1976

Live load distribution factors for prestressed concrete i-beam bridges, January 1976

C. N. Kostem

M. A. Zellin

D. A. VanHorn

J. M. Kulicki

Technical Report Documentation Page

1. Report No.	2. Government Accession No.	3. Recipient's Catalog No.
FHWA-PA-RD-72-4-2B		

4. Title and Subtitle	5. Report Date
LIVE LOAD DISTRIBUTION FACTORS FOR PRESTRESSED CONCRETE I-BEAM BRIDGES	January 1976
	6. Performing Organization Code
7. Author(s) Martin A. Zellin, Celal N. Kostem, David A. VanHorn, John M. Kulicki	8. Performing Organization Report No. No. 387.2B
9. Performing Organization Name and Address Department of Civil Engineering Fritz Engineering Laboratory Lehigh University (Bldg. 13) Bethlehem, Pennsylvania 18015	10. Work Unit No. (TRAIS) 11. Contract or Grant No. Project 72-4
12. Sponsoring Agency Name and Address Pennsylvania Department of Transportation P. O. Box 2926 Harrisburg, Pennsylvania 17120	13. Type of Report and Period Covered Interim Report 14. Sponsoring Agency Code

15. Supplementary Notes

Prepared in cooperation with the U. S. Department of Transportation, Federal Highway Administration.

16. Abstract

This is the third report on the research investigation entitled "Development and Refinement of Load Distribution Provisions for Prestressed Concrete Beam-Slab Bridges" (PennDOT 72-4). The beam-slab bridges included in this study are of the I-beam type. Included are: (1) a structural analysis, based on the finite element method, which describes superstructure response to design-vehicle loading, (2) a comparison of the structural analysis with results from the field tests of two in-service bridge superstructures, (3) the analysis of 150 superstructures ranging in length from 30 ft. to 135 ft. and in roadway width from 24 ft. to 72 ft., and (4) equations for evaluating live-load distribution factors for interior and exterior beams, based on the definition of traffic lanes set forth in the AASHTO "Interim Specifications - Bridges: 1974".

17. Key Words	18. Distribution Statement
Prestressed Concrete I-Beam Bridge Design, Live Load Distribution for Highway Bridges	

19. Security Classif. (of this report)	20. Security Classif. (of this page)	21. No. of Pages	22. Price
Unclassified	Unclassified	107	

COMMONWEALTH OF PENNSYLVANIA

Department of Transportation

Bureau of Materials, Testing and Research

Leo D. Sandvig - Director
Wade L. Gramling - Research Engineer
Kenneth L. Heilman - Research Coordinator

Project 72-4: Development and Refinement of Load Distribution Provisions for Prestressed Concrete Beam-Slab Bridges

LIVE LOAD DISTRIBUTION FACTORS FOR PRESTRESSED CONCRETE I-BEAM BRIDGES

by

Martin A. Zellin
Celal N. Kostem
David A. VanHorn
John M. Kulicki

Prepared in cooperation with the Pennsylvania Department of Transportation and the U. S. Department of Transportation, Federal Highway Administration. The contents of this report reflect the views of the authors who are responsible for the facts and the accuracy of the data presented herein. The contents do not necessarily reflect the official views or policies of the Pennsylvania Department of Transportation, the U. S. Department of Transportation, Federal Highway Administration, or the Reinforced Concrete Research Council. This report does not constitute a standard, specification or regulation.

LEHIGH UNIVERSITY

Office of Research

Bethlehem, Pennsylvania

January, 1976

Fritz Engineering Laboratory Report No. 387.2B

TABLE OF CONTENTS

ABSTRACT

This is the third report on the research investigation entitled "Development and Refinement of Load Distribution Provisions for Prestressed Concrete Beam-Slab Bridges" (PennDOT 72-4). The beam-slab bridges included in this study are of the I-beam type. Included are: (1) a structural analysis, based on the finite element method, which describes superstructure response to design-vehicle loading, (2) a comparison of the structural analysis with results from the field tests of two in-service bridge superstructures, (3) the analysis of 150 superstructures ranging in length from 30 ft. to 135 ft. and in roadway width from 24 ft. to 72 ft., and (4) equations for evaluating live-load distribution factors for interior and exterior beams, based on the definition of traffic lanes set forth in the AASHTO "Interim Specifications - Bridges: 1974".

1. INTRODUCTION

1.1 General

Over the past eleven years, Lehigh University has conducted a major research program on the structural behavior of prestressed concrete beam-slab highway bridge superstructures subjected to design vehicle loading conditions. The superstructures basically consist of a number of longitudinal precast prestressed concrete beams, equally spaced and spread apart, along with a cast-in-place composite reinforced concrete deck slab. The research program has included: (1) field studies of eight in-service bridges, (2) laboratory studies of 1/16-scale model bridges, and (3) the development of a complex mathematical computer-based analysis.

The first part of the overall research program was devoted to a study of spread box-beam superstructures. Based on the results from the study, a new specification provision was proposed, covering lateral distribution of live loads. This provision was adopted by AASHTO in Fall, 1972, and now appears as Article 1.6.24 in the 1973 AASHTO Standard Specifications for Highway Bridges[1]. Currently, the overall investigation is progressing under PennDOT Research Project No. 72-4, entitled "Development and Refinement of Load Distribution for Prestressed Concrete Beam-Slab Bridges".

1.2 Objectives

The primary objectives of the overall investigation are:

1. To develop a new provision for live-load distribution in prestressed concrete I-beam bridge superstructures, paralleling the already adopted provision for spread box-beam bridges.

2. To expand the live-load distribution provisions for spread box-beam bridges (Article 1.6.24[1]), and the proposed new provisions for I-beam bridges, to include provisions for the inclusion of the effects of skew.

3. To investigate the possibility of extending the analysis and specification development to cover: (a) the effects of interior-span diaphragms, (b) the effects of curb-parapet sections, and (c) continuous-span construction.

Currently, the AASHTO provisions for the distribution of live load in prestressed concrete I-beam superstructures are listed under Article 1.3.1 of the 1973 AASHTO Standard Specifications for Highway Bridges[1]. Both field tests and preliminary analytical work have indicated the inadequacy of the current specifications. Under Objective No. 1, two separate analyses have been conducted. The first analysis, described in Report No. 387.2A entitled "Lateral Distribution of Live Load in Prestressed Concrete I-Beam Bridges"[15], was based on the definition of traffic lanes as specified in

Article 1.2.6 of the 1973 AASHTO Specifications. The second analysis, reported herein, is based on the current definition of traffic lanes as specified under the revised Article 1.2.6 as set forth in the 1974 AASHTO Interim Specifications - Bridges[2]. There will be two additional reports on this Project, Nos. 387.3 and 387.4, which will cover Objectives Nos. 2 and 3, respectively.

1.3 Previous Studies

Load distribution in highway bridges has been studied for many years, both in this country and abroad. Though the previous work has resulted in a greater understanding of the behavior of bridges, a number of simplifying assumptions were made in each case in order to overcome the mathematical difficulties involved in the solution procedures. The methods used to study the behavior of bridges have been the grillage analysis, folded and orthotropic plate theories, the finite difference method, the finite strip method, and the finite element method. Of all of the methods, the finite element method requires the fewest simplifying assumptions in accounting for the greatest number of variables which govern the structural response of the bridge. Therefore, the technique chosen was a structural analysis for stiffened plate structures, developed at Lehigh University, which utilized the finite element displacement approach.

It is not the purpose of this report to provide a discussion of previous work. An up-to-date annoted bibliography containing references which are directly or indirectly applicable to the structural behavior, analysis, and design of beam-slab type highway bridges was presented in a previous report[14] from this project.

2. ANALYSIS BY THE FINITE ELEMENT METHOD

2.1 Assumptions

The following assumptions were made in the finite element analysis of the bridge superstructures investigated as part of this research.

1. A small strain - small deflection theory was used.
2. Linearly elastic behavior of materials was assumed.
3. All superstructures were analyzed with simple supports. The effects of continuity were not included.
4. The longitudinal beams were prestressed concrete I-beams, either from Pennsylvania Standard[8] or from AASHTO-PCI Standard cross-sections.
5. All loading conditions were static. No dynamic effects were considered.
6. The response of the slab was divided into out-of-plane and in-plane behavior. The out-of-plane behavior accounted for actions such as the normal stress associated with composite action of the beams and slab.
7. The in-plane and out-of-plane responses were superimposed.
8. The mid-plane of the deck slab was taken as the reference plane for the analysis technique.
9. The deck slab was assumed to have a constant thickness. Haunching for grade or camber was not included, nor was

the presence of permanent metal deck forms or the concrete below the top surface of the deck form. These are conservative assumptions.

10. Local stresses produced by the individual wheel loads were considered to have a negligible effect on the live load distribution factors, and were not considered in the analysis.

11. Beams and slabs were assumed to act in a completely composite manner. Thus, the strain compatibility between the deck slab and the beam was maintained.

12. The beams were modeled as eccentric stiffeners to the slab.

13. The action of each beam was satisfactorily represented by a normal force, a bending moment about one axis, and a torsional moment. Weak-axis bending was ignored because of the relative stiffnesses of I-beam sections, and because only vehicular loading was considered.

14. The St. Venant torsional stiffness of the beams was considered. Warping torsion was assumed to be small because of the shape of the I-beams (Ref. 12). Appropriate values of the St. Venant torsional stiffness coefficient were computed and reported in Ref. 7.

15. The cross-sections of the structures analyzed in this research were reasonably proportioned. That is, for a particular structure, the beam size and spacing were appropriate for the span length, and the slab thickness was appropriate for the beam spacing.

16. The effect of the curb-parapet section was considered, as discussed in Sec. 3.3.4.

17. Intra-span diaphragms were not included in this analysis, since past research[10,12] has shown that while these diaphragms are effective in distributing the live load from a single vehicle, the effect becomes minimal when several lanes are loaded.

18. The number of loaded lanes conformed to the revised Article 1.2.6[2], as discussed in Section 4.2.

19. AASHTO type HS20 standard truck loading was used throughout the entire study, Ref. 1, Article 1.2.5.

2.2 Finite Element Analysis

The finite element method has three basic phases:

1) Structural Idealization
2) Evaluation of element properties
3) Assembly and analysis of the structural system.

In the current analysis, the beams and slab were treated separately, and then combined in the third phase. This presentation will follow the same pattern by discussing first the analysis of deck slabs, then the analysis of beams, and finally the assembly of beam and slab elements. This analysis is based on the formulation by Wegmuller and Kostem.[12,13]

2.2.1 The Deck Slab

As mentioned in Sec. 2.1, the response of the deck slab was further divided into out-of-plane (bending) and in-plane (membrane) actions.

2.2.1.1 The Out-of-Plane Behavior of the Deck Slab

The deck slab was analyzed using thin plate theory. Hence, the following assumptions were made:

1. Sections which were plane and normal to the middle surface before deformation remained plane and normal after deformation.
2. Transverse displacements were small compared to the plate thickness.

Tension in Concrete :

long time ago — not allowable

— fatigue problem — didn't consider

Introduction.

Six kinds of Standard P. C. Beam.

Different span length range

Different Size.

3. Since stresses normal to the plane of the plate were negligible, shearing stresses in the transverse direction were neglected, and the transverse displacement of any point on the plate was essentially the displacement of the corresponding point on the middle surface of the plate.

The deck slab was discretized into rectangular plate bending elements. The element developed by Adini, Clough, and Melosh[3] was used. The plate elements were connected at node points. A node point was common to all of the elements which surrounded it. The displacements at the node points were the basic unknowns of the finite element stiffness analysis. There were three out-of-plane displacements assigned to each plate element node point. These displacements were the transverse displacement, W, and the bending rotations θ_x and θ_y. These displacements occured at the mid-plane of the plate. Thus, there were a total of twelve out-of-plane degrees of freedom (i.e., unknown displacements) associated with each plate bending element.

A polynomial displacement function was used to describe the displacements within the plate bending element.

$$W = \alpha_1 + \alpha_2 X + \alpha_3 Y + \alpha_4 XY + \alpha_5 X^2 + \alpha_6 Y^2 + \alpha_7 XY^2 \qquad (2.1)$$
$$+ \alpha_8 X^2Y + \alpha_9 X^3 + \alpha_{10} Y^3 + \alpha_{11} X^3Y + \alpha_{12} XY^3$$

The nodal rotations are given as derivatives of the transverse displacement, W.

$$\theta_x = \partial w/\partial y \tag{2.2}$$

$$\theta_y = -\partial w/\partial x \tag{2.3}$$

There are twelve unknown constants in Eq. 2.1 and twelve boundary conditions for each element: three displacements at each of four nodes. Substituting Eq. 2.1 into Eqs. 2.2 and 2.3, and then substituting the coordinates of the corners of the elements with respect to the element axes (shown in Fig. 1), the following equation is obtained:

$$\{\delta^e\}_o = [C]_o \{\alpha\} \tag{2.4}$$

the subscript "o" indicates out-of-plane displacements. The constants (α) are evaluated by matrix inversion.

$$\{\alpha\} = [C]_o^{-1} \{\delta^e\}_o \tag{2.5}$$

The strains within the element are related to the displacement field by the strain displacement equations. Within the context of the finite element method, strains and stresses are usually referred to as <u>generalized strains</u> and <u>generalized stresses</u>.

The generalized strains for out-of-plane behavior are the bending curvatures. Thus, it is possible to define the strains as:

$$\{\varepsilon\} = \begin{Bmatrix} \phi_x \\ \phi_y \\ \phi_{xy} \end{Bmatrix} = \begin{Bmatrix} -\partial^2 w/\partial x^2 \\ -\partial^2 w/\partial y^2 \\ 2\,\partial^2 w/\partial_x\,\partial_y \end{Bmatrix} \tag{2.6}$$

Substitution of Eq. 2.1 into Eq. 2.6 results in the matrix equation:

$$\{\varepsilon\} = [Q]\ \{\alpha\} \tag{2.7}$$

Substitution of Eq. 2.5 into Eq. 2.7 relates the generalized strains to the unknown nodal equations:

$$\{\varepsilon\} = [Q]\ [C]_o^{-1}\ \{\delta^e\}_o \tag{2.8}$$

Stresses are related to strains by an elasticity matrix:

$$\{\sigma\} = [D]\ \{\varepsilon\} \tag{2.9}$$

The stresses corresponding to the strains given by Eq. 2.6 are the bending moments per unit distance: M_x, M_y, and M_{xy}. Using the well-known equations of plate analysis (Ref. 9), the elasticity matrix is defined as:

$$\begin{Bmatrix} M_x \\ M_y \\ M_{xy} \end{Bmatrix} = \frac{Eh^3}{12(1-\nu^2)} \begin{bmatrix} 1 & \nu & 0 \\ \nu & 1 & 0 \\ 0 & 0 & \frac{1-\nu}{2} \end{bmatrix} \begin{Bmatrix} \phi_x \\ \phi_y \\ \phi_{xy} \end{Bmatrix} \tag{2.10}$$

where E is the modulus of elasticity of the plate, h is the plate thickness, and ν is Poisson's Ratio. Once these matrices have been defined, the well-established procedures of the finite element

method lead to the following stiffness matrix (Ref. 14):

$$[K]_o = [C]_o^{-1^T} \int_A [Q]^T [D] [Q] \, dx \, dy \, [C]_o^{-1} \tag{2.11}$$

The out-of-plane stiffness matrix, $[K]_o$ is given explicitly in Refs. 6, 12, and 16.

2.2.1.2 The In-Plane Behavior of the Deck Slab

The in-plane behavior of the plate is analyzed as a plane-stress elasticity problem. The discretization remains the same as discussed of out-of-plane behavior. There are two in-plane displacements at each node. The displacement in the x-direction (Fig. 1) is called U, the displacement in the y-direction is V. There are a total of eight in-plane degrees of freedom. The polynomial displacement functions are given by Eqs. 2.12 and 2.13.

$$U = \alpha_{13} + \alpha_{14} X + \alpha_{15} Y + \alpha_{16} XY \tag{2.12}$$

$$V = \alpha_{17} + \alpha_{18} X + \alpha_{19} Y + \alpha_{20} XY \tag{2.13}$$

As in the out-of-plane case, the eight unknown constants in Eqs. 2.12 and 2.13 are evaluated using the eight nodal displacements:

$$\{\delta^e\}_I = [C]_I \{\alpha\} \tag{2.14}$$

$$\{\alpha\} = [C]_I \{\delta^e\}_I \tag{2.15}$$

The generalized strains are taken as:

$$\{\varepsilon\} = \begin{Bmatrix} \partial u/\partial x \\ \partial v/\partial y \\ \partial u/\partial x + \partial v/\partial y \end{Bmatrix} = \begin{Bmatrix} \varepsilon_x \\ \varepsilon_y \\ \gamma_{xy} \end{Bmatrix} \tag{2.16}$$

Substitution of Eqs. 2.12 and 2.13 into 2.16 results in:

$$\{\varepsilon\} = [Q]\ \{\alpha\} \tag{2.17}$$

Substituting Eq. 2.15 into Eq. 2.19 results in the strain-displacement relations:

$$\{\varepsilon\} = [Q]\ [C]_I^{-1}\ \{\delta^e\}_I \tag{2.18}$$

The stresses are chosen as the membrane stresses σ_x, σ_y and τ_{xy}. The resulting elasticity matrix, based on the assumption of plane stress, is given by:

$$\begin{Bmatrix} \sigma_x \\ \sigma_y \\ \tau_{xy} \end{Bmatrix} = \frac{E}{1-\nu^2} \begin{bmatrix} 1 & \nu & 0 \\ \nu & 1 & 0 \\ 0 & 0 & \frac{1-\nu}{2} \end{bmatrix} \begin{Bmatrix} \varepsilon_x \\ \varepsilon_y \\ \gamma_{xy} \end{Bmatrix} \tag{2.19}$$

The basic matrices necessary to evaluate Eq. 2.13 are now known for the in-plane case, and the in-plane stiffness matrix, $[K]_I$, can now be evaluated. The in-plane stiffness matrix is also given explicitly in Ref. 12.

2.2.1.3 Superposition of In-Plane and Out-of-Plane Behaviors

Since the analysis is based on a small deflection theory with linear material properties, as mentioned in Sec. 2.1, the in-plane and out-of-plane stiffness matrices may be superimposed as follows:

$$\begin{Bmatrix} F_I \\ F_o \end{Bmatrix} = \begin{bmatrix} K_I & 0 \\ 0 & K_o \end{bmatrix} \begin{Bmatrix} \delta_{e_I} \\ \delta_{e_o} \end{Bmatrix} \tag{2.20}$$

$[F]_I$ and $[F]_o$ are the in-plane and out-of-plane nodal force vectors, respectively.

2.2.2 The Beams

Figure 2 shows a beam element, nodal points, coordinate axes, and degrees of freedom. The degrees of freedom consist of an in-plane axial displacement, U, out-of-plane bending displacements, W and θ_y, and a torsional rotation, θ_x, at each node. Beam elements are positioned between plate nodes in the x-coordinate direction.

The in-plane and out-of-plane response of beam elements are considered simultaneously. The torsional response is treated separately.

2.2.2.1 The In-Plane and Out-of-Plane Behavior of Beams

The polynomial displacement functions for the response of beam element, not including the effects of torsion, are given by:

$$U = \alpha_{21} + \alpha_{22} X \tag{2.21}$$

$$W = \alpha_{23} + \alpha_{24} X + \alpha_{25} X^2 + \alpha_{26} X^3 \tag{2.22}$$

These displacements occur in the same reference plane that is used for calculation of the plate displacements (Fig. 2). In this formulation the reference plane was the mid-plane of the deck slab. It should be noted that Eqs. 2.21 and 2.22 have the same form as Eqs. 2.12 and 2.1 when the coordinate y is equal to a constant. This fact, combined with a choice of beam eccentricity referenced to the mid-plane of the deck slab, provides strain compatibility between the deck slab and the beam. This is necessary to correctly model composite beam-slab bridges. The bending rotation, θ_y, is defined by Eq. 2.3.

The six unknown constants in Eqs. 2.21 and 2.22 are evaluated using the six nodal displacements, three at each end of the beam:

$$\{\delta^e\}_B = [C]_B \{\alpha\} \tag{2.23}$$

$$\{\alpha\} = [C]_B^{-1} \{\delta^e\}_B \tag{2.24}$$

The generalized strains are taken as the bending curvature and axial strain.

$$\{\epsilon\} = \begin{Bmatrix} dy/dx \\ - d^2w/dx^2 \end{Bmatrix} \tag{2.25}$$

The generalized stresses corresponding to these strains are the axial force and bending moment.

$$\{\sigma\} = \begin{Bmatrix} N \\ M \end{Bmatrix} \tag{2.26}$$

The strain in the beam can be related to Eq. 2.25 as shown in Fig. 3.

$$\bar{\varepsilon} = \frac{du}{dx} - Z \frac{d^2w}{dx^2} \tag{2.27}$$

The bar indicates that the strain is referred to the reference plane. The stress is equal to Young's modulus times the strain.

$$\bar{\sigma} = E \bar{\varepsilon} = E\left[\frac{du}{dx} - Z \frac{d^2w}{dx^2}\right] \tag{2.28}$$

The generalized stresses are related to $\bar{\sigma}$ by the integrals:

$$N = \int_A E \bar{\varepsilon} \, dA = E \frac{du}{dx} \int_A dA - E \frac{d^2w}{dx^2} \int_A Z \, dA = E \bar{A} \frac{du}{dx} - E \bar{S} \frac{d^2w}{dx^2} \tag{2.29}$$

$$M = \int_A E Z \bar{\varepsilon} \, dA = E \frac{du}{dx} \int_A Z \, da - E \frac{d^2w}{dx^2} \int_A Z^2 \, dA = E \bar{S} \frac{du}{dx} - E\bar{I} \frac{d^2w}{dx^2} \tag{2.30}$$

The elasticity matrix is defined by using Eqs. 2.29 and 2.30:

$$\begin{Bmatrix} N \\ M \end{Bmatrix} = \begin{bmatrix} \bar{A} & \bar{S} \\ \bar{S} & \bar{I} \end{bmatrix} \begin{Bmatrix} dy/dx \\ - d^2w/dx^2 \end{Bmatrix} \tag{2.31}$$

The bars in Eq. 2.31 indicate that the appropriate quantities are referred to the reference plane, not necessarily to the centroidal

axis of the beam.

Substituting Eqs. 2.21 and 2.22 into Eq. 2.25 leads to the definition of [Q]. Once this is done, all of the matrices are defined to evaluate the nontorsional stiffness matrix of the eccentric beam element:

$$[K] = [c]_B^{-1^T} \int_\ell [Q]^T [D] [Q] \, dx \, [c]_B^{-1} \tag{2.32}$$

The beam stiffness matrix above is given explicitly in Ref. 12.

2.2.2.2 The Torsional Behavior of the Beams

The St. Venant torsional stiffness of the prestressed concrete I-beams is included in the analysis. The warping torsion effects are neglected. The St. Venant torsional moment[12] can be related to the unit angle of twist by:

$$T_{sv} = GK_T \phi' \tag{2.33}$$

The unit angle of twist can be related to the axial rotation of the beam by:

$$\{\varepsilon\} = \phi' = \frac{\partial}{\partial x} \theta_x = \frac{\partial}{\partial x} \frac{\partial w}{\partial y} \tag{2.34}$$

Substitution of the displacement function for the plate (Eq. 2.1) into Eq. 2.34 results in the assumed displacement function for θ_x along a line defined by a constant y coordinate.

$$\theta_x = \frac{\partial w}{\partial y} = \alpha_{27} + \alpha_{28} X \tag{2.35}$$

The elemental displacement vector consists of values of θ_x at each end of the beam. Thus, a connection matrix analogous to Eqs. 2.4, 2.14, 2.15, and 2.23 can be defined.

$$\{\delta_e\}_T = [C]_T \{\alpha\} \tag{2.36}$$

$$\{\alpha\} = [C]_T^{-1} \{\delta_e\}_T \tag{2.37}$$

The generalized stress and strain are the torsional bending moment and the unit angle of twist, respectively. Thus, an elasticity matrix is defined as shown above.

$$\{T\} = [GK_T] \{\phi'\} \tag{2.38}$$

The matrix [Q] is again defined by substituting the displacement functions given by Eq. 2.35 into the definition of strain given by Eq. 2.34. When this is done, all of the matrices needed to define the stiffness matrix are known, and evaluation may proceed. An explicit torsional stiffness matrix is given in Ref. 12.

2.3 Assembly of Elements

The assembly of elements in the finite element method is analogous to the assembly of member-stiffness matrices in conventional matrix structural analysis. The slab element stiffness matrix relates a force at one node to the displacements of the remaining nodes in that element. Each node may be surrounded by as many as four slab elements which join that node. Thus, a force at one node may be related to the displacements of all the nodes in four elements. This means that, including the fact that some nodes will be common to the adjoining elements, a total of 9 nodes having forty-five degrees of freedom could be related to the single force component. The process of relating the force to all of the adjoining ele-

ments and their degrees of freedom is called assembly of the global stiffness matrix. The problem of finding the appropriate node points related to a given node point is a matter of specifying structural topology to the computer program which actually performs the arithmetic operations, and will not be discussed in this report.

The superposition of beam stiffness components is accomplished by straight-forward addition of corresponding beam and slab element stiffness components. This includes isolating the nodes to which beam elements are attached. The force at a node having a beam element is related to the beam displacements at the adjacent nodes in the x-direction. This is also a matter of topology which is specified as input to the computer program, and will not be discussed in this report.

2.4 Solution and Back Substitution

The assembly of the element stiffness matrices results in a set of simultaneous equations relating nodal forces to nodal displacements. These equations are solved for the nodal displacements after the boundary conditions are enforced. Once the displacements are known, it is possible to back-substitute them into appropriate equations to compute the generalized stresses. Thus, substitution of nodal displacements into the beam stiffness matrix results in the normal force, bending moment, and torsional moment at the beam node points. These forces act at the plane of reference, i.e., the midplane of the plate. This fact is important in evaluating the lateral load distribution in bridges.

Substitution of the appropriate nodal displacements into Eq. 2.8, followed by substitution of the results into Eq. 2.9, enables the evaluation of the unit bending moments M_x, M_y, and M_{xy} at the node points. The inplane stresses (or forces) can be evaluated in a similar manner.

2.5 Computation of Moment Percentages

A moment percentage is defined as the bending moment carried by one beam, where the beam can be considered as the total composite cross-section, divided by the total of the moments carried by all the beams, and multiplied by 100. The moment carried by one composite cross-section is given by:

$$M_c = \int_{beam} \sigma_x Z \, dA + \int_{slab} \sigma_x Z \, dA \qquad (2.39)$$

where Z is a coordinate from any reference plane. If the reference plane is chosen as the mid-plane of the plate, Eq. 2.39 may be rewritten as:

$$M_c = M_{x_{beam}} + \int_0^{b_{eff}} (M_{x_{slab}}) \, d\ell \qquad (2.40)$$

in which b_{eff} is the effective width of the slab. It was noted in Sec. 2.2 that provisions were made to reference the beam moment to any arbitrary reference plane, including the mid-plane of the plate. It is this moment which is found by back-substitution, as discussed in Sec. 2.2.4.

The problem of finding the effective flange width is simplified by the relative sizes of the unit slab bending moment, $M_{x_{slab}}$, and the beam bending moment about the mid-plane of the plate. The total slab moment across the bridge width is only a small percentage of the total of the composite beam moments. Sample calculations indicate that for beam-slab bridges, the total slab moment is generally $\leq$ 5% of the total. Therefore, the effect of a small error in the effective flange width is an insignificant difference in the moment percentages as calculated in this research. As a result, the following approximate effective flange widths were used in lieu of more exact calculations:

1. For interior beams, the actual beam spacing was used.
2. For exterior beams, one half of the spacing, plus the over-hang was used.

Having the effective flange width and choosing the slab moment at the node over the beam as representative width of the superstructure, Eq. 2.40 reduces to:

$$M_c = M_{beam} + (M_{x_{slab}}) (b_{eff}) \tag{2.41}$$

The moment percentage of one beam is then calculated as:

$$M_{pi} = \frac{M_{c_i}}{\sum_{i=1}^{n} M_{c_i}} \tag{2.42}$$

in which i denotes the beam in question and n is the total number of beams. These moment percentages were used to produce influence lines for a given bridge. These influence lines were then loaded to determine the maximum distribution factor for a given bridge.

3. ANALYTIC MODELING STUDY

3.1 Purpose of Analytic Modeling Study

The finite element technique described in Chapter 2 of this report was used in the study of lateral load distribution in I-beam bridges. A preliminary study was undertaken to investigate different methods of analytically modeling the I-beam bridges so as to use the finite element method effectively and efficiently. In this study the analytic models were compared to the field test results[4,5,10,11] of two in-service I-beam bridges located near Lehighton and Bartonsville, Pennsylvania.

The results of the analytic modeling study were threefold. First, important design parameters of a bridge were isolated, described, and analyzed using analytic approximations. Thus, the influence of these design parameters such as the curb-parapet section and permanent metal deck forms were taken into account. Second, the analysis was verified by comparison with the results from the field tests. Third, the analytic bridge model was refined, to enable an accurate and efficient study of lateral load distribution.

3.2 Description of Field Test Bridges

The field testing of the Lehighton and Bartonsville bridges analyzed in this investigation is described in detail by Chen and VanHorn,[4,5,10] and Wegmuller and VanHorn.[11] Initially, only the field

test results of the Lehighton bridge were used in comparison with different analytic models. The reason for the emphasis on the Lehighton bridge was two-fold. First, the Lehighton bridge was tested both with and without midspan diaphragms between beams. Second, there was only one curb-parapet section on the Lehighton bridge, which allowed the effect of the curb-parapet section on load distribution to be seen more readily. The Bartonsville bridge test results were then compared to an analytic model which included all of the features of modeling discussed in this chapter which are appropriate to the Bartonsville bridge.

The cross-section of the Lehighton Bridge is shown in Fig. 4. The main supporting members were six identical PennDOT 24/45 prestressed concrete I-beams spaced 6 feet 9 inches center-to-center. The slab was cast-in-place over a permanent metal deck form, with a nominal thickness of 7-1/2 inches. With a curb and parapet section on only one side of the superstructure, the roadway width was 35 feet 11-1/2 inches. The span length was 71 feet 6 inches, center-to-center of bearings.

The cross-section of the Bartonsville Bridge is shown in Fig. 5. The main supporting members were five identical AASHTO-PCI Type III prestressed concrete I-beams spaced 8 feet center-to-center. The slab was cast-in-place with a nominal thickness of 7-1/2 inches. The roadway width was 32 feet. The span length was 68 feet 6 inches, center-to-center of bearings.

3.3 Analytic Modeling

3.3.1 Discretization of the Superstructure

Using the finite element technique, the actual bridges were modeled by a discretized bridge containing a suitable number of finite elements. Figure 6 shows the cross-section of the Bartonsville test bridge. Also shown is the plan view of the bridge, with the discretization indicated. The lines indicate boundaries between elements, and the intersections of those lines are nodal points. The beams were also discretized into beam elements, connected at the appropriate nodal points. In the discretization shown in Fig. 6, there are two plate elements between the beams. In the analytic modeling study, the discretization was varied according to the requirements of a particular analytic model.

In comparing the analytic and field test results, the moments at a cross-section called the maximum moment section of the bridge were used. The maximum moment section, shown as section M in Fig. 6, is the section at which the absolute maximum moment would occur in a simple beam of the same span as the bridge, when loaded with the test vehicle. The test vehicle, which closely approximated the AASHTO HS20 design vehicle, is shown in Fig. 7.

Comparisons of different analytic models were made using moment percentage diagrams. The definition of moment percentage for a particular beam is defined in Section 2.5 of this report.

3.3.2 Refinement of Slab Discretization

Figure 8 shows a typical segment of the cross-section of the test bridge. The figure shows that portions of the slab are supported by the relatively stiff flange of the I-beams. Because of the support provided by the flanges, the first investigation undertaken was the analytic modeling of the effective bending span of the slab between the beams.

Two different models were used to model the effective bending span of the slab. The first model was a mathematical approximation that was an accurate and efficient modeling technique. The second model was a theoretically better approximation, but was a far less efficient model. Though this second model would not be used in an extensive study, it was used here to verify the first modeling technique.

The first model, shown in Fig. 8, consisted of nodes positioned above the center of the beams and midway between the beams. This discretization, which consisted of two slab elements between beams was designated the 2 PL mesh. Using this discretization, the effective bending span was approximated by introducing an orthotropy factor (D_y) in the analysis. This factor was defined as the ratio of the transverse-to-longitudinal stiffness of a unit area of slab. The orthotropy factor was calculated as the square of the ratio of the center-to-center beam spacing to the flange-to-flange spacing.

As shown in Fig. 8, the orthotropy factor calculated for the Lehighton Bridge was 1.69.

The moment percentage diagram (Section 2.5) shown in Fig. 9 is a comparison of two analytic models with the field test results. One model included the orthotropy factor in the analysis, while the other did not. As shown in Fig. 9, the test vehicle is located between the third and fourth beams, as indicated by the wheels and axle. Comparison of the analytic models with the field test results showed that a closer correlation to the field test results was obtained when the orthotropy factor was included in the analysis.

To verify that this method was an effective way of modeling the bending span of the slab, a comparison was made with another theoretical model. The discretization for the latter model is shown in Fig. 10. There are four slab elements between the beams, with two elements over the flange of each beam, and two elements between the flanges of the beams. This discretization was designated the 4 PL mesh. The slab elements over the flanges of the beams were assigned an orthotropy factor of 100.0. This orthotropy factor defined the stiffness of the slab elements, above the beam flanges, in the transverse direction to be 100 times greater then stiffness in the longitudinal direction. In effect, the slab elements above the flanges were allowed to deform in the longitudinal direction, while essentially remaining rigid in the transverse direction. This prevented relative deformation of the slab with respect to the beam flange in

the transverse direction. The elements between the beams were assigned an orthotropy factor of 1.00, therefore those elements would deform in an isotropic manner.

In Fig. 11, the results from use of the 4 PL mesh are compared with those from the 2 PL mesh. The position of the test vehicle is indicated. It is seen in this comparison that both models yielded virtually the same results. Thus, the methods of modeling the appropriate bending span were verified. Based on the comparison, the 2 PL mesh was selected for the remainder of the study because it was as equally effective as, and more efficient than, the 4 PL model in representing the bending span of the slab.

A further investigation was then performed to determine the effect of a different slab discretization on the analysis. The discretization in Fig. 12(a) is the 2 PL mesh, described earlier in this section, while the discretization in Fig. 12(b) has one slab element between the beams, and will be designated the 1 PL mesh. Both of these models contain the appropriate orthotropy factors and results from their use are compared in Figs. 13 & 14. Two different truck positions are indicated. These figures both show that there was no perceptible difference between either of the modeling techniques.

3.3.3 Permanent Metal Deck Form

The concrete slab of the test bridge was placed over a permanent metal deck form which had ribs running in the transverse direction (Fig. 15). The effects of the deck form on lateral load distribution were modeled by introducing another orthotropy factor (D_y). As indicated in Fig. 16 the orthotropy factor was claculated as the ratio of moments of inertia I'/I, where I' was defined as the moment of inertia of the transformed concrete section and the metal deck form in the transverse direction, and I was the moment of inertia of the concrete slab of nominal thickness in the longitudinal direction. For the Lehighton test bridge, the orthotropy factor was calculated as 1.48. The effect of including this factor in the analysis is shown in Fig. 17. When the permanent metal deck form was included in the analysis, the agreement between analytic and field test results was improved.

3.3.4 Curb-Parapet Section

In order to verify that the analytic model accurately represented the actual superstructure behavior, it was also necessary to make an investigation to assess the effect of the single curb-parapet section, shown on the right side of the cross-section in Fig. 4. The curb-parapet section was considered as a beam element in the analysis. Two different models of the section were studied: (1) The section, shown in Fig. 18, was considered to be

fully effective. (2) The section was considered to be partially effective. That is, only the cross-sectional properties up to the dashed line were considered, as indicated in Fig. 18. In the actual bridge, the curb-parapet section was interrupted by deflection joints one inch in width at intervals of approximately 14 feet along the span length. The joints were filled with a pre-molded joint filler in the portion of the section between the top of the slab and the dotted line. Therefore, the two models represented the upper and lower bounds of effectiveness.

Both modeling techniques are compared to the field test results in Figs. 19, 20, and 21. Each figure corresponds to a different truck position. It is seen in Fig. 19 that there is very little difference between results from the two models. This was expected for a truck position which was as far as possible from the curb-parapet section. In this case the bending moments in the beams in the vicinity of the curb-parapet are negligible, and therefore, the influence of the curb-parapet would be small. In Fig. 20 the test vehicle is placed between the third and fourth beams of the bridge. For this load case, there was a noticeable difference between the fully effective and partially effective models. Use of the partially effective section produced results which correlated better with the field test than those obtained with the fully effective section. In Fig. 21 the truck is positioned as close as possible to the curb-parapet section.

With this position of the truck, use of the fully effective curb-parapet section, resulted in an over-estimation of the moment carried by the exterior beam under the curb-parapet section, while use of the partially effective curb-parapet section, yielded very good correlation with the field test results. Thus, it was concluded that the effect of the curb-parapet section on lateral load distribution increases as the load approaches that section. These studies have also indicated that the partially effective section is a more realistic model of the curb-parapet than a fully effective section.

3.4 Summary

A study of different analytic modeling techniques has been presented. In this study, an accurate and efficient model was developed for use in the study of lateral load distribution. Figures 22 and 23 show the correlation between analytic and field test results for two additional load cases on the Lehighton Bridge. Figures 24 and 25 compare analytic and field test results for two load cases on the Bartonsville Bridge. The difference between the analytic and field test results is no greater than 6% for any load case.

Based on this study, the following conclusions are drawn:

1) The permanent metal deck form and the top flanges of the beams stiffen the slab in the transverse direction. This stiffening effect can be accounted for by using an orthotropy

factor. Suggested methods of computing these orthotropy factors are presented in Sec. 3.3.2 and Sec. 3.3.3.

2) The number of elements between beams can be reduced with a considerable increase in efficiency, but without a significant loss in accuracy.

3) The curb-parapet section affects the distribution of live load. The results from this preliminary study indicate that a partially effective curb-parapet model yields more realistic results than a fully effective model.

4. DESIGN OF ANALYTIC EXPERIMENT

4.1 General

To obtain a general method for the evaluation of distribution factors that will be reliable for all bridges over a range of different dimensions, many bridges were considered in the investigation. Although field tests were important in establishing the validity of analytical techniques, an investigation of the number of structures required in this study eliminates the possibility of sufficient field testing to provide the basis for a general specification provision. Therefore, an analytic experiment was designed to yield the information which would form the basis for development of new design provisions for live-load distribution factors. In this analytic experiment, 150 bridges were designed and analyzed. The experiment was a computer based analytic simulation, based on the theoretical technique described in Chapter 2, and the analytic model developed in Chapter 3.

4.2 Type of Superstructure and Loading Configuration

The bridges that were considered in the analytic experiment were all simple-span, without skew. The bridges consist of a reinforced concrete deck slab supported longitudinally by equally spaced prestressed concrete I-beams. The effects of the curb-parapet section and the intra-span diaphragms were neglected. All bridges were designed using the provisions of the 1973 AASHTO specification[1], the 1974

AASHTO interim specification[2], and the PennDOT Standards for Bridge Design, BD-201[8]. AASHTO HS20 truck loadings were used.

4.3 Bridge Dimensions and Variation of Parameters

The following bridge design parameters were varied in the analytic experiment. A representative range of roadway widths were chosen, using Art. 1.2.6 of the 1974 AASHTO interim specification[2] as a guide. The roadway widths used were 24, 36, 48, 60, and 72 ft. For each roadway width, the number of beams was varied, which provided a range in beam spacing from 4 ft. to 10 ft. - 3-1/2 in. For each beam spacing, the length of the bridge was varied from approximately 35 ft. to approximately 135 ft. The slab thickness used for each case was the thickness appropriate for the beam spacing and length, as specified in PennDOT BD-201[8]. The beams for each bridge were selected as the straight strand beams, having the smallest cross-sectional area, which would meet all current design requirements. The consideration of draped-strand beams would have yielded smaller beams in many cases. The use of larger beams in the analysis yielded distribution factors which were slightly larger, and therefore, were on the conservative side. Both PennDOT and AASHTO-PCI prestressed I-beam shapes were used.

Table 1(a) gives the overall scope of the range of the analytical experiment. For each roadway width (W_c), the table indicates the number of beams (N_B), the beam spacing (S), the maximum and minimum lengths (L_{max} and L_{min}), and the number of bridges analyzed.

Table 1(b) demonstrates the scheme used to vary the bridge parameters in the analytic experiment. The table provides a detailed outline of the experiment for all bridges. Each X represents one of the 150 bridges that were designed and analyzed. The table is divided into five broad vertical columns, each representing a roadway width (W_c). Each broad column contains several single columns, each representing a number of beams (N_B), for that width. Each horizontal line in the table represents the S/L ratio indicated in the left column.

5. RESULTS OF THE EXPERIMENT

5.1 General

The design of the analytic experiment to study lateral load distribution was presented in Chapter 4. This chapter presents the procedure in which the results of the bridge analyses were utilized to develop the maximum distribution factors for interior and exterior beams in the 150 bridge superstructures included in the overall investigation. The development of the proposed new specification provisions for live-load distribution is presented in Chapter 6.

Following is a brief outline of the steps leading to the proposed specification provisions:

1. Analyze the bridges listed in Tables 1(a) and 1(b).
2. Obtain influence lines for each beam of each bridge (Sec. 5.2).
3. Calculate the maximum distribution factors for the interior and exterior beams of each bridge, for one loaded lane, two loaded lanes, -- up to the N_B specified in the revised Art. 1.2.6[2].
4. Plot maximum distribution factors versus the S/L ratio, for both interior and exterior girders.
5. Determine new lateral load distribution equations, one for interior and one for exterior girders, by fitting the data plotted in step 4 with appropriate equations.

This chapter provides a description of steps 2-4.

5.2 Development of Influence Lines

The finite element method described in Chapter 2 was the method used to analyze the bridges in the experiment. For each bridge, a single HS20 vehicle was placed in a number of positions across the width, and an analysis was performed for each position. The longitudinal position of the vehicle was always the one that would produce an absolute maximum moment in an analogous single beam of length equal to the span length of the bridge. The bridge was discretized in such a way that the maximum moment was obtained directly in the analysis.

For each position of the vehicle, a moment percentage diagram was obtained, similar to the diagrams shown in Figs. 19-25. The moment percentage diagrams were then used to produce the influence lines for each beam. The influence line for a particular beam is a plot of the moment percentage for that beam, as a function of the lateral location of the center of the design vehicle. A series of influence lines representing all of the beams in one of the bridges (W = 48 ft., S = 8 ft., L = 96 ft.) is shown in Figs. 26-29. These influence lines were then used to produce two distribution factors, one for the exterior beam (Beam 1) and one for the interior beams (taken as the maximum value developed in Beam 2, 3, or 4). Each of the 150 bridges was analyzed in this manner.

5.3 Determination of Maximum Distribution Factors

The widths of the bridges analyzed (24, 36, 48, 60, and 72 ft.) were chosen as multiples of the 12 ft. wide design traffic

lanes specified in Art. 1.2.6[2]. Since any bridge with $24 \leq W < 36$ would be considered as a two-lane bridge, bridges with $W = 24$ and 36 ft. were analyzed with two design traffic lanes to represent the two extremes for two-lane bridges. Likewise, since any bridge with $36 \leq W < 48$ would be considered as a three-lane bridge, bridges with $W = 36$ and 48 ft. were analyzed with three design traffic lanes. This process was continued with analyses of bridges with $W = 48$ ft. as a four-lane bridge; of bridges with $W = 60$ ft. as four-lane and five-lane bridges; and of bridges with $W = 72$ ft. as five-lane and six-lane bridges.

As an illustration of the determination of maximum distribution factors, consider the analysis of the bridge shown in Figs. 26-29. This bridge has a roadway width of 48 ft., which is the minimum width for four 12 ft. wide design traffic lanes. The width of 48 ft. also represents the maximum width for three design traffic lanes.

In the analysis, the bridge was first considered as a three-lane structure. For the exterior beam (Beam 1, represented by the influence line in Fig. 26), a design vehicle was placed in each of the three design traffic lanes. The lanes were then positioned across the width, and the vehicles were positioned within the lanes, to produce the maximum positive moment percentage. For this exterior beam, only two lanes were loaded to produce the maximum positive value. Since the influence line indicates negative ordinates over the right portion of the roadway, only two vehicles, appropriately placed within two lanes crowded to the left side of the roadway, would produce a maximum

positive moment in the exterior beam. The sum of the two ordinates was then multiplied by two to yield the maximum distribution factor for the exterior beams in this bridge. The reason for the multiplication by two was to produce a distribution factor which would be applied to a single longitudinal line of wheel loads. Since the moment percentages were developed considering truck loadings (which consist of two longitudinal lines of wheel loads), the multiplication by two was appropriate.

To develop a distribution factor for interior beams (Beams 2, 3, and 4, represented by the influence lines in Figs. 27-29), the process described in the previous paragraph was repeated for each of the three interior beams.

The distribution factors for the three beams were then compared, and the maximum value was taken as the distribution factor for the interior beams in the bridge - for the three-lane case. For the four-lane case, the entire process was repeated, again yielding one distribution factor for exterior beams and one factor for interior beams.

The bridge cross-section, used in the previous illustration with a span length of 80 ft., had a roadway width of 48 ft. and was supported by seven beams spaced at 8.00 ft. This same bridge cross-section was analyzed with six other span lengths, ranging from 32 ft. to 120 ft., representing S/L ratios ranging from 1/4 to 1/15. These analyses represent seven of the 150 bridge superstructures included in the overall investigation.

5.4 Presentation of Results

The maximum distribution factors derived from the analyses of the 150 bridge superstructures were plotted as a function of the ratio of the beam spacing to span length, S/L. The plots are presented in Figs. 30-43. Figures 30-34 represent the interior beams of bridges with the five widths W = 24, 36, 48, 60, and 72 ft., loaded with 2, 3, 4, 5, and 6 design lanes, respectively. Figures 35-39 represent the exterior beams of the same bridges, loaded with the same design lanes. Figures 40-43 represent the interior beams of bridges with W = 36, 48, 60, and 72 ft., loaded with 2, 3, 4, and 5 design lanes, respectively. It would appear that there should be an additional four figures, representing the exterior beams of the combination of bridges and design loadings on which Figs. 40-43 are based. However, the analyses of bridges with W = 36, 48, 60, and 72 ft., loaded with 2, 3, 4, and 5 design lanes yielded results identical to the results obtained from analyses of the same bridges loaded with 3, 4, 5, and 6 design lanes. These identical results can be explained by referring back to the discussion presented in the third paragraph of Art. 5.3. That discussion described the analysis used to develop the maximum distribution factor for the exterior beams in a bridge with W = 48 ft., loaded with three design lanes. It was explained that because of the negative-ordinate portion of the influence line (Fig. 26), only two design lanes were used to develop the maximum distribution factor. Therefore, when the same bridge was considered as a four-lane bridge, again, only two design lanes were required to develop the maximum distribution factor.

This phenomenon for exterior beams was consistent throughout the entire range of bridges analyzed with the two load conditions.

The following summary relates Figs. 30-43 to the appropriate roadway width and number of design traffic lanes.

Interior Beam Fig. No.	Exterior Beam Fig. No.	W (ft.)	No. of Design Traffic Lanes
30	35	24	2
40	--	36	2
31	36	36	3
41	--	48	3
32	37	48	4
42	--	60	4
33	38	60	5
43	--	72	5
34	39	72	6

6. PROPOSED SPECIFICATION PROVISIONS

6.1 Current Design Provisions

The current provisions for determining live-load bending moments in the longitudinal beams in beam-slab type highway bridges are set forth in Art. 1.3.1(B) of the 1973 AASHTO Specification[1]. For interior beams, the live-load bending moments are determined by applying factored design-vehicle wheel loads to the beam. For prestressed concrete I-beams, the factor (D.F.) applied to each wheel is given by:

$$D.F. = \frac{S}{5.5}$$

where S is the average beam spacing, in feet. For exterior beams, the loading is determined by applying to the beam the reactions produced by the individual wheel loads, considering the floor slab to act as a simple span between beams.

6.2 Development of Proposed Design Provisions

In the analysis described in Chapters 4 and 5, a total of 24 different cross-sections were analyzed, each with six or seven span lengths in the approximate range 35 to 125 feet. A typical plot of the distribution factor for interior beams, as a function of the ratio S/L, is shown in Fig. 44. This plot is representative of the 45 plots included in Figs. 30-34 and Figs. 40-43. The problem was to generate a single equation which would represent all of the 45 plots. The form of the equation was selected as:

$$D.F. = \frac{2N_L}{N_B} + k_1 \left(\frac{S}{L}\right)^n \qquad (6.1)$$

where N_L = number of design traffic lanes

$= \frac{W}{12}$, reduced to nearest whole number

N_B = number of beams

S = beam spacing, in ft.

L = span length, in ft.

W = roadway width (curb-to-curb), in ft.

This form was chosen to match the form of the equation for interior beams in prestressed concrete spread box-beam bridges, as set forth in Art. 1.6.24[1]. Based on an extensive analysis of the results, the terms k_1 and n were established as:

$$k_1 = \frac{1}{9}\left(\frac{W}{N_B}\right)\left(\frac{W}{12N_L}\right)^{\frac{3}{2}}$$

$$n = \frac{1}{3}$$

Plots of the distribution factors (D.F.) yielded by Eq. 6.1 are shown in Figs. 30-34 and Figs. 40-43.

For exterior beams, it was found that an equation of the same general form could be used. However, one modification was necessary - the addition of another term, k_2 - resulting in the following equation:

$$D.F. = \frac{2N_L}{N_B} + k_1 \left(\frac{S}{L}\right)^n + k_2 \qquad (6.2)$$

A typical plot of the distribution factor for exterior beams, as a function of the ratio S/L, is shown in Fig. 45, along with a typical plot of Eq. 6.2. For exterior beams, the terms k_1, k_2, and n were established as follows:

$$k_1 = -\frac{1}{11}\left(\frac{W_o}{N_B}\right)$$

$$k_2 = \frac{2}{5N_L}$$

$$n = \frac{1}{3}$$

where $W_o = 12\ N_L$, in ft.

Although the form of the equations for exterior and interior beams is the same, there is a basic difference in the use of the equations. For the interior beams, Eq. 6.2 can be used directly for any roadway width (W) in the range 24-72 ft. However, for the exterior beams, Eq. 6.2 can be used directly only for roadway widths (W_o) which are multiples of 12 ft., in the range 24-72 ft. Then, to obtain the distribution factor for exterior beams with $12\ N_L < W < 12\ (N_L + 1)$, a linear interpolation is made between values of D.F. computed from Eq. 6.2 with $W_o = 12\ N_L$ and $W_o = 12\ (N_L + 1)$.

The following example will illustrate the use of Eqs. 6.1 and 6.2 in determing the distribution factors for interior and exterior beams in a given bridge. The bridge has the following characteristics

W = 32 ft. S = 8 ft.

L = 80 ft. N_B = 5

With five beams ($N_B = 5$), the beam spacing (S) would be 8 ft., assuming that the center of the exterior beam is directly under the face of the curb. With W = 32 ft., $\frac{W}{12} = 2.67$; therefore $N_L = 2$

For the interior beam (Eq. 6.1):

$$D.F. = \frac{2(2)}{(5)} + \frac{1}{9}\frac{(32)}{(5)}\left(\frac{32}{12(2)}\right)^{\frac{3}{2}}\left(\frac{8}{80}\right)^{\frac{1}{3}}$$

$$= 1.308$$

For the exterior beam, since W lies between $12\ N_L = 24$ ft. and $12\ (N_L + 1) = 36$ ft., Eq. 6.2 is used to compute the D.F. for $W_o = 24$ ft. and $W_o = 36$ ft. For $W_o = 24$ ft., $N_L = 2$, and for $N_B = 5$, S would be 6 ft. Equation 6.2 would yield:

$$(D.F.)_{24} = \frac{2(2)}{(5)} - \frac{1}{11}\frac{(24)}{(5)}\left(\frac{6}{80}\right)^{\frac{1}{3}} + \frac{2}{5(2)}$$

$$= 0.816$$

For $W_o = 36$ ft., $N_L = 3$, and for $N_B = 5$, S would be 9 ft., Eq. 6.2 would yield:

$$(D.F.)_{36} = \frac{2(3)}{(5)} - \frac{1}{11}\frac{(36)}{(5)}\left(\frac{9}{80}\right)^{\frac{1}{3}} + \frac{2}{5(3)}$$

$$= 1.017$$

Then, to determine the D.F. for W = 32 ft., a linear interpolation is made:

$$(D.F.)_{32} = 0.816 + \frac{8}{12}(1.017 - 0.816)$$

$$= 0.950$$

6.3 Accuracy of Proposed Equations

To assess the accuracy of the proposed equations for distribution factors (Eqs. 6.1 and 6.2), a statistical analysis was performed. For each of the structures analyzed, the ratio $(D.F.)_E/(D.F.)_A$ was computed, where $(D.F.)_E$ is the distribution factor yielded by the appropriate proposed equation (6.1 or 6.2), and $(D.F.)_A$ is the distribution factor determined from the computer analysis of the structure. From the analysis of the 150 superstructures, many under two loading conditions, 281 comparisons were made for the interior beams and 150 comparisons for the exterior beams.

For the interior beams, the arithmetic mean of the ratios was 0.996, with a standard deviation of 0.036. Assuming a normal distribution, this would indicate that 68.3% of the values would fall in the range 1.032 and 0.960, and 99.7% of the values would fall in the range 1.104 and 0.888.

A similar analysis was used to compare values yielded by the current specification (D.F. = S/5.5) with values determined from the computer analysis. The statistical analysis of the resulting values of $(D.F.)_E/(D.F.)_A$ resulted in an arithmetic mean of 0.971, and a standard deviation of 0.070. This indicates that 99.7% of the values would fall in the range 1.181 and 0.761.

For the exterior beams, the statistical analysis based on the proposed equation (Eq. 6.2) yielded an arithmetic mean of 1.011, with a standard deviation of 0.036. Therefore, 99.7% of the values would fall

in the range 1.119 and 0.903. No comparison was made to evaluate the current specification provision for exterior beams.

To illustrate the difference between the proposed equations and the current specification provisions, Fig. 46 was prepared. This illustration is intended to indicate the variation in distribution factors for a 5-beam bridge, as a function of roadway width and span length, and was not chosen to indicate maximum differences between the proposed and current provisions. In this particular illustration, it is evident that the current and proposed specifications for interior beams are nearly identical only for L = 50 ft. and for 36 ft. $< W_c <$ 44 ft. Otherwise, in this example, the current provisions consistently yield greater values than the proposed equation for interior beams. The reverse is true for exterior beams.

6.4 Proposed Specification Provisions

Based on the analyses presented in this report, the following new specification provisions are proposed for the evaluation of live load distribution factors in beam-slab highway bridge superstructures supported by prestressed concrete I-beams. These new provisions would replace the current provisions which are set forth in Art. 1.3.1(B) of the 1973 AASHTO Specification[1]. The proposed new provisions are stated as follows:

Interior Beams

The live load bending moment for each interior beam shall be determined by applying to the beam the fraction (D.F.) of the wheel load (both front and rear) determined by the following equation:

$$D.F. = \frac{2N_L}{N_B} + k_1 \left(\frac{S}{L}\right)^{\frac{1}{3}}$$

where $$k_1 = \frac{1}{9}\left(\frac{W}{N_B}\right)\left(\frac{W}{12N_L}\right)^{\frac{3}{2}}$$

N_L = number of design traffic lanes

$= \frac{W}{12}$, reduced to nearest whole number

N_B = number of beams $(3 \leq N_B \leq 17)$

S = beam spacing, in feet $(4 \leq S \leq 11)$

L = span length, in feet $(30 \leq L \leq 135)$

W = roadway width between curbs, in feet $(24 \leq W \leq 72)$

Exterior Beams

The live load bending moment for each exterior beam shall be determined by applying to the beam the fraction (D.F.) of the wheel load (both front and rear) obtained by use of the following equation. For roadway widths (W) which are multiples of 12, the equation yields the value of D.F. directly. For widths $12N_L < W < 12(N_L + 1)$, determine D.F. for $W_o = 12N_L$ and for $W_o = 12(N_L + 1)$, then linearly interpolate between the two values to determine D.F. for W.

$$D.F. = \frac{2N_L}{N_B} + k_1 \left(\frac{S}{L} \right)^{\frac{1}{3}} + k_2$$

where $k_1 = -\frac{1}{11}\left(\frac{W_o}{N_B} \right)$

$k_2 = \frac{2}{5N_L}$

$W_o = 12N_L$; in feet

N_L, N_B, S, and L are defined under Interior Beams

7. SUMMARY AND RECOMMENDATION

This report describes the development of new specification provisions for the evaluation of live-load distribution factors in beam-slab highway bridge superstructures supported by prestressed concrete I-beams.

Initially, a structural analysis based on the finite element method was developed to evaluate the response of the superstructures to design-vehicle loading. The analysis was then refined and verified through comparison with results from previous field tests of two in-service bridges. Next, an analytic experiment was designed to study the effects of various parameters on live-load distribution. In the experiment, 150 superstructures were analyzed under numerous loading conditions. The results from the analyses provided the data base which was then utilized in the development of two equations. The equations, one for interior beams and the other for exterior beams, yield the distribution factors needed in the design of bridge superstructures. Finally, a statistical analysis was made of comparisons of values yielded by the structural analyses (1) with values from the equations, and (2) with values based on the current specification provisions.

Based on the results from this study, the proposed new specification provisions for live-load distribution, as presented in Chapter 6, are recommended for adoption. The proposed provisions are relatively simple in form and clearly yield more accurate values than those based on the current provisions.

8. ACKNOWLEDGMENTS

This study was conducted in the Department of Civil Engineering and Fritz Engineering Laboratory, under the auspices of the Lehigh University Office of Research, as a part of the research investigation entitled "Development and Refinement of Load Distribution Provisions for Prestressed Concrete Beam-Slab Bridges" sponsored by the Pennsylvania Department of Transportation; the U. S. Department of Transportation, Federal Highway Administration; and the Reinforced Concrete Research Council.

The basic research planning and administrative coordination in this investigation were in cooperation with the following individuals representing the Pennsylvania Department of Transportation: B. F. Kotalik, Chief Bridge Engineer; H. P. Koretzky, and Hans Streibel, all from the Bridge Division; and K. L. Heilman, Research Coordinator; all from the Bureau of Materials, Testing, and Research.

The following members of the staff at Lehigh University made significant contributions: E. S. deCastro and W. S. Peterson in the programming and execution of the computer analysis, and S. Tumminelli in the review of parts of this report.

9. TABLES

TABLE 1(a) BRIDGES ANALYZED

Roadway Width W_c ft.	No. of Beams N_B	Beam Spacing S ft.	Span Length		Number of Bridges
			L_{max} ft.	L_{min} ft.	
24	4	8.00	120.0	32.0	6
	5	6.00	120.0	36.0	7
	6	4.80	120.0	38.4	6
36	5	9.00	108.0	36.0	6
	6	7.20	108.0	36.0	6
	7	6.00	105.0	36.0	6
	8	5.14	128.6	36.0	7
	9	4.50	135.0	36.0	7
48	6	9.60	115.2	38.4	6
	7	8.00	120.0	32.0	7
	8	6.86	120.0	41.1	6
	9	6.00	120.0	36.0	7
	11	4.80	120.0	38.4	6
60	7	10.00	100.0	30.0	6
	8	8.57	102.9	34.3	6
	9	7.50	112.5	37.5	6
	11	6.00	105.0	36.0	6
	13	5.00	125.0	35.0	7
72	8	10.29	102.9	30.9	6
	9	4.00	108.0	36.0	6
	10	8.00	120.0	32.0	6
	12	6.55	114.5	34.3	6
	14	5.54	110.8	38.8	6
	16	4.80	120.0	38.4	6
				Total	150

TABLE 1(b) BRIDGES ANALYZED

S/L	W_c, ft.																							
	24			36					48					60					72						
	N_B																							
	4	5	6	5	6	7	8	9	6	7	8	9	11	7	8	9	11	13	8	9	10	12	14	16
1/30								X																
1/25			X				X	X					X					X						X
1/20		X	X				X	X				X	X					X					X	X
1/17.5		X	X			X	X	X			X	X	X				X	X				X	X	X
1/15	X	X			X	X	X			X	X	X				X	X	X			X	X	X	
1/12	X		X	X	X	X		X	X	X	X	X	X		X	X	X			X	X	X	X	X
1/10		X	X	X	X		X	X	X	X	X		X	X	X	X		X	X	X		X		X
1/8	X	X	X	X		X	X	X	X	X		X	X	X	X	X	X	X	X	X	X		X	X
1/7		X			X	X	X		X		X	X		X	X		X	X	X			X	X	
1/6	X	X		X	X	X				X	X	X		X		X	X			X	X	X		
1/5	X			X	X				X	X					X	X			X	X	X			
1/4	X			X					X	X				X	X				X	X	X			
1/3														X					X					

10. FIGURES

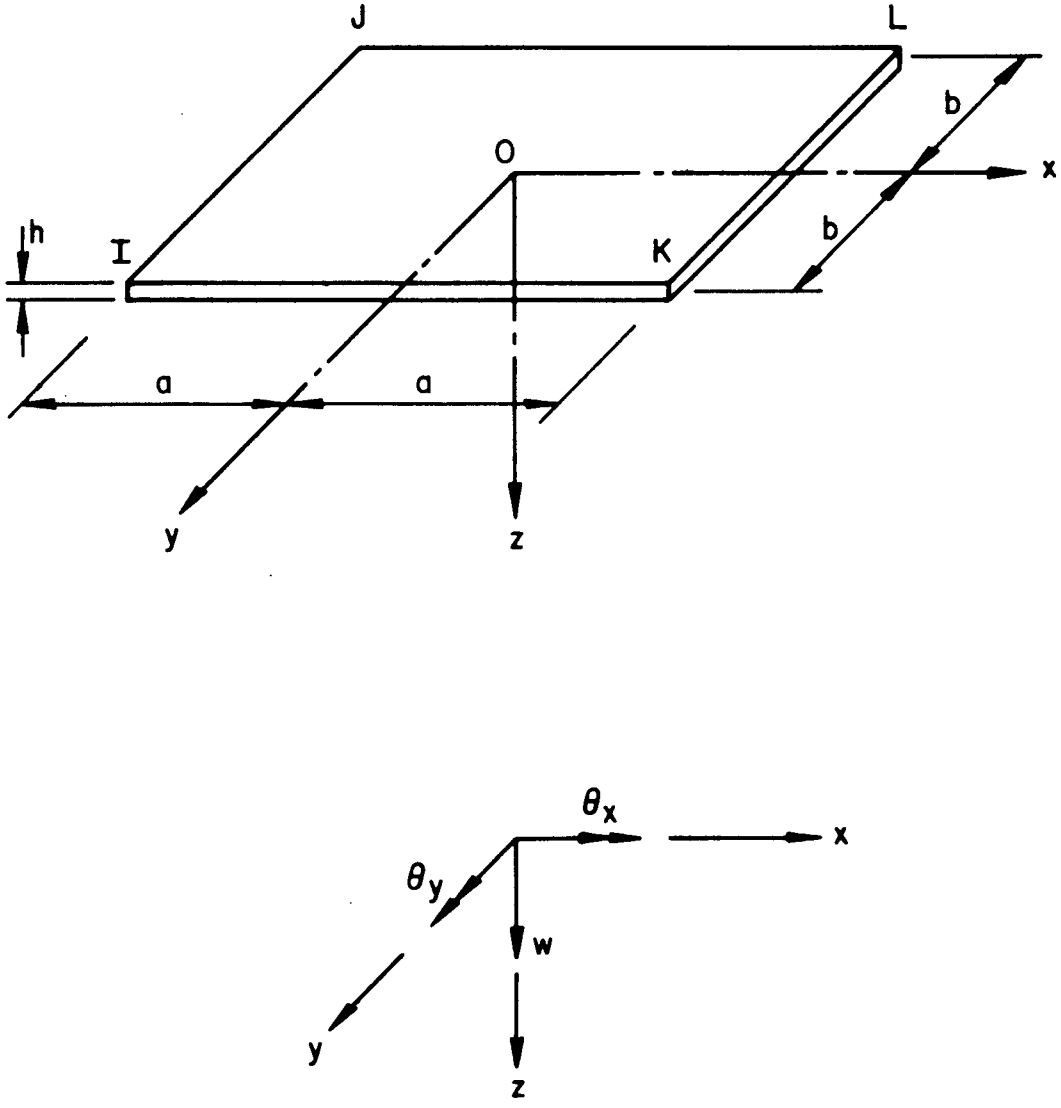

Fig. 1 Rectangular Plate Element and Basic Displacement Components

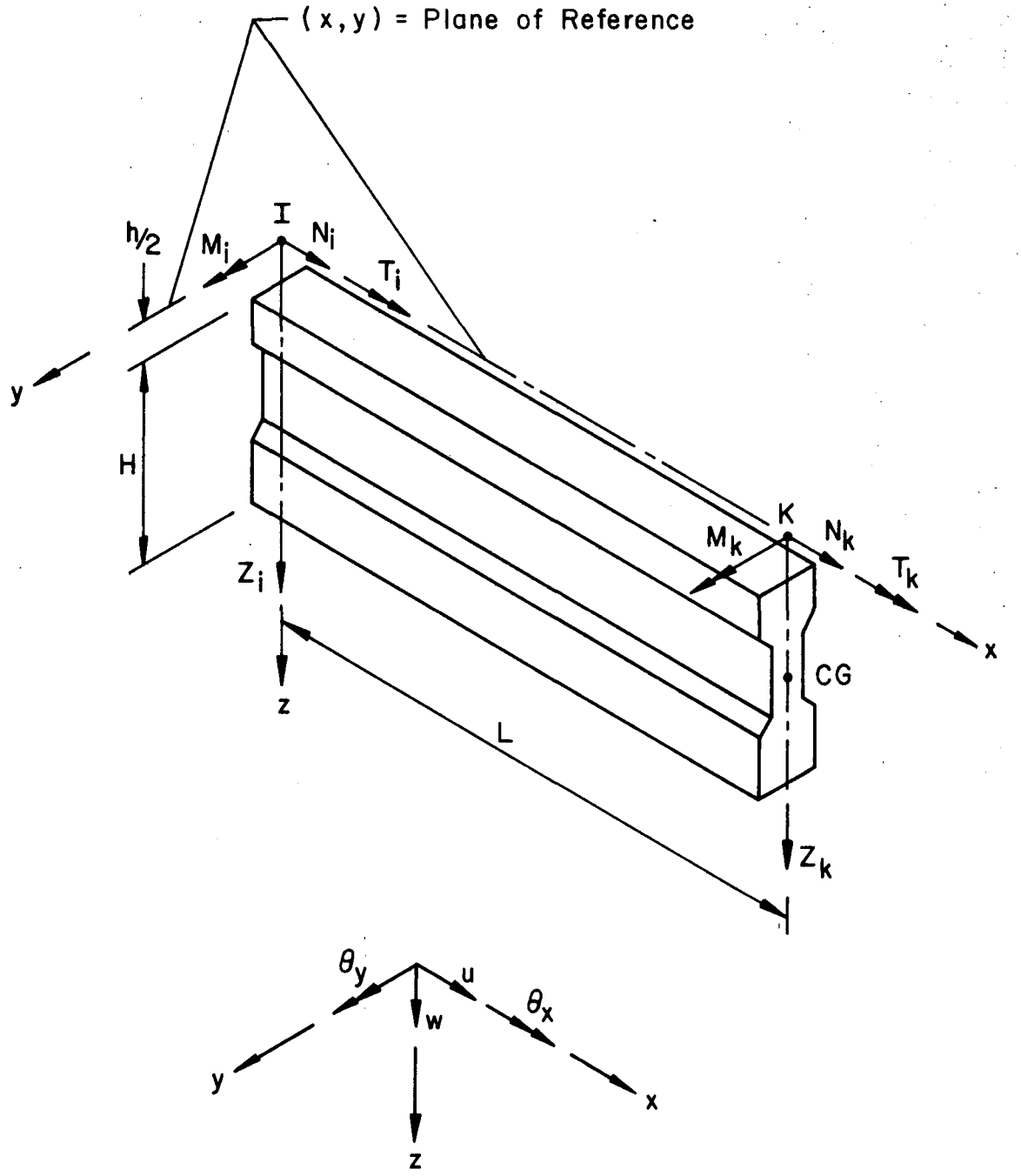

Fig. 2 Eccentrically Attached Beam Element

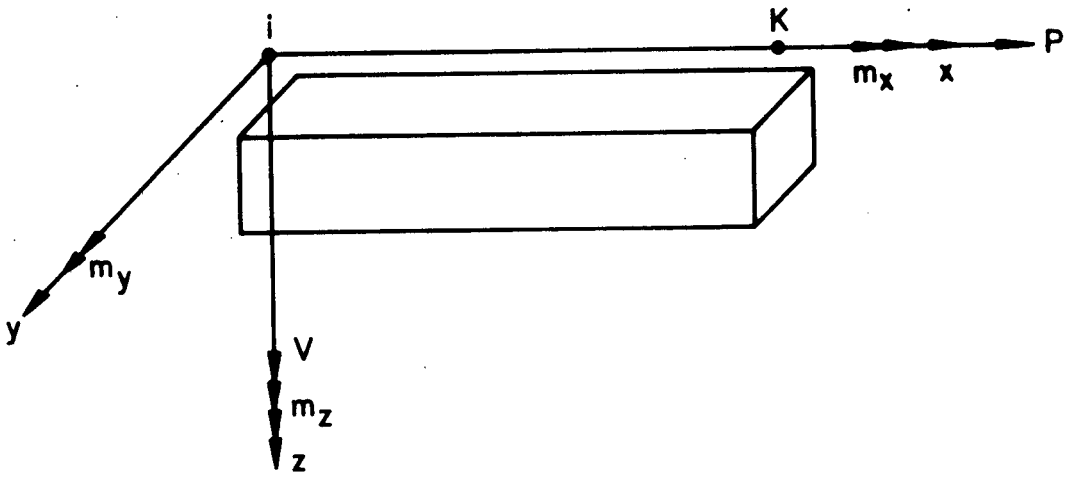

Fig. 3(a) Coordinate System and Positive Sign Convention

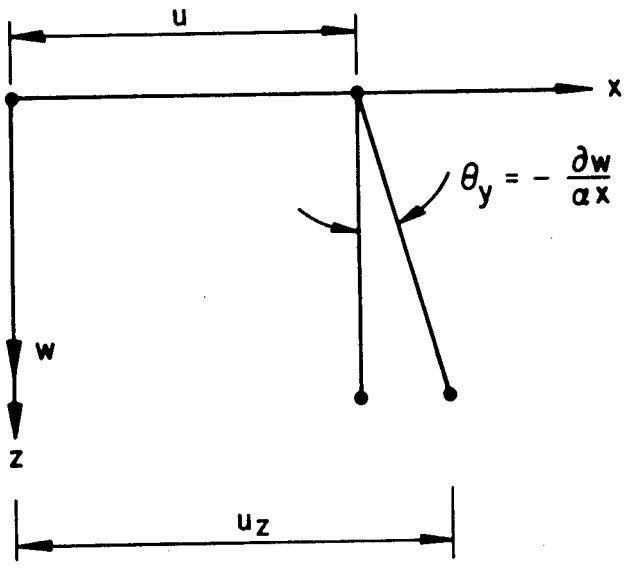

Fig. 3(b) Coordinate System and Generalized Displacements

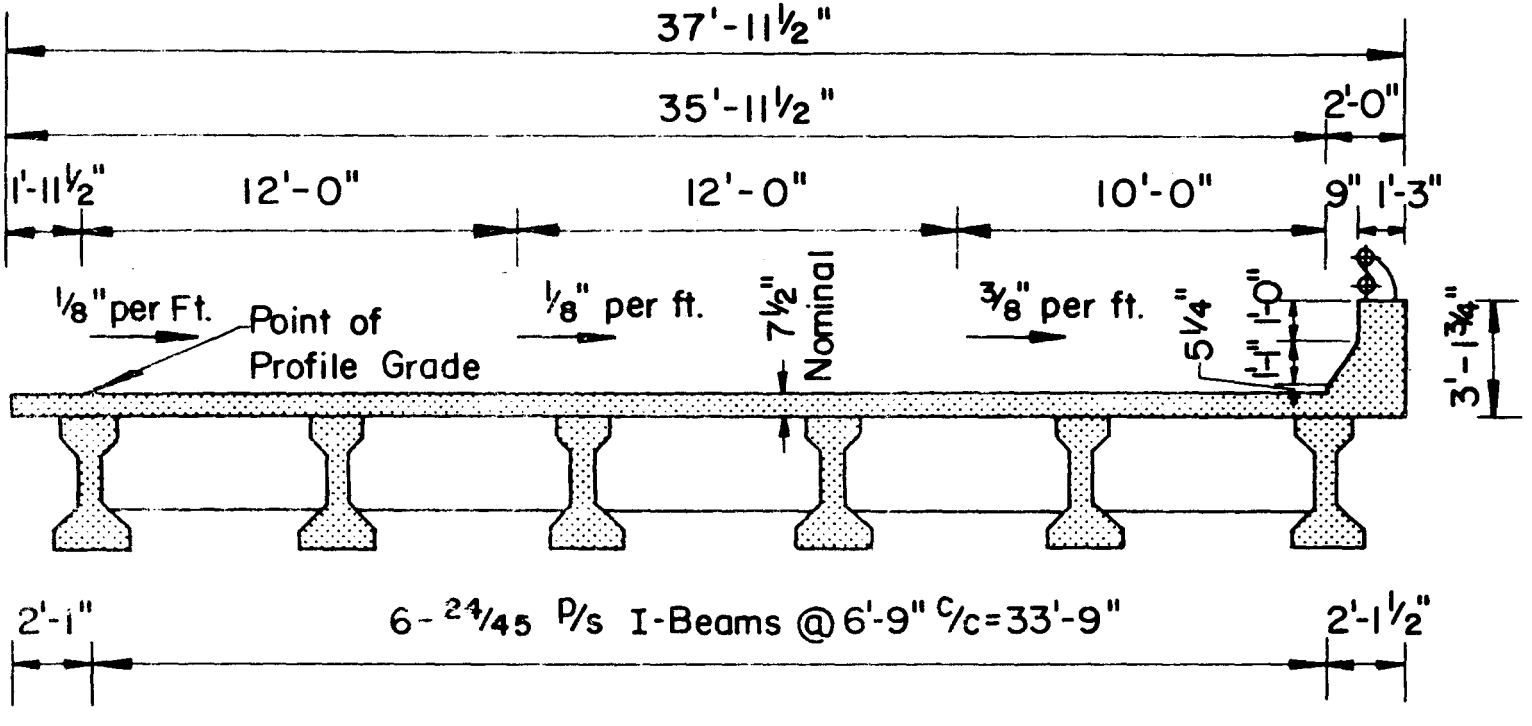

Fig. 4 Cross-section of Lehighton Bridge

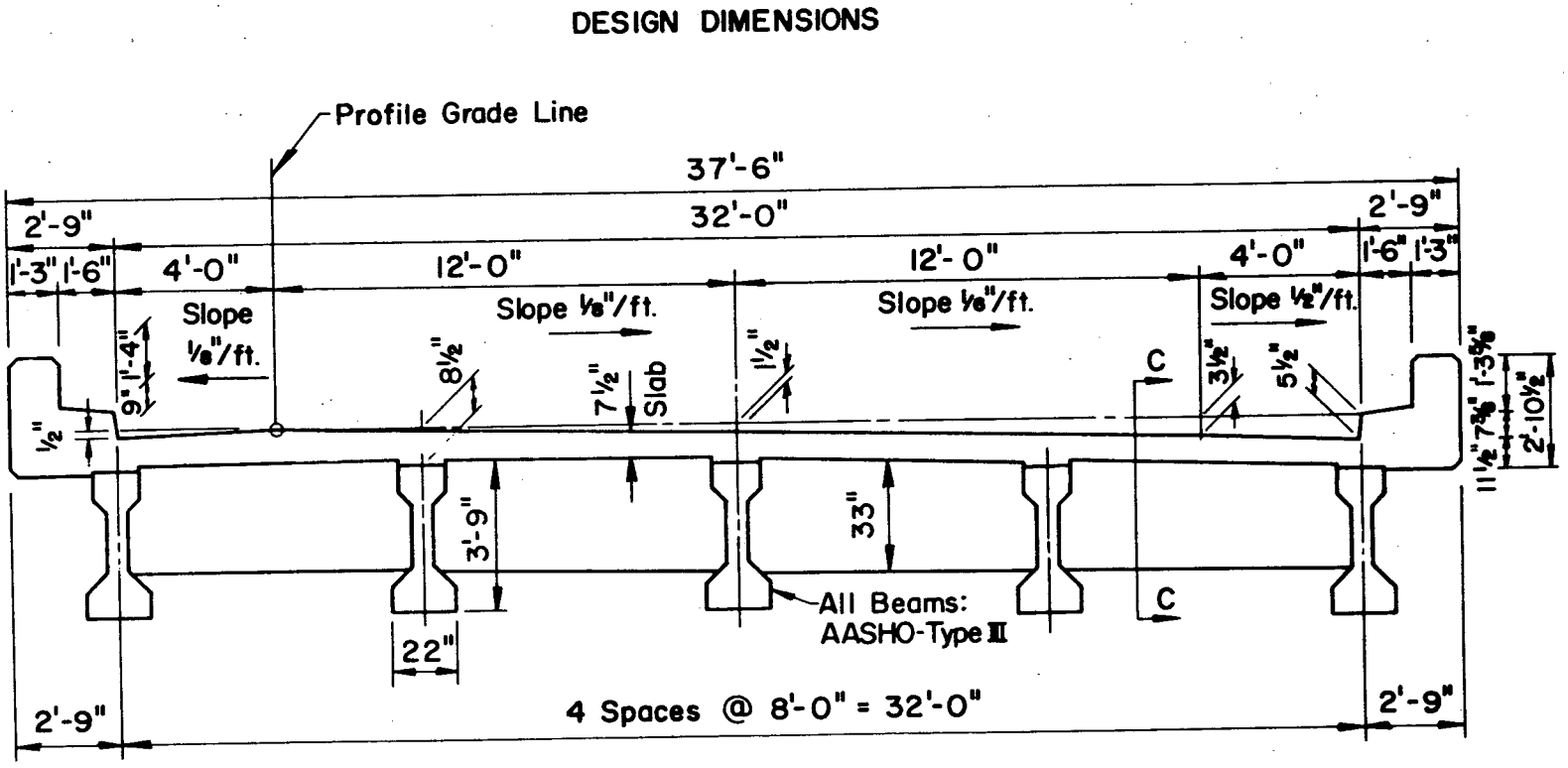

Fig. 5 Cross-section of Bartonsville Bridge

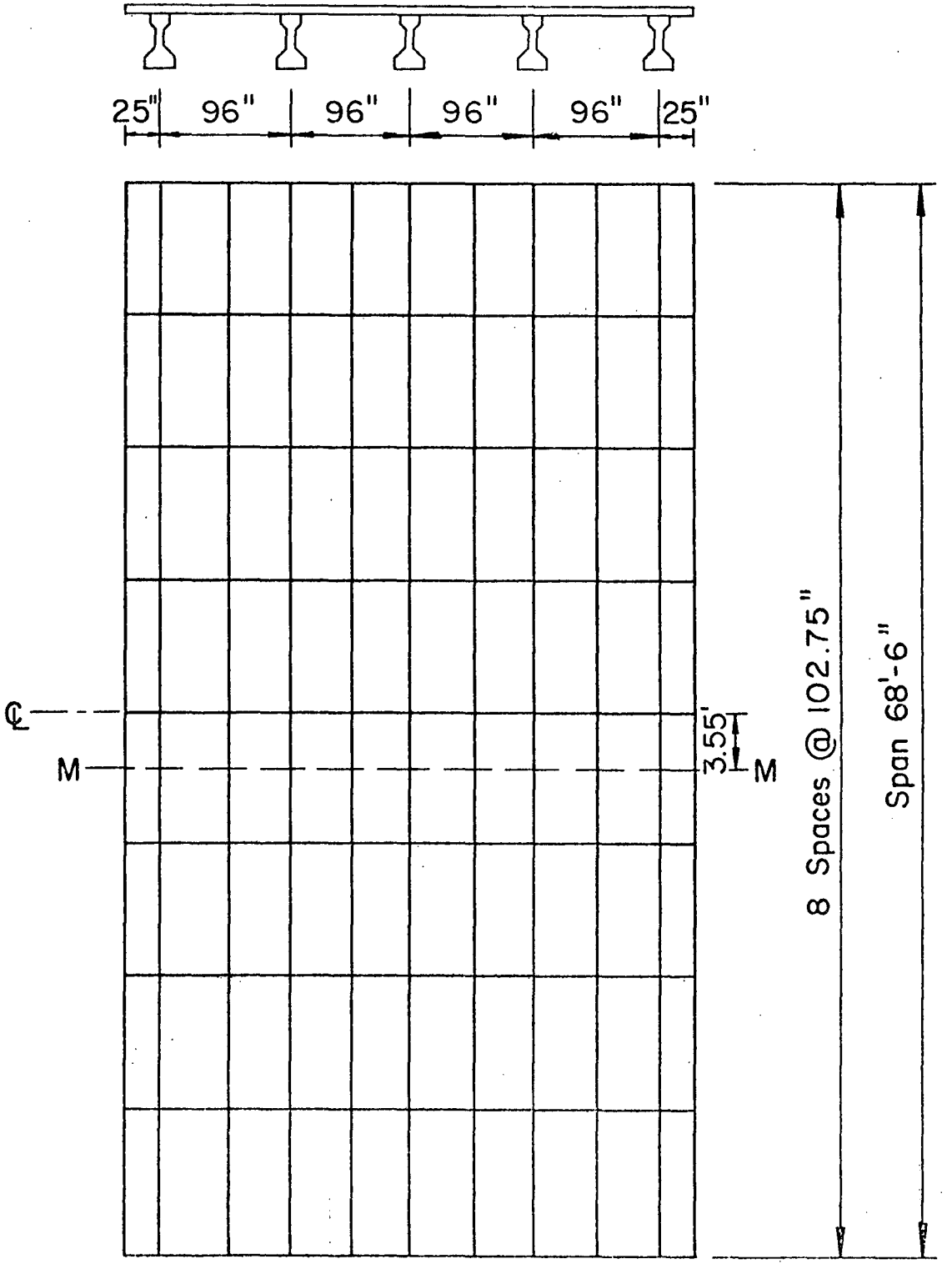

Fig. 6 Discretization of Bartonsville Bridge

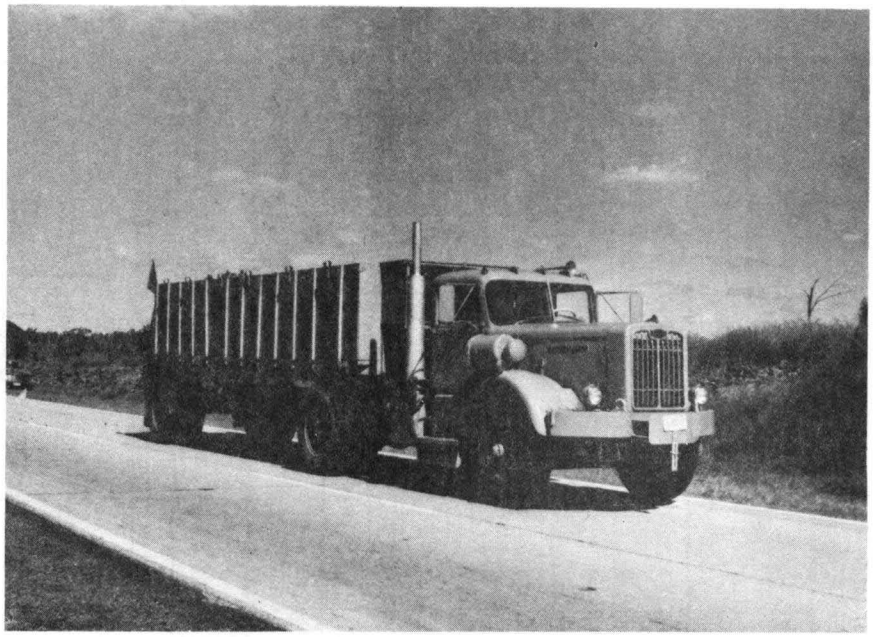

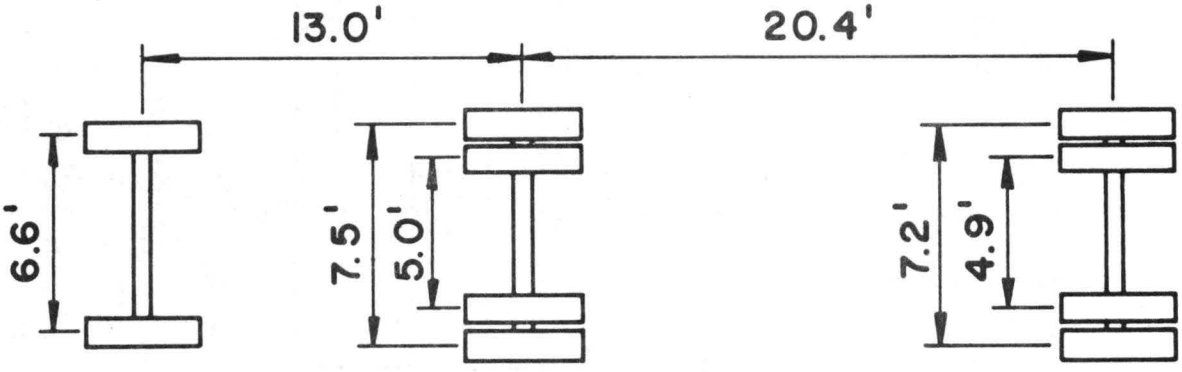

AXLE AND WHEEL SPACING

FRONT	DRIVE	REAR
↓	↓	↓
10.36k	32.20k	32.20k

AXLE LOADS

Fig. 7 Test Vehicle

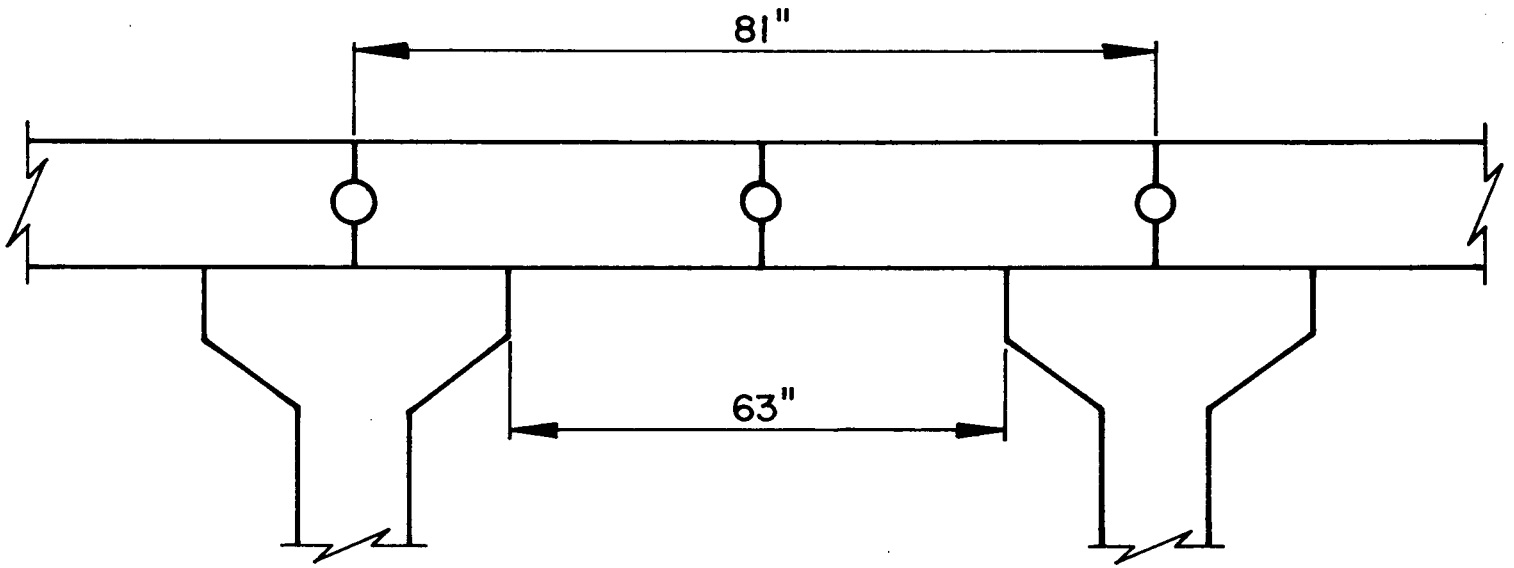

Fig. 8 2 PL Mesh Discretization and Orthotropy Factor for Lehighton Bridge

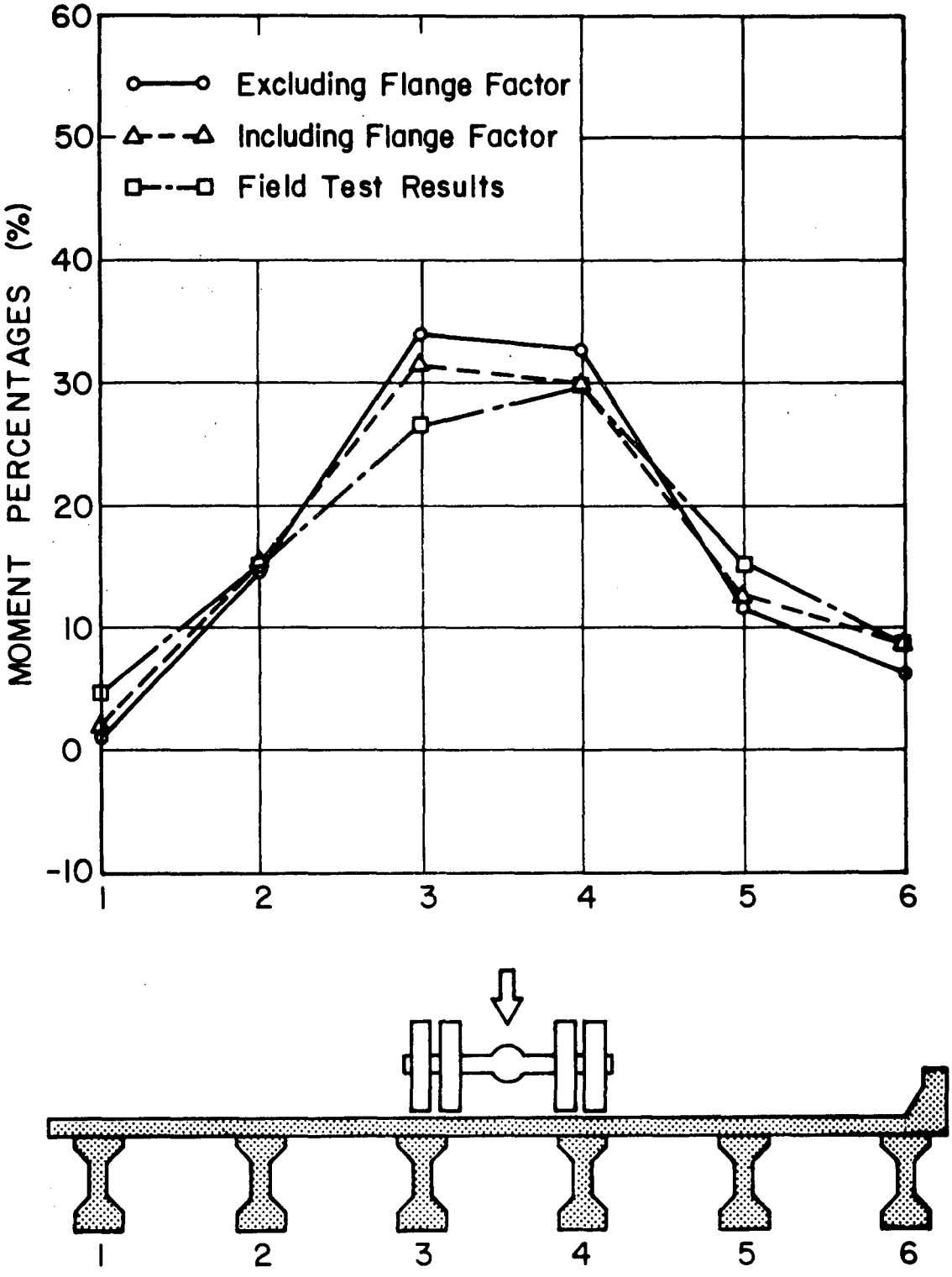

Fig. 9 Comparison of Moment Percentages Derived From Analyses and Field Test Results

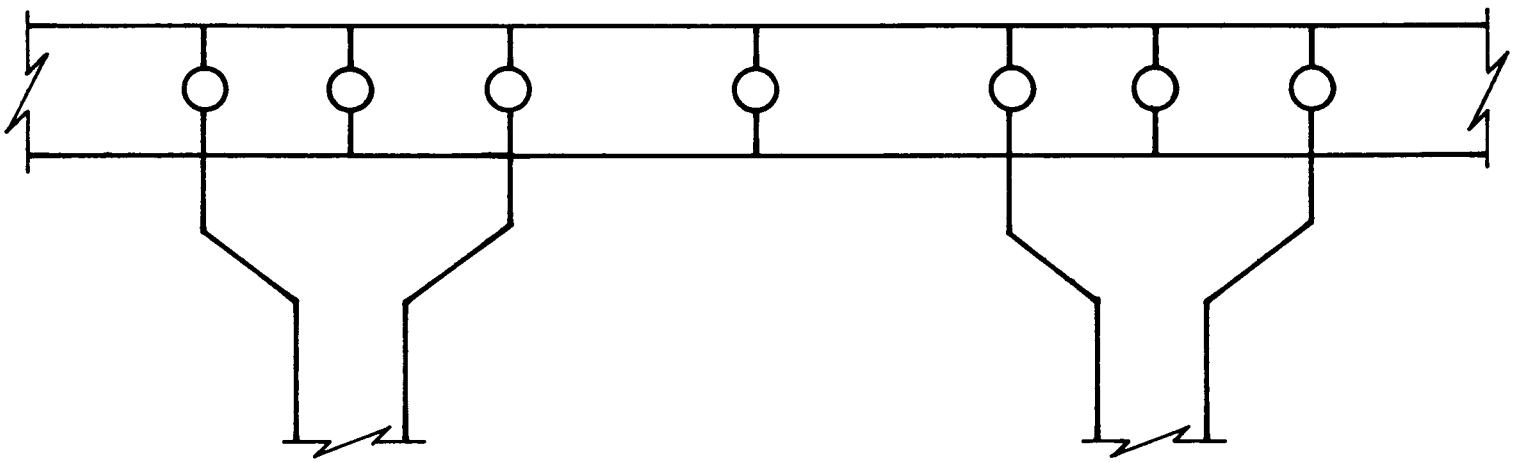

Slab Elements Over Flanges $D_Y = 100.0$

Slab Elements Between Beams $D_Y = 1.0$

Fig. 10 4 PL Mesh Discretization and Orthotropy Factors

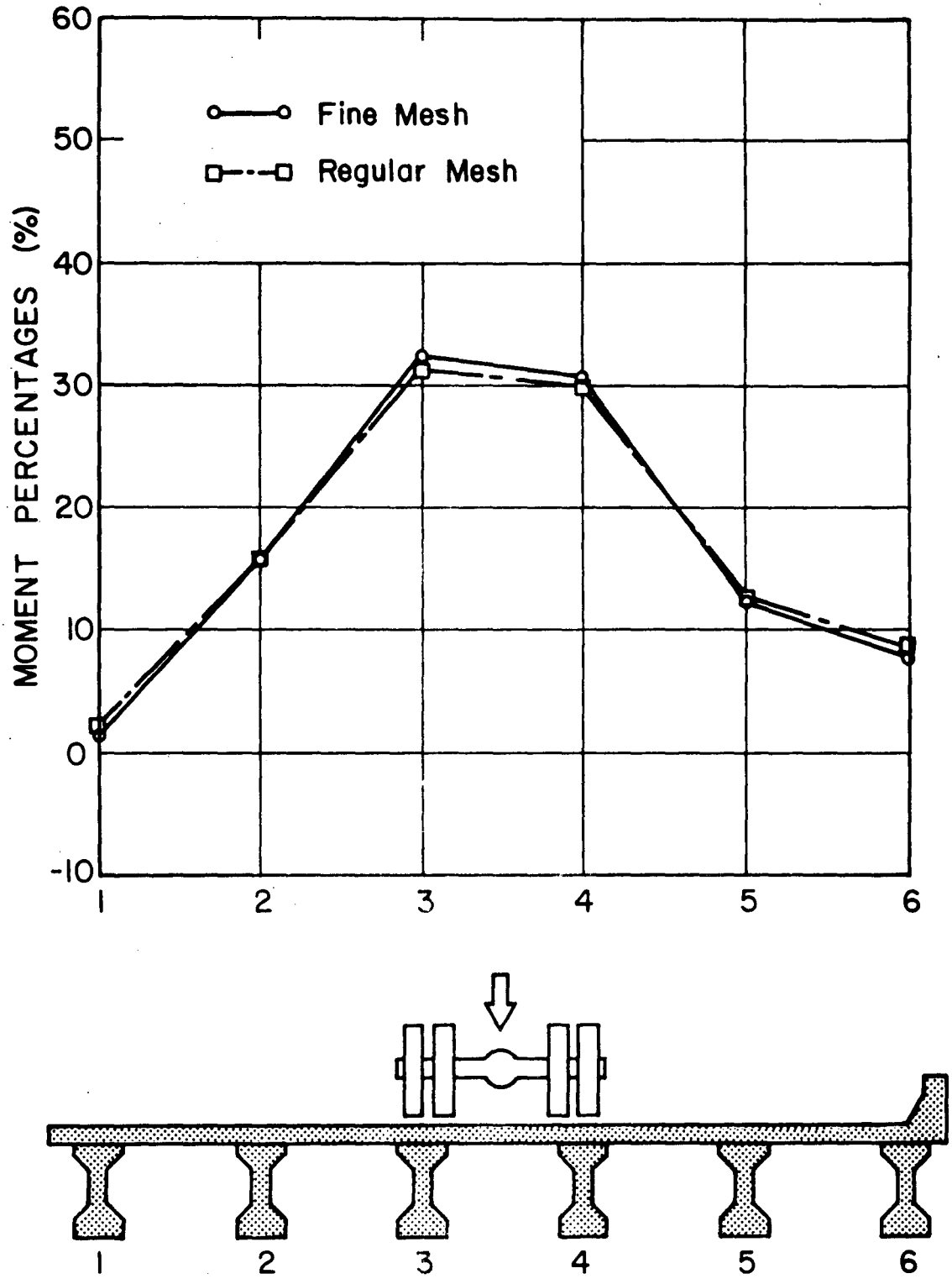

Fig. 11 Comparison of Moment Percentages Derived from Analysis Using 2 PL Mesh and 4 PL Mesh

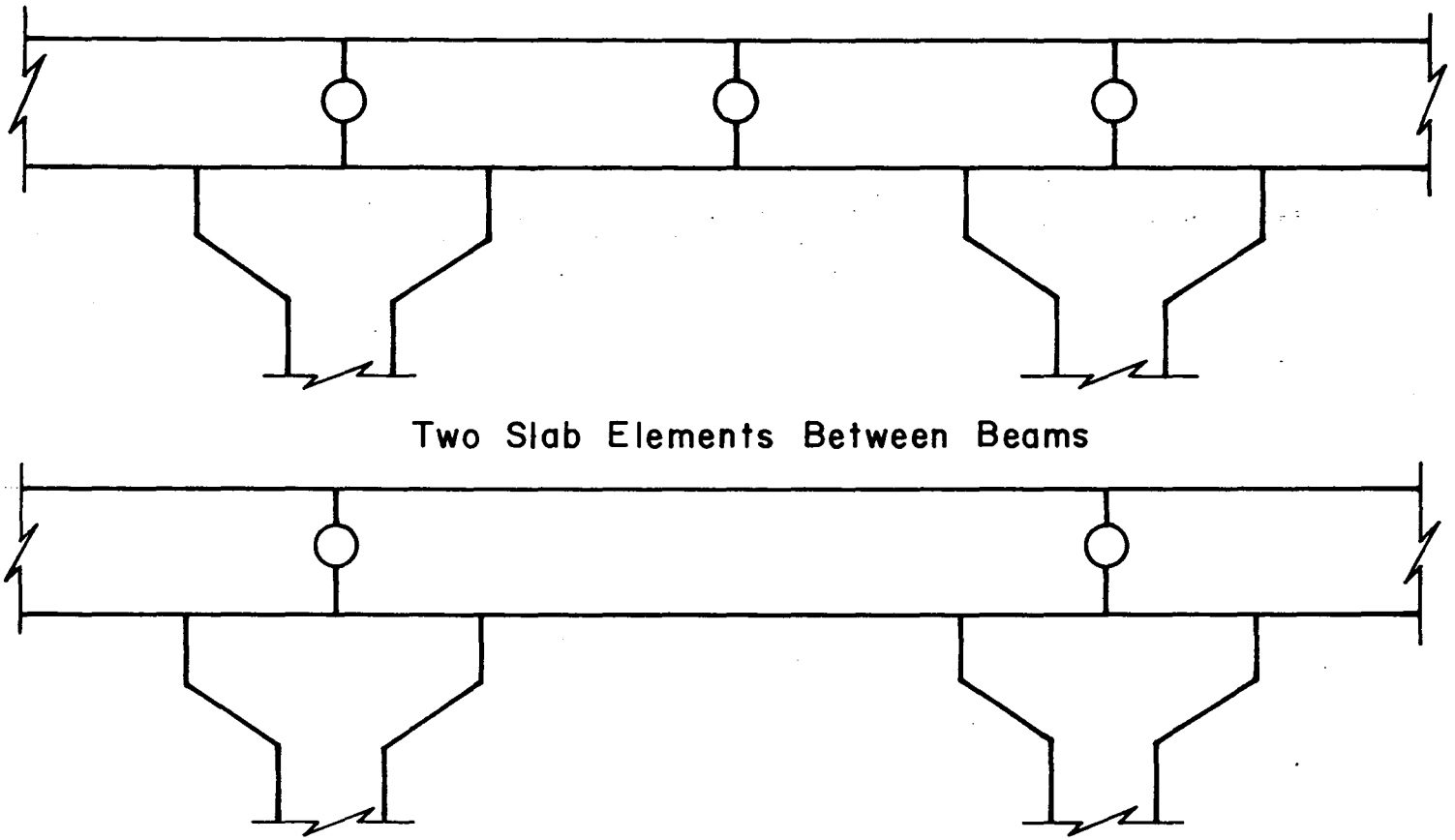

Fig. 12 2 PL and 1 PL Mesh Discretization

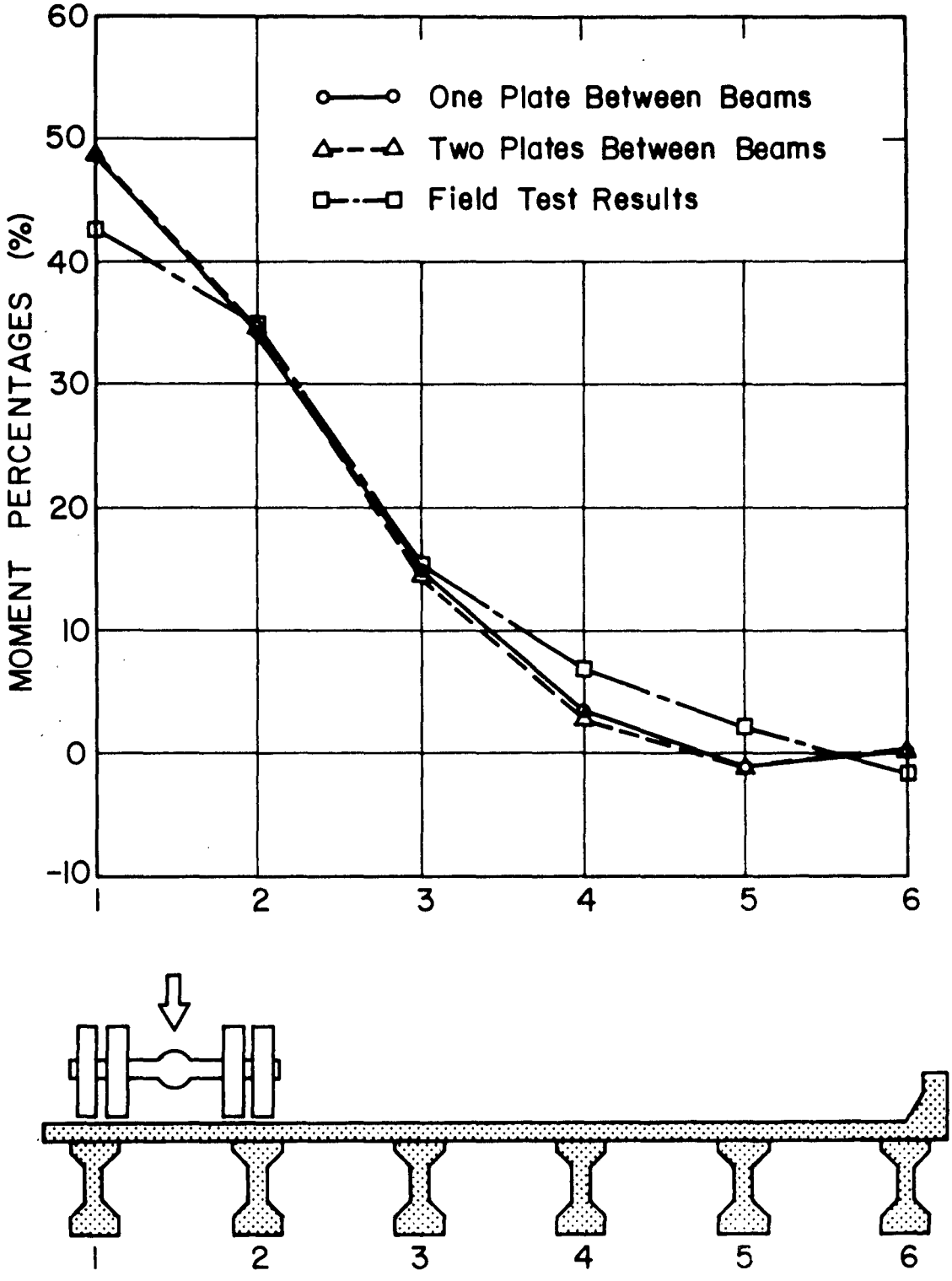

Fig. 13 Comparison of Moment Percentages Derived from Analyses and Field Test Results

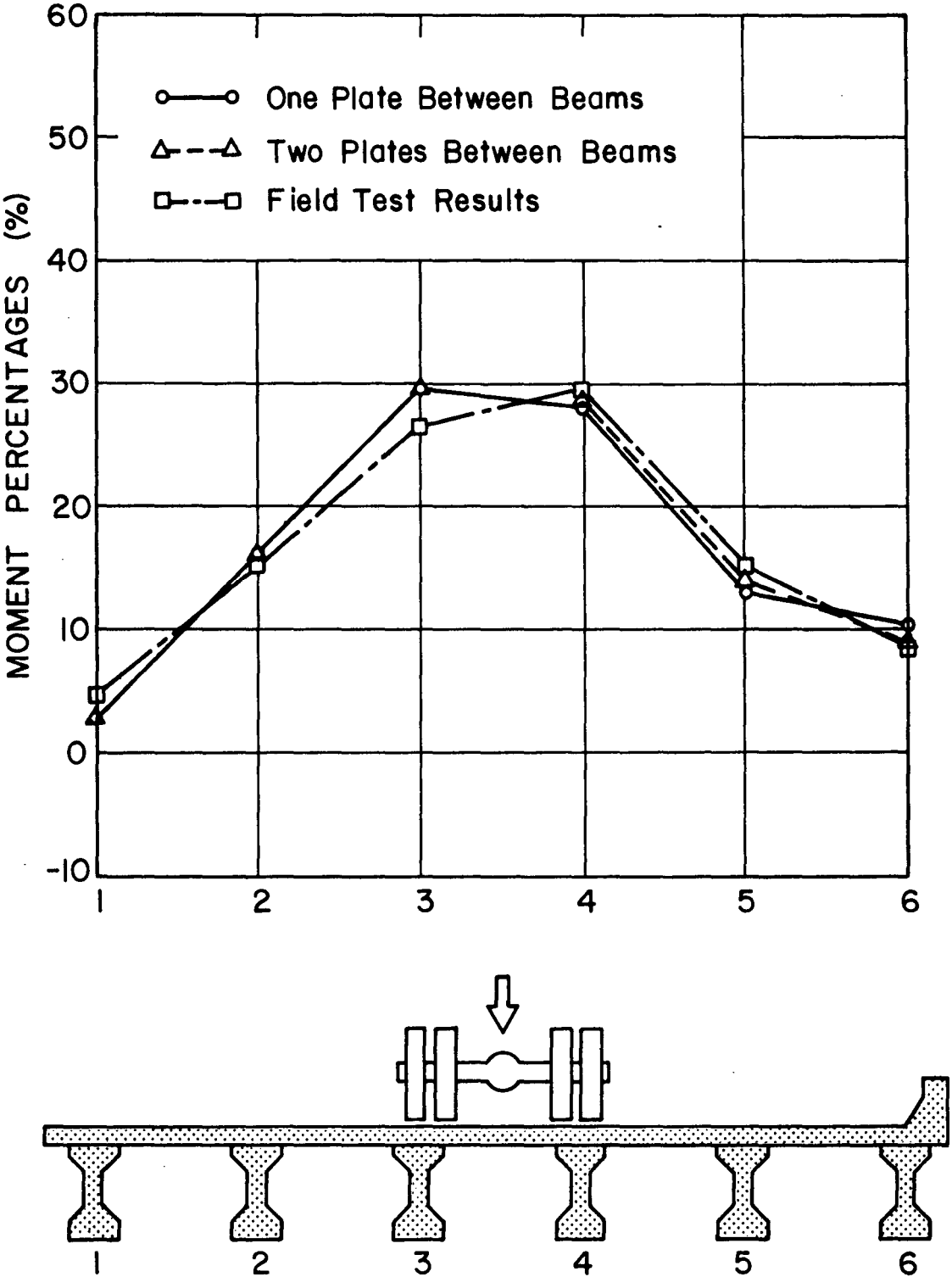

Fig. 14 Comparison of Moment Percentages Derived from Analyses and Field Test Results

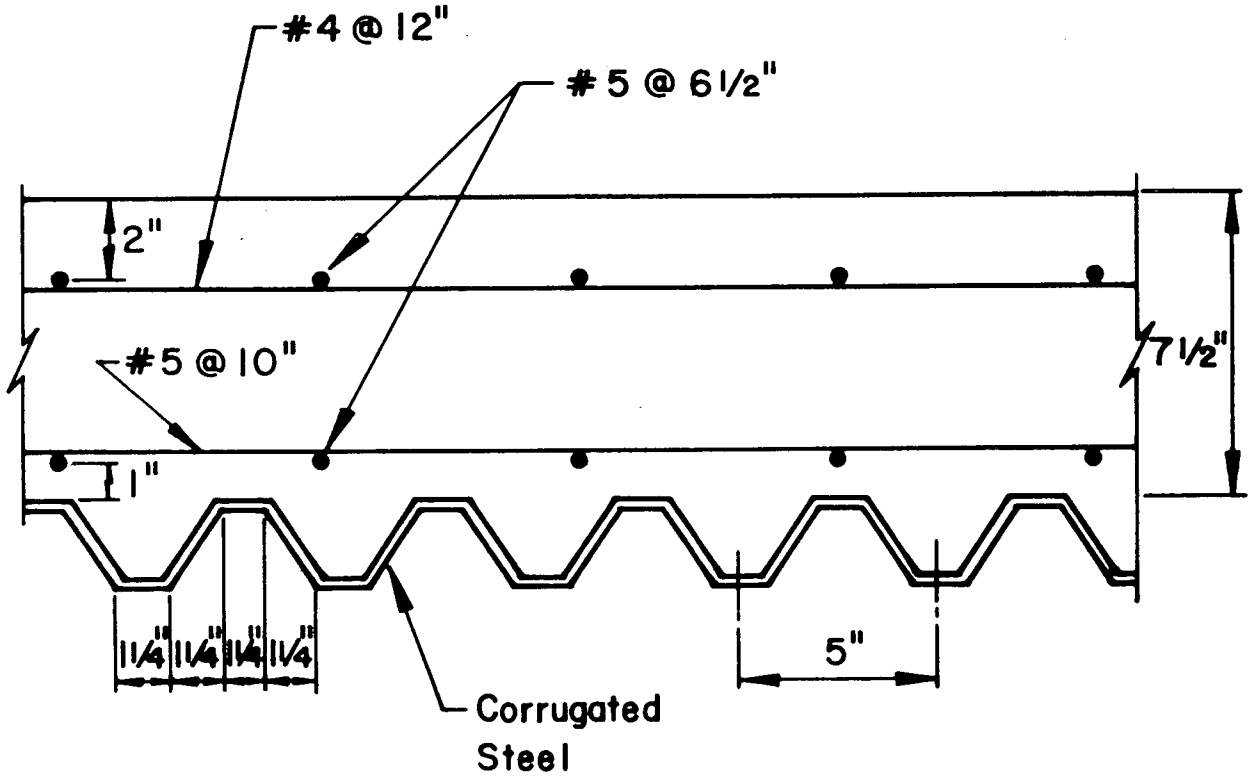

Transverse Cross-section Of Slab

Fig. 15 Transverse Cross-section of Lehighton Bridge Slab

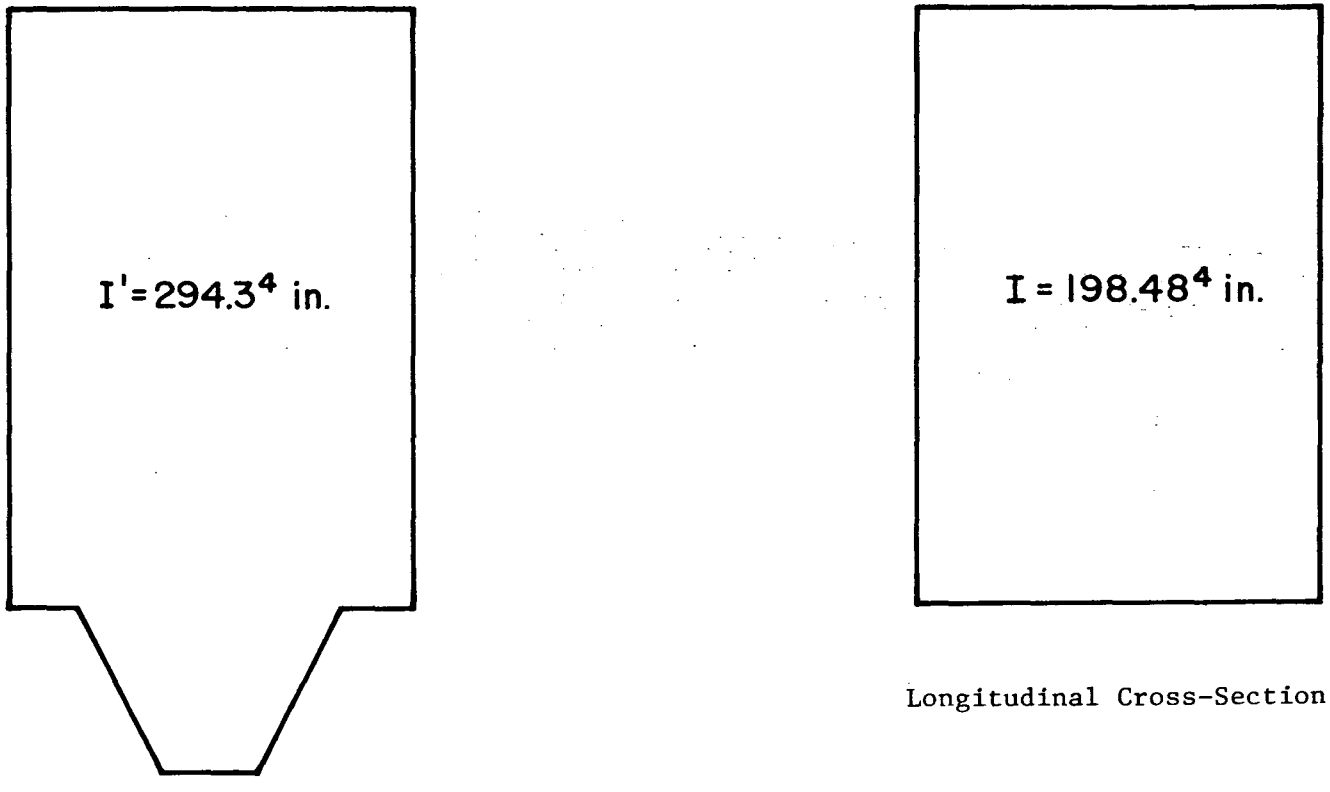

Fig. 16 Determination of Orthotropy Factor for Slab - Lehighton Bridge

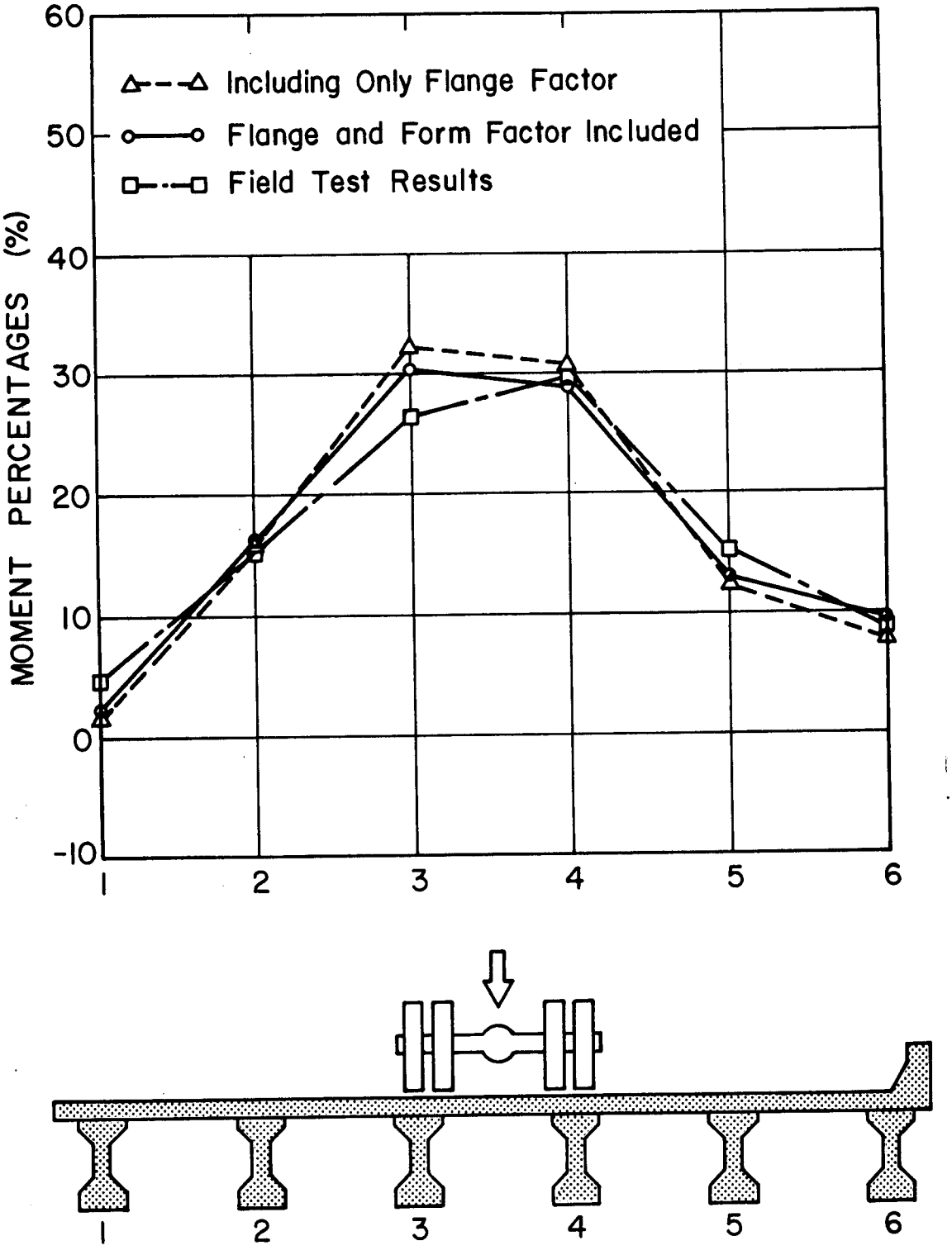

Fig. 17 Comparison of Moment Percentages Derived from Analyses and Field Test Results - Lehighton Bridge

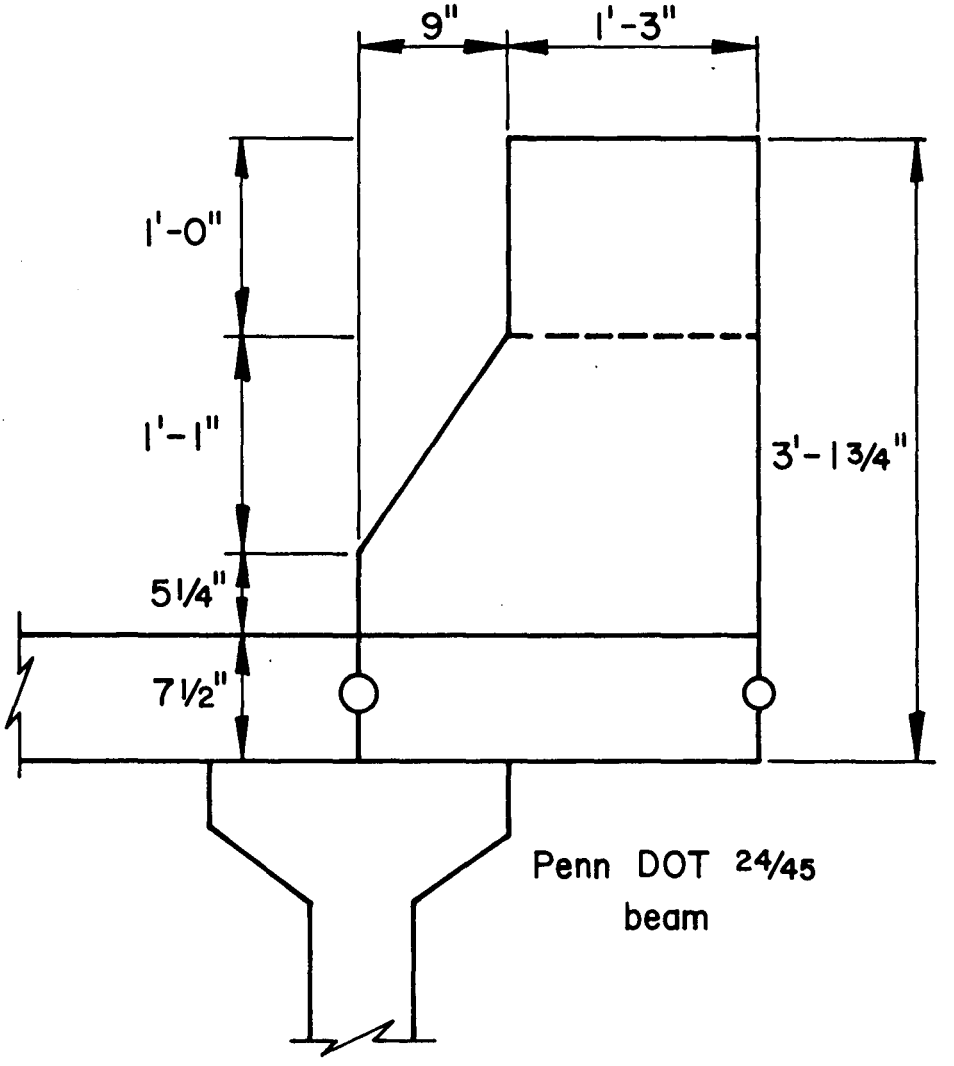

Fig. 18 Curb-Parapet Section - Lehighton Bridge

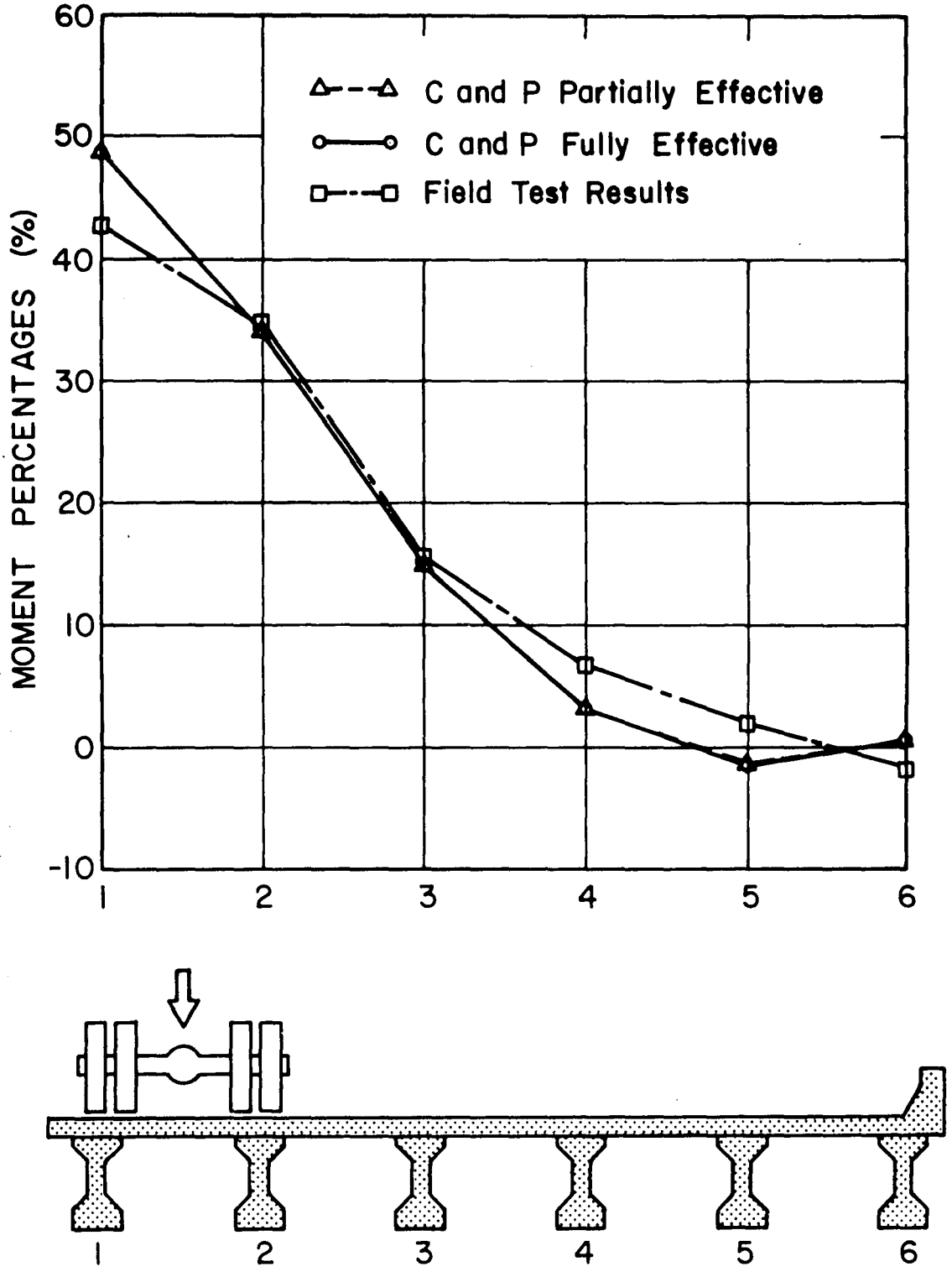

Fig. 19 Comparison of Moment Percentages Derived from Analyses and Field Test Results - Lehighton Bridge

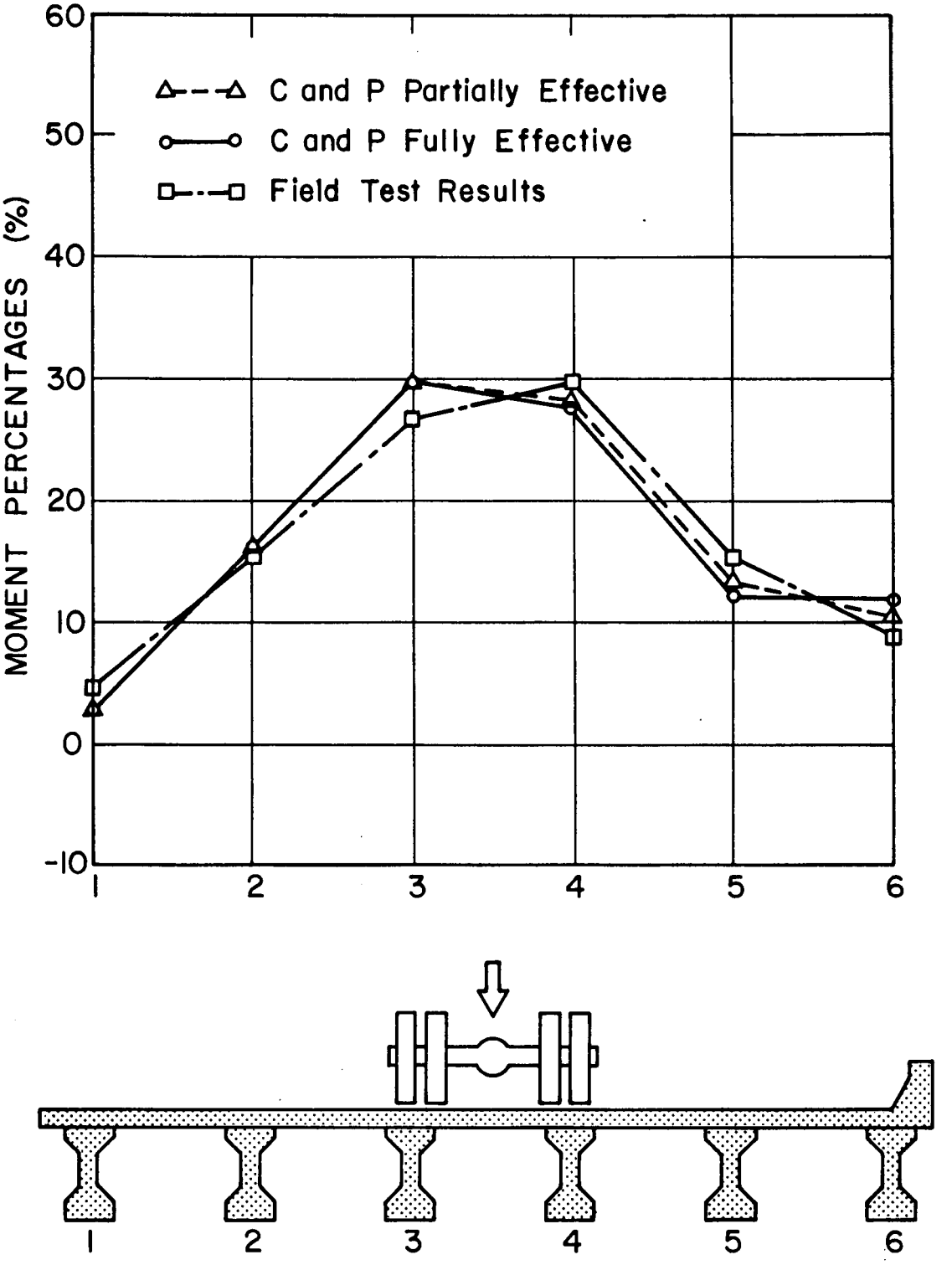

Fig. 20 Comparison of Moment Percentages Derived from Analyses and Field Test Results - Lehighton Bridge

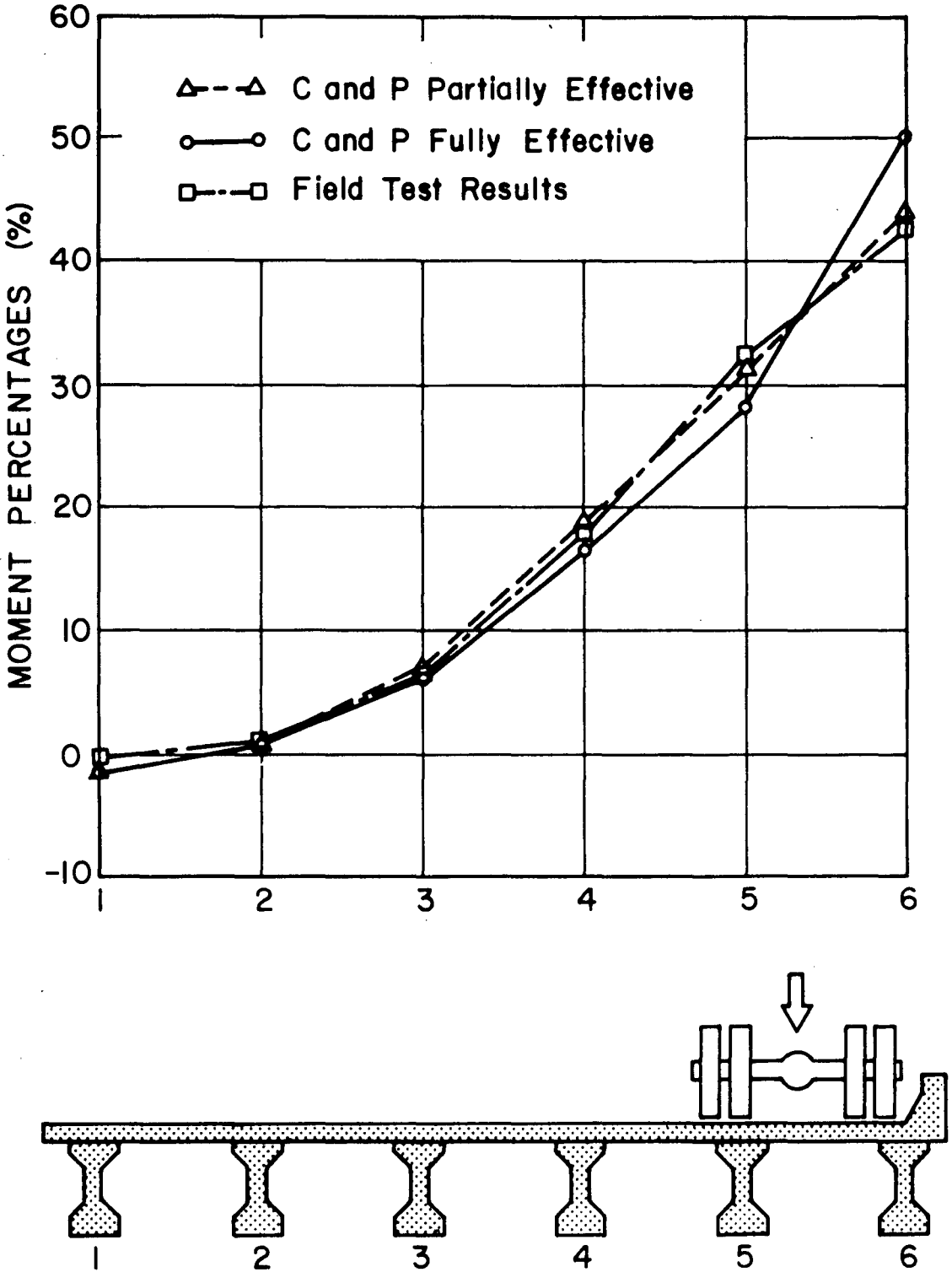

Fig. 21 Comparison of Moment Percentages Derived from Analyses and Field Test Results - Lehighton Bridge

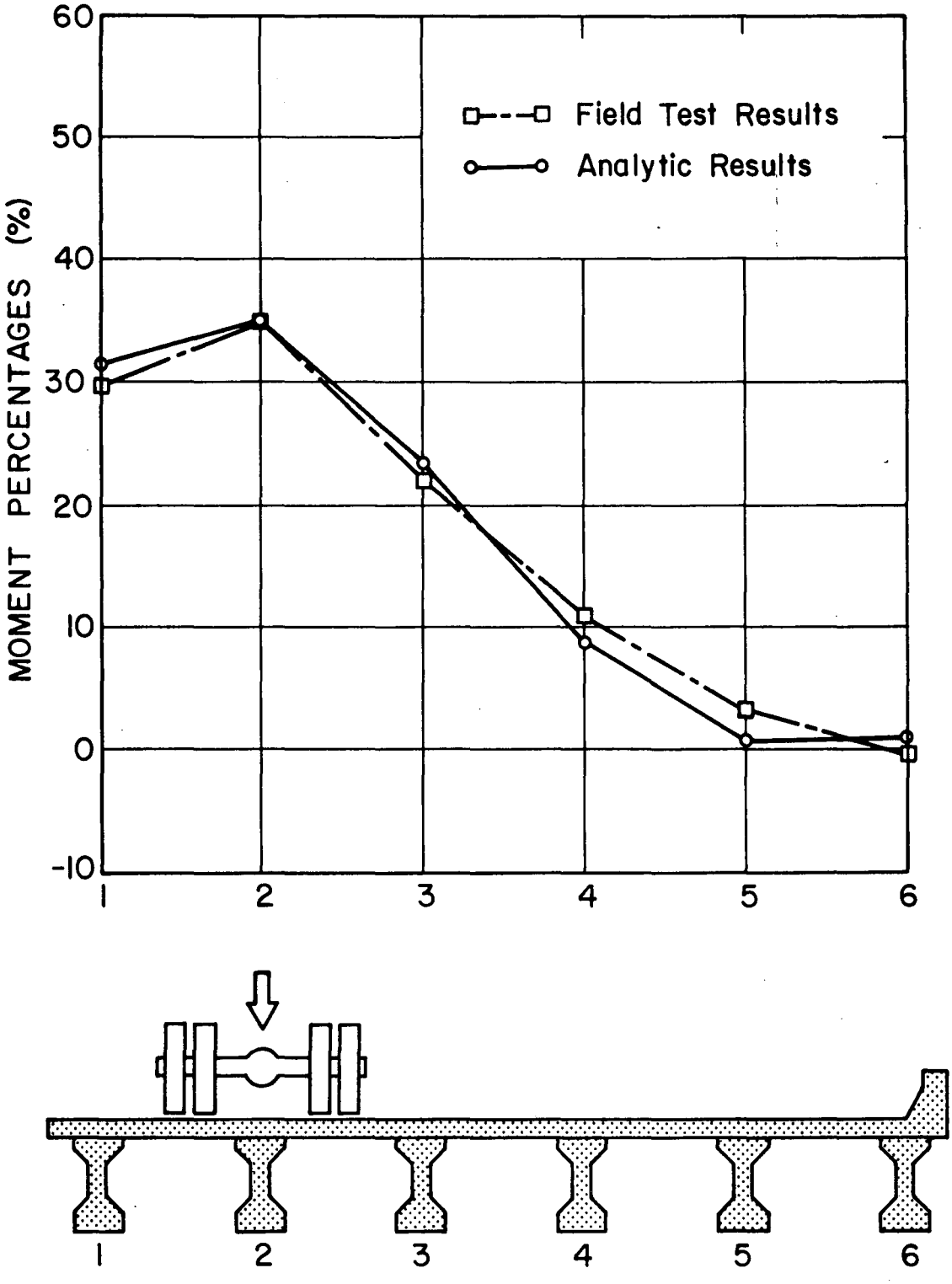

Fig. 22 Comparison of Moment Percentages Derived from Analyses and Field Test Results - Lehighton Bridge

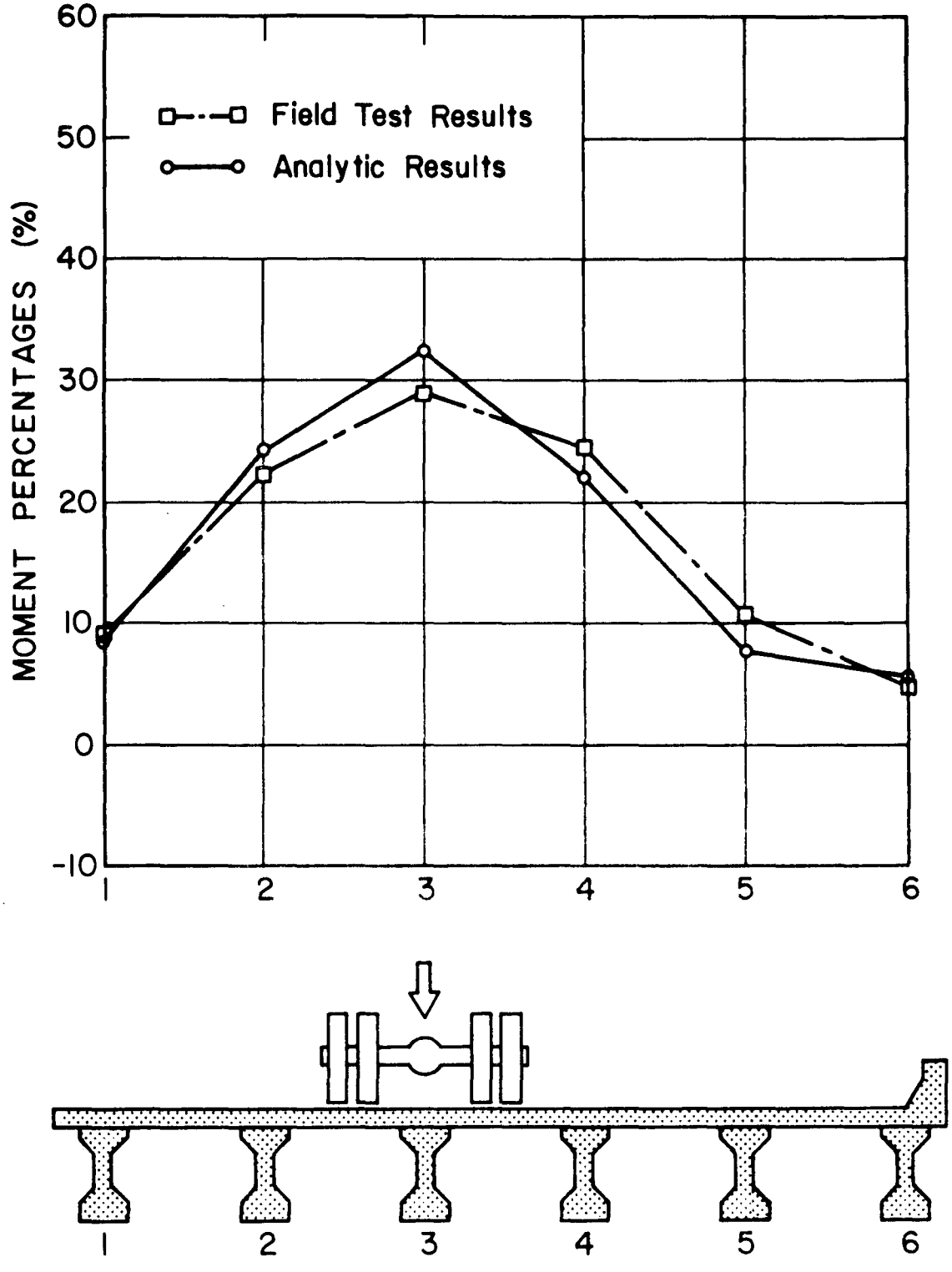

Fig. 23 Comparison of Moment Percentages Derived from Analyses and Field Test Results - Lehighton Bridge

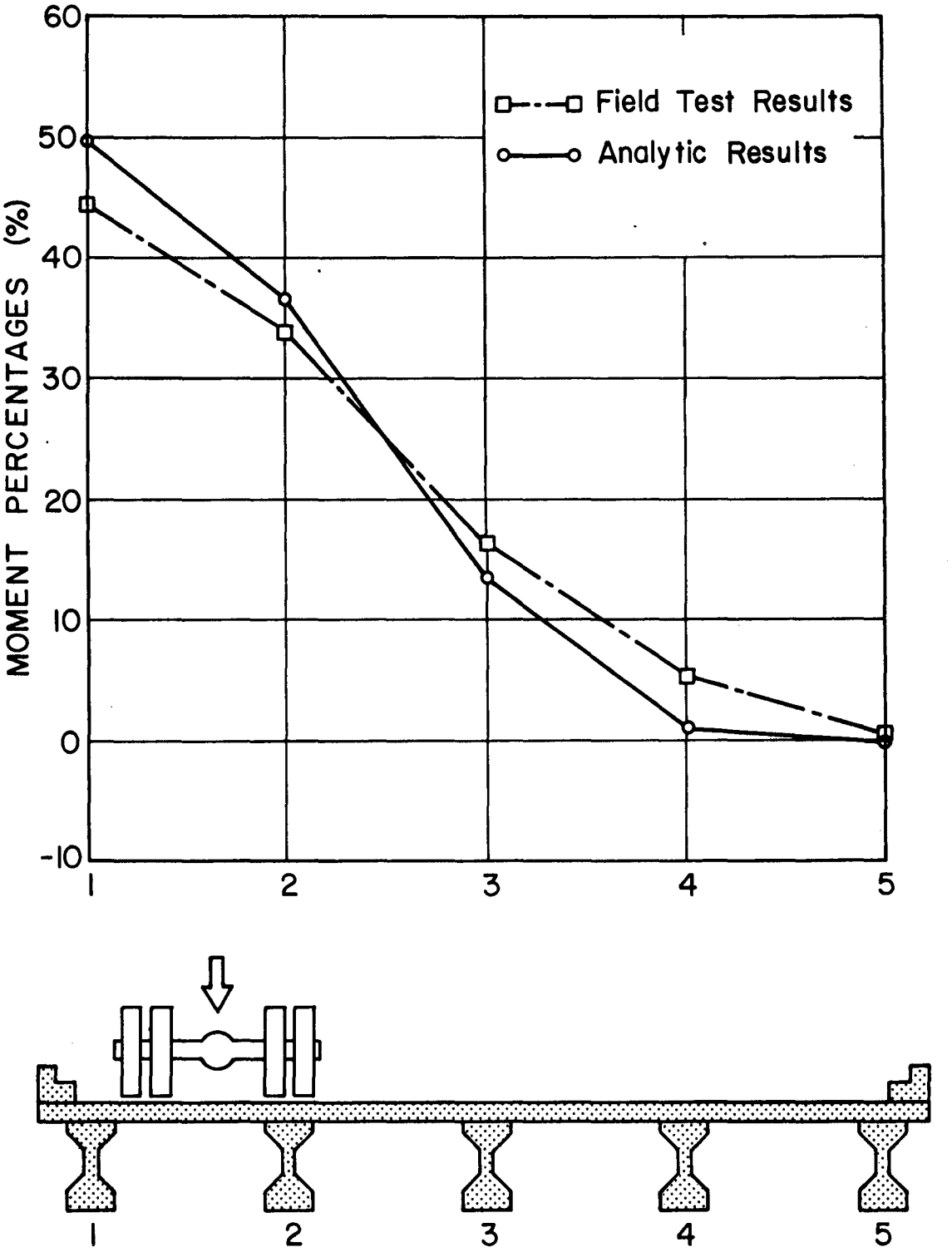

Fig. 24 Comparison of Moment Percentages Derived from Analyses and Field Test Results - Bartonsville Bridge

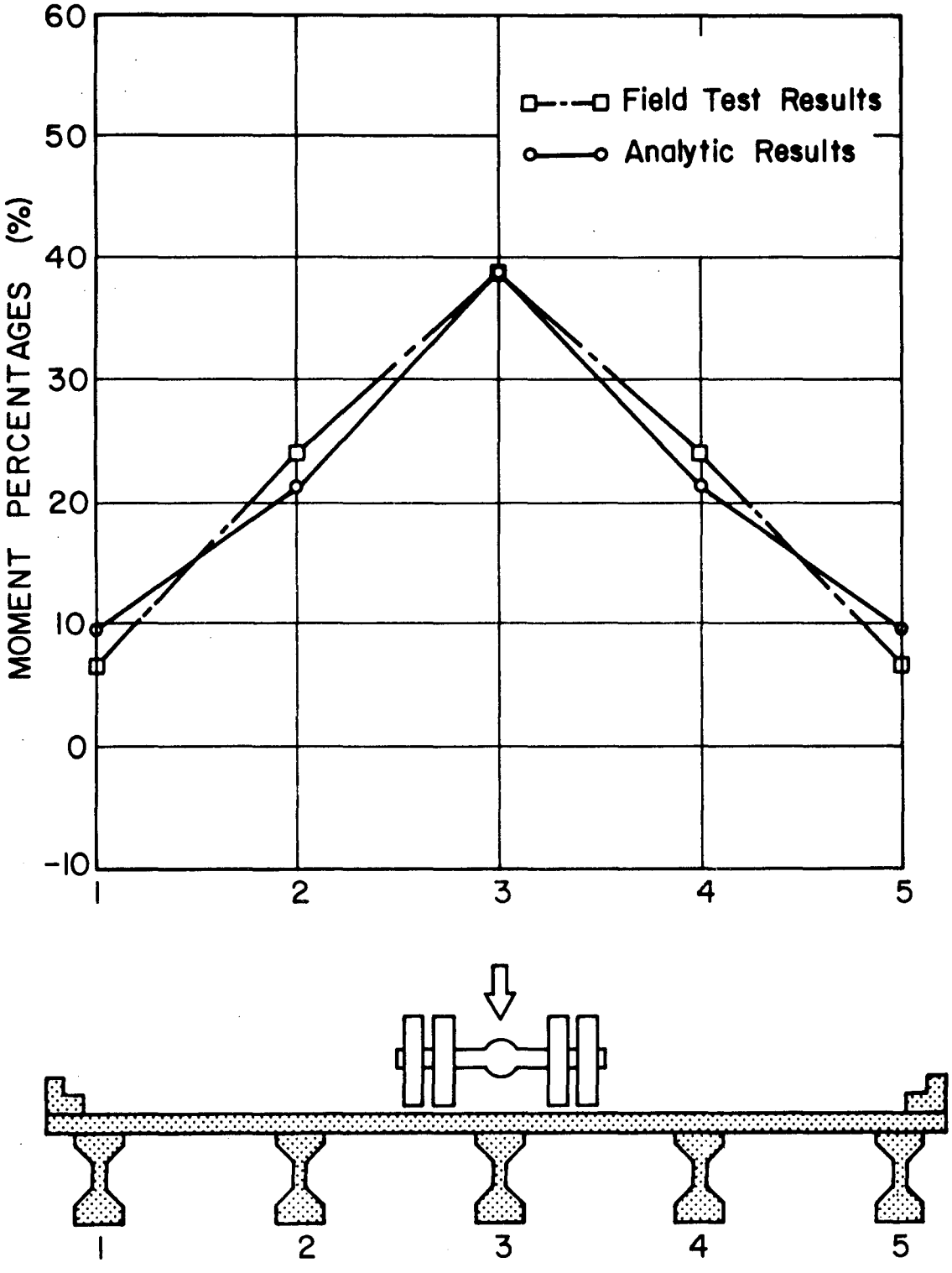

Fig. 25 Comparison of Moment Percentages Derived from Analyses and Field Test Results - Bartonsville Bridge

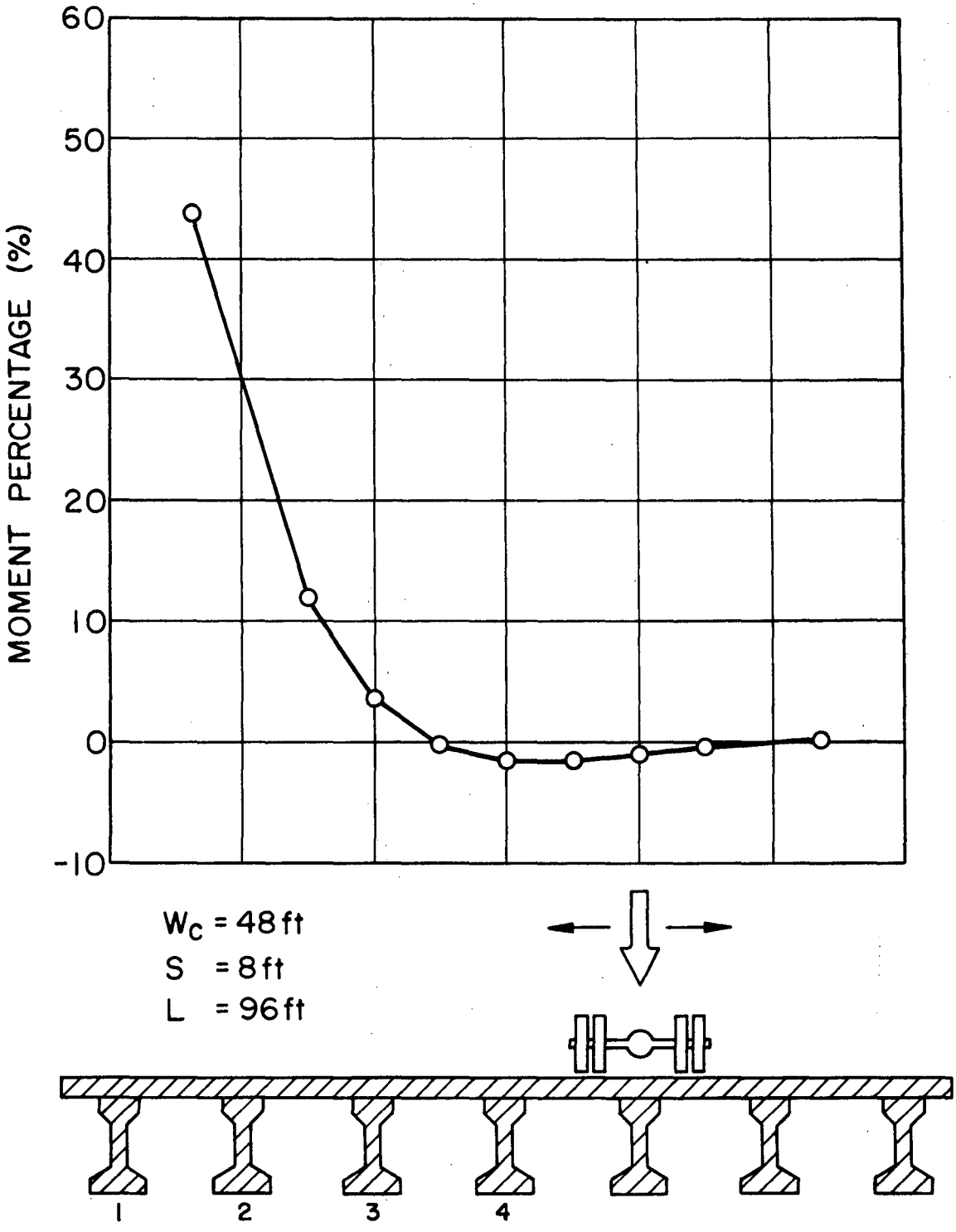

Fig. 26 Influence Line for Moment Percentage - Beam 1

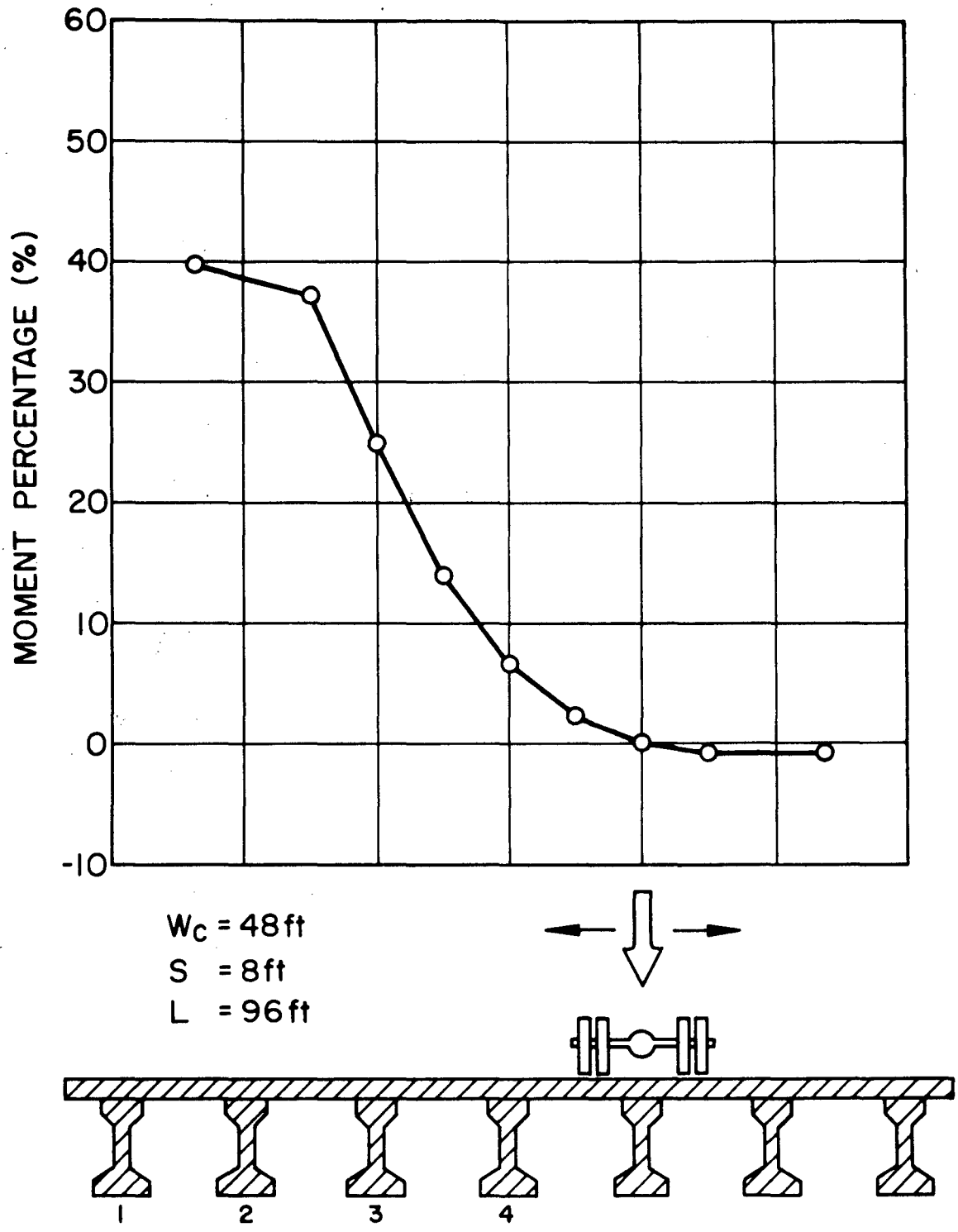

Fig. 27 Influence Line for Moment Percentage - Beam 2

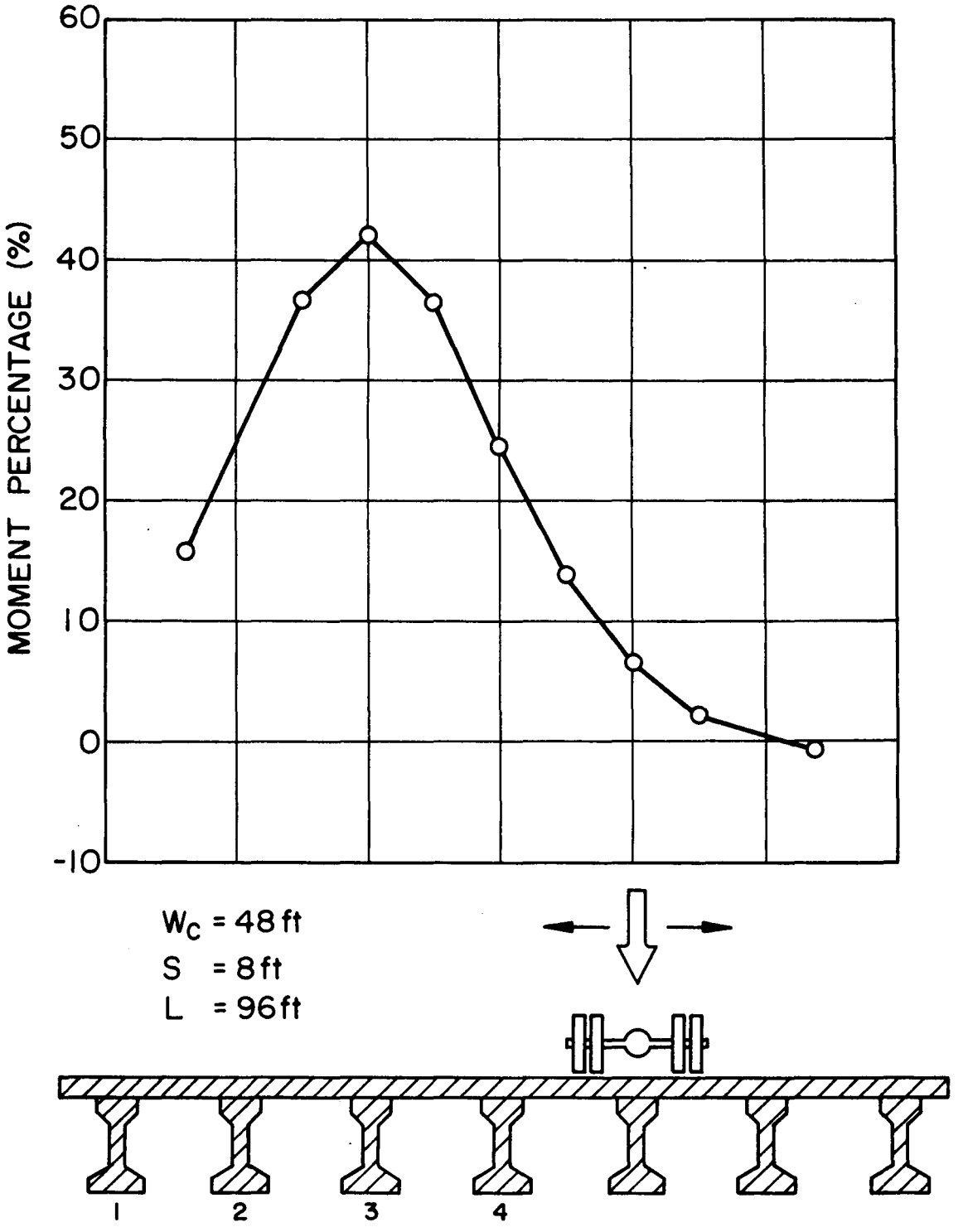

Fig. 28 Influence Line for Moment Percentage - Beam 3

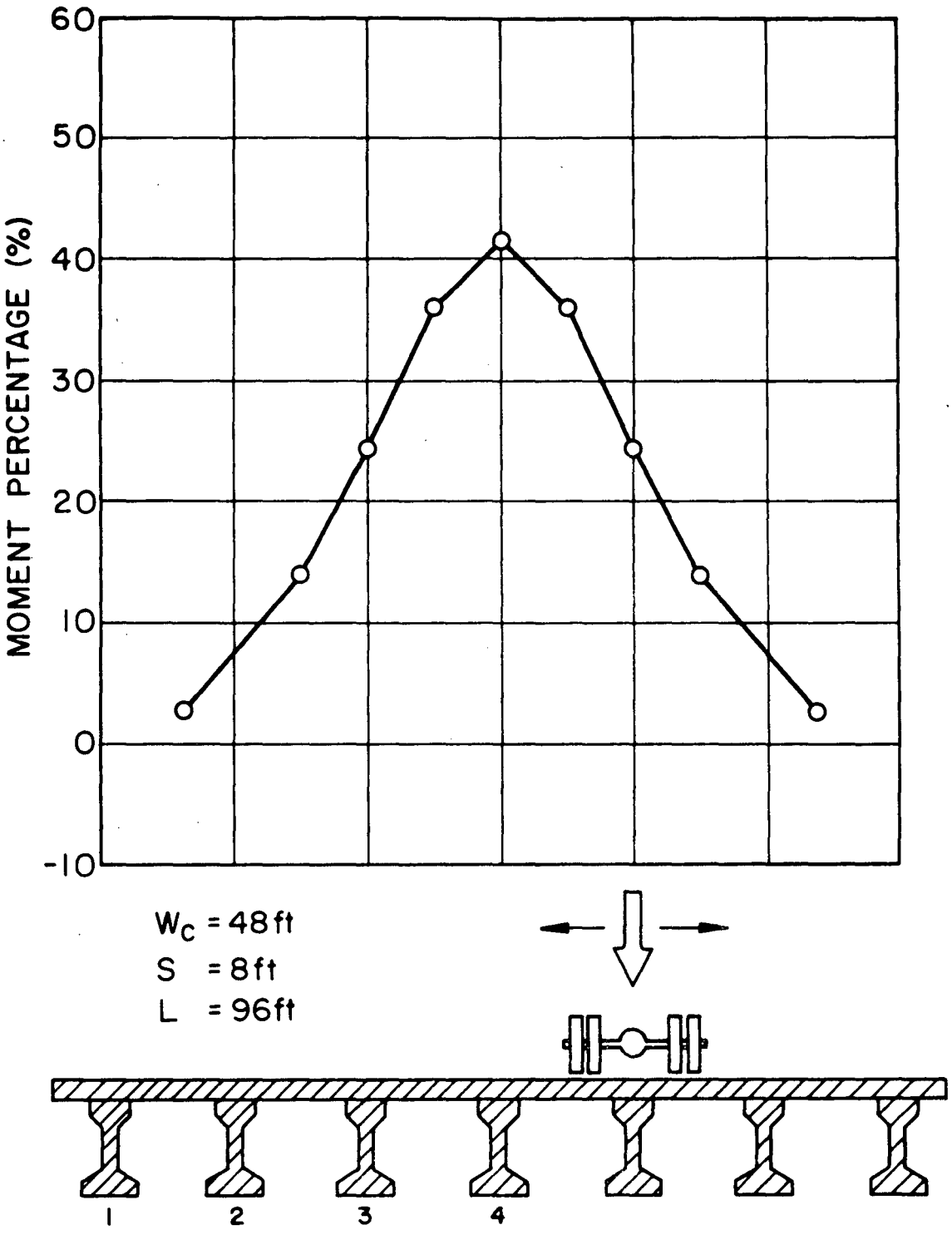

Fig. 29 Influence Line for Moment Percentage - Beam 4

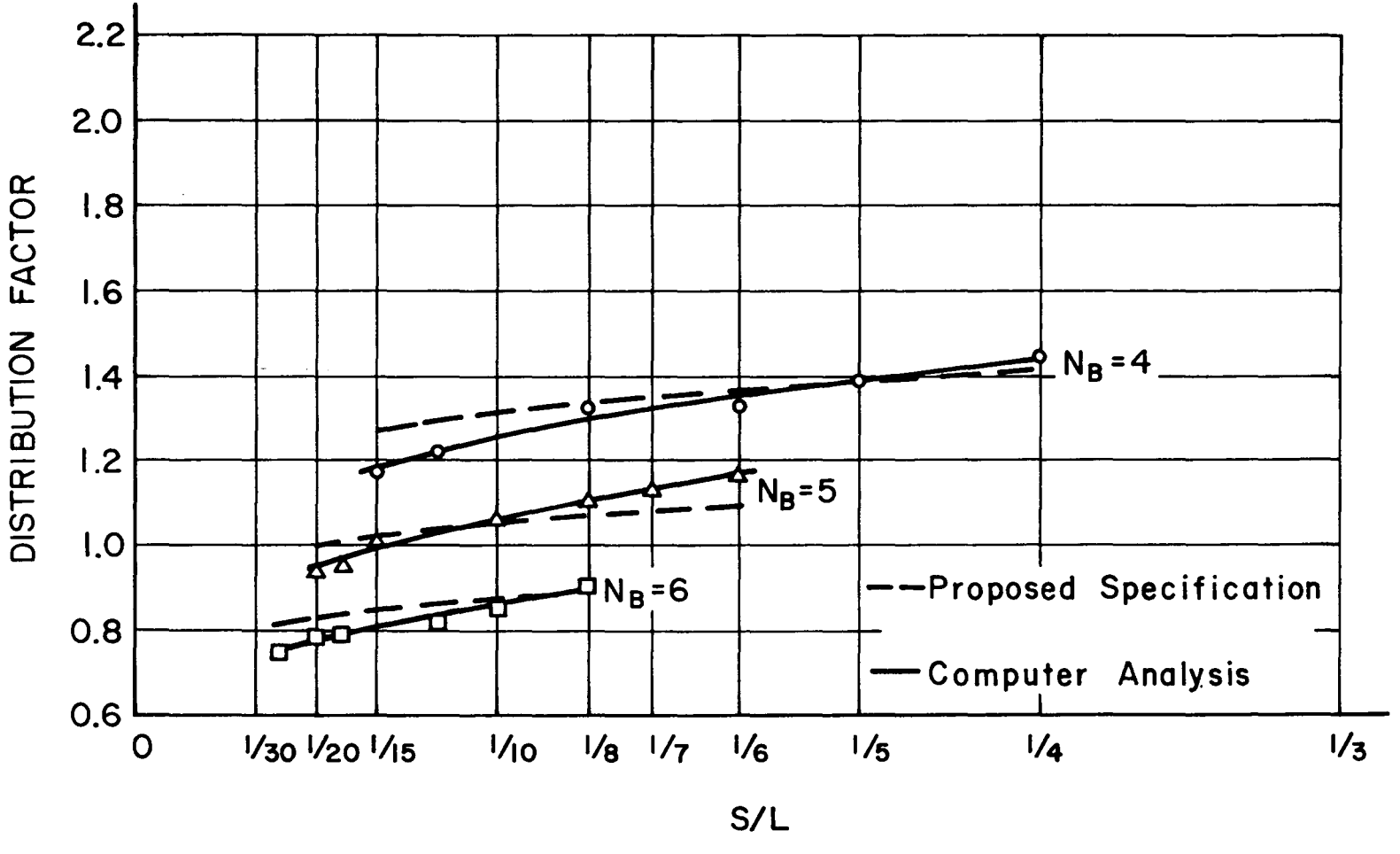

Fig. 30 Distribution Factors for Interior Beams - W = 24 ft. N_L = 2

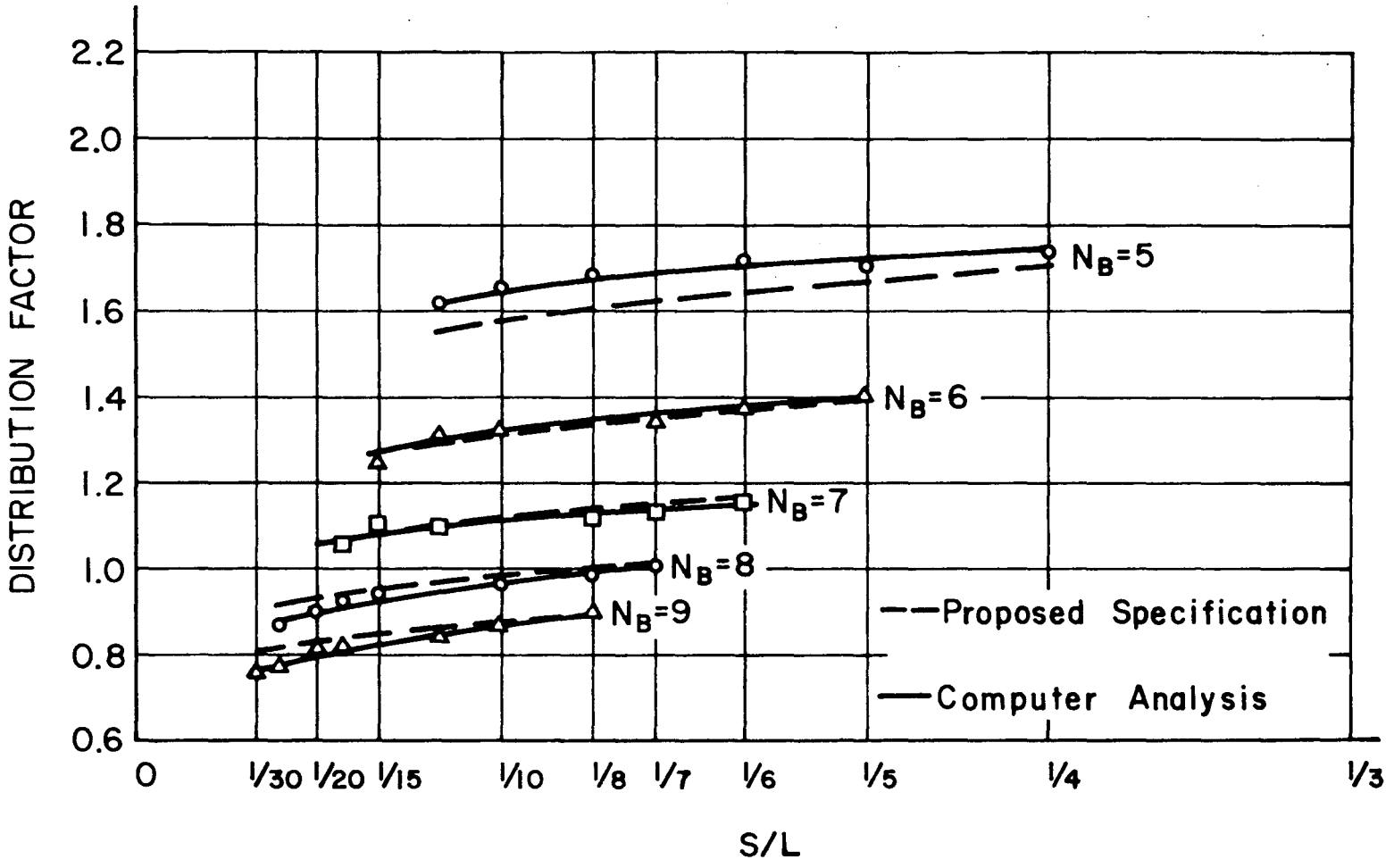

Fig. 31 Distribution Factors for Interior Beams - W = 36 ft. N_L = 3

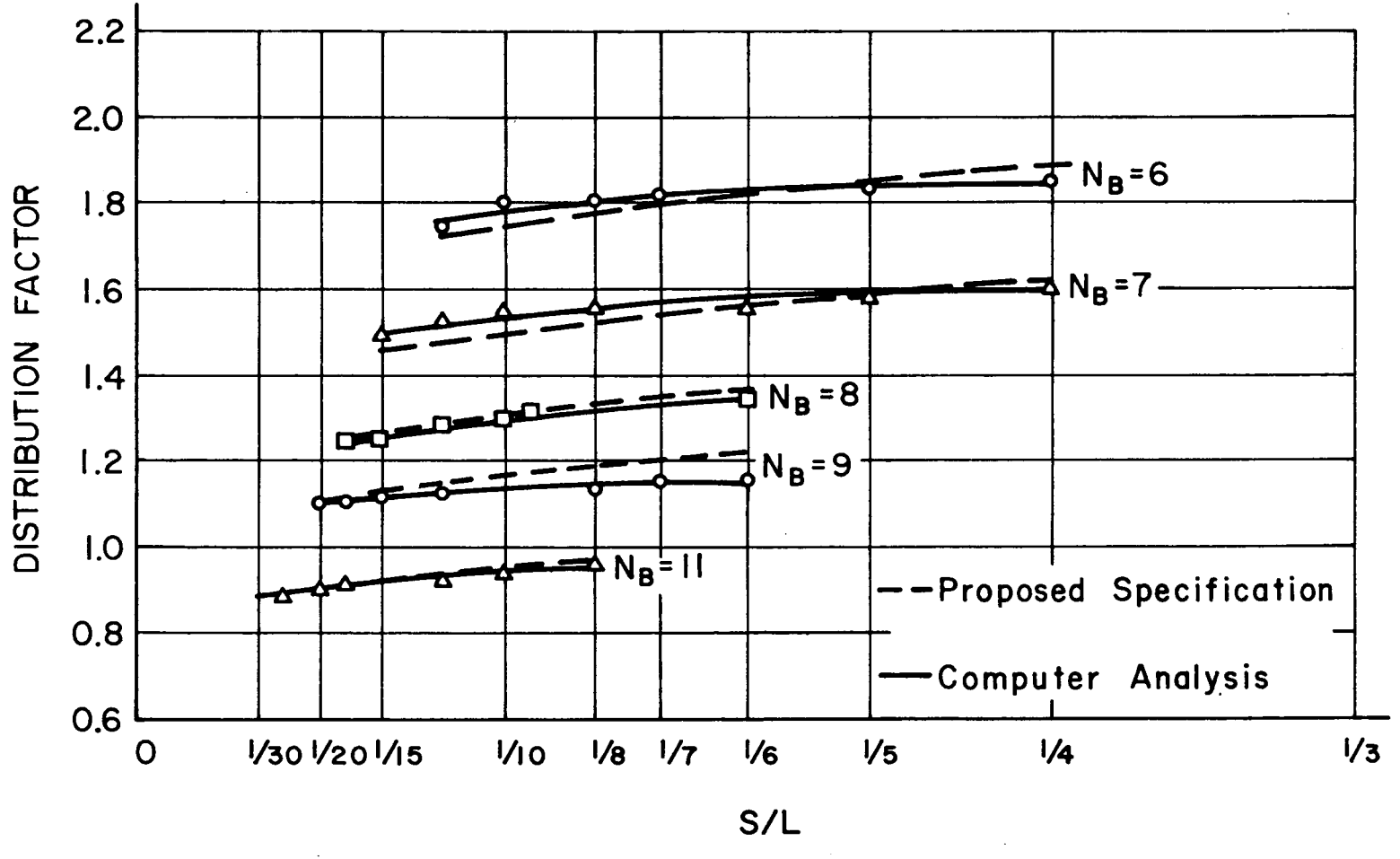

Fig. 32 Distribution Factors for Interior Beams - W = 48 ft. N_L = 4

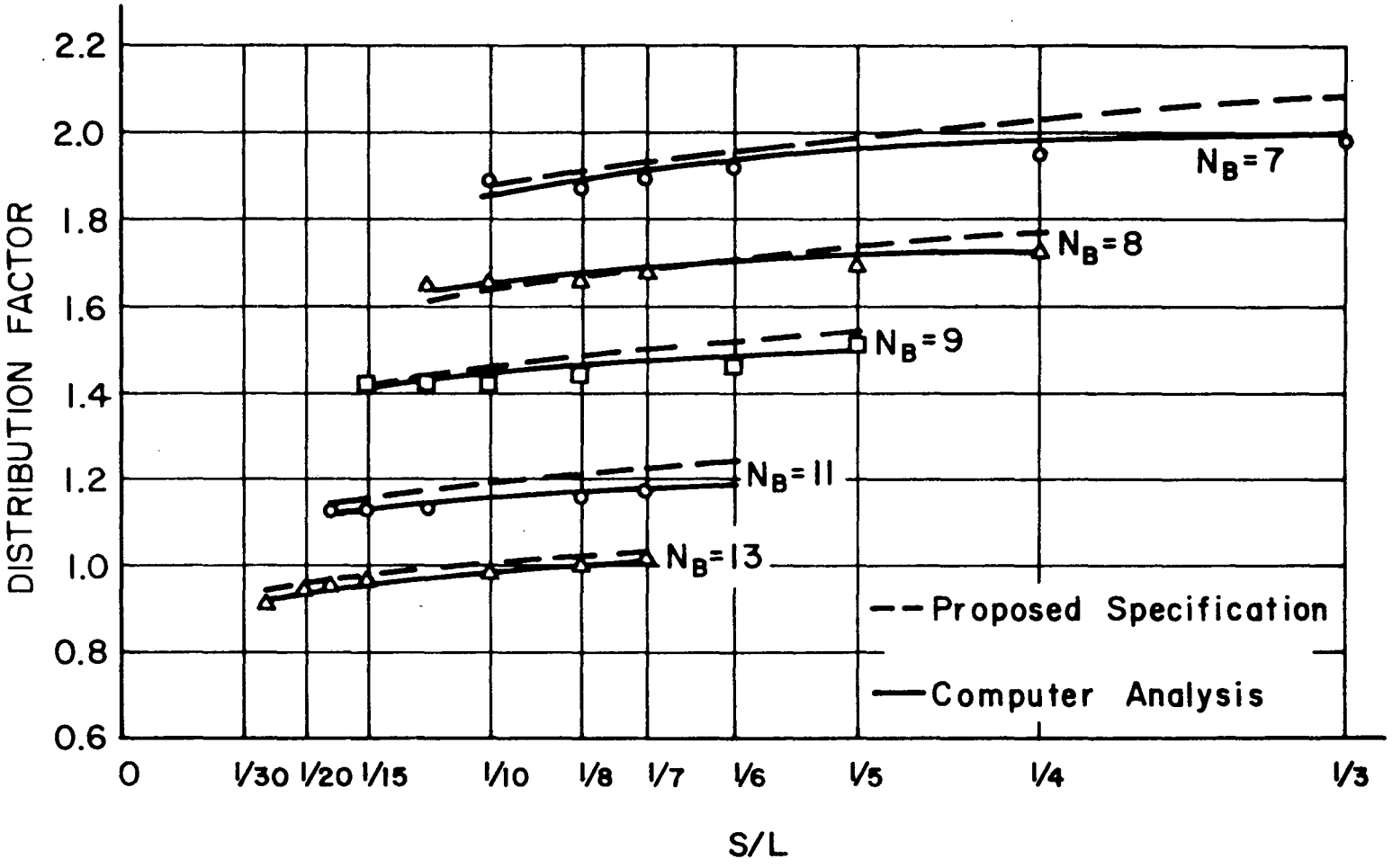

Fig. 33 Distribution Factors for Interior Beams - W = 60 ft. N_L = 5

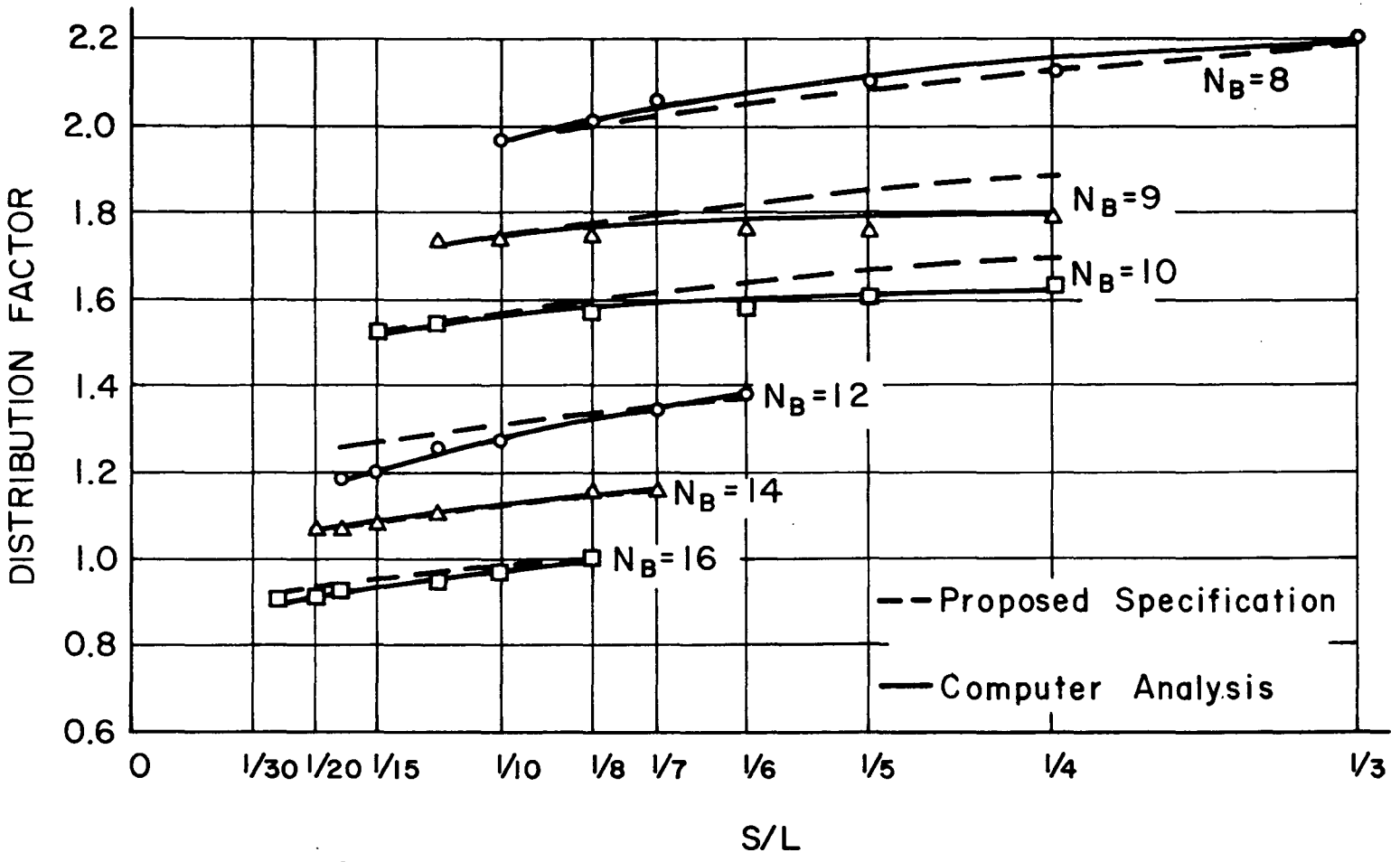

Fig. 34 Distribution Factors for Interior Beams - W = 72 ft. N_L = 6

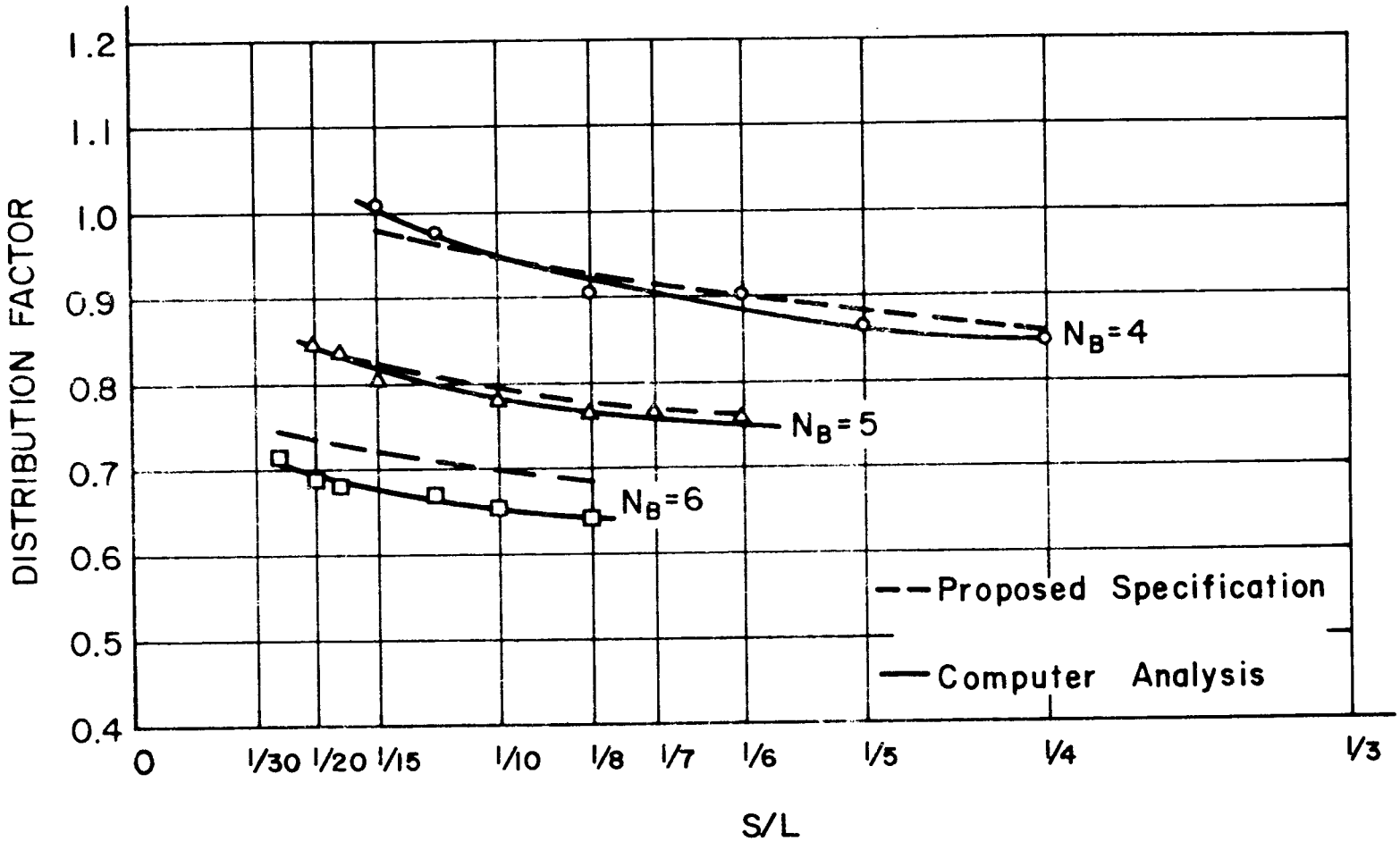

Fig. 35 Distribution Factors for Exterior Beams - W = 24 ft. N_L = 2

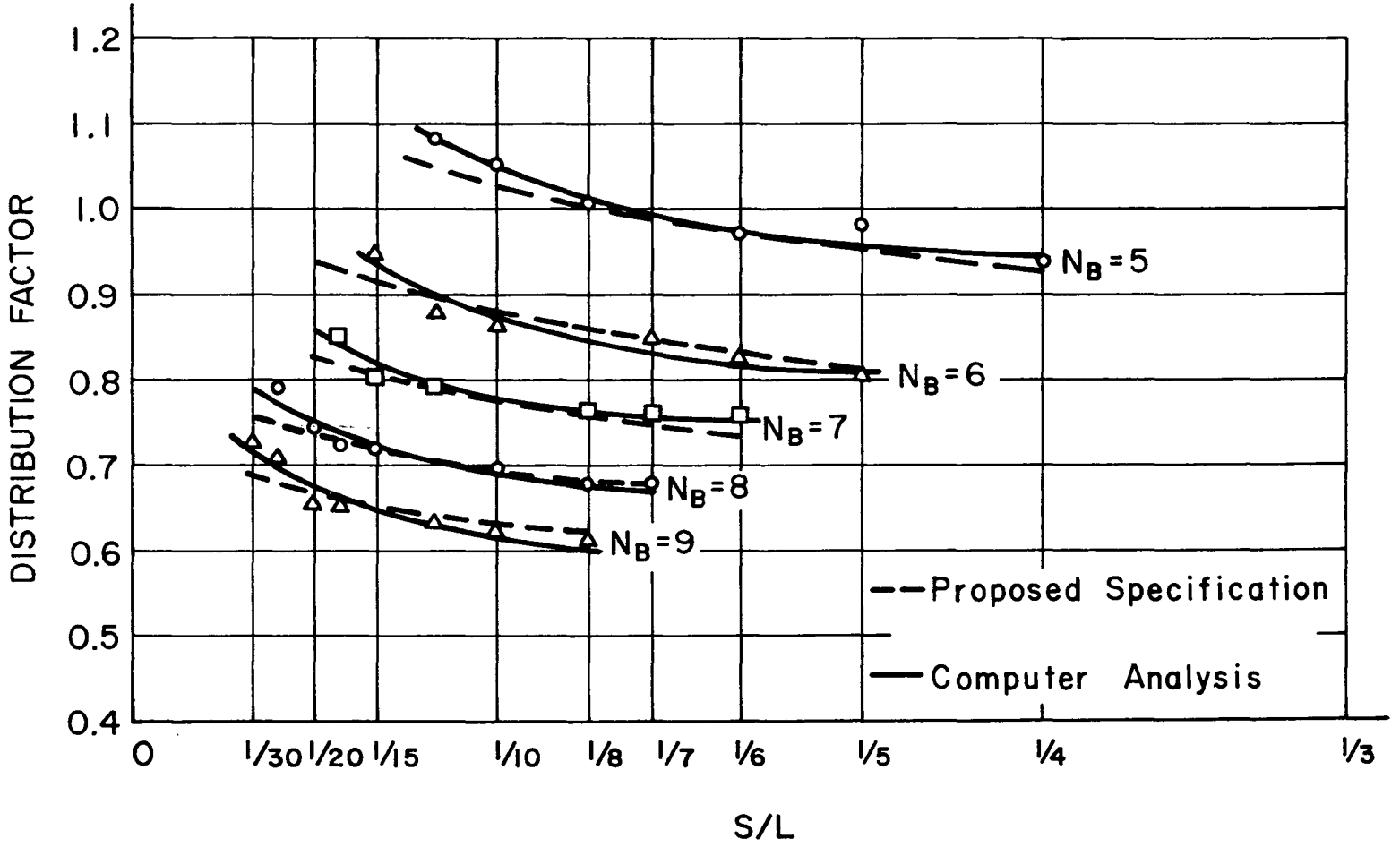

Fig. 36 Distribution Factors for Exterior Beams - W = 36 ft. N_L = 3

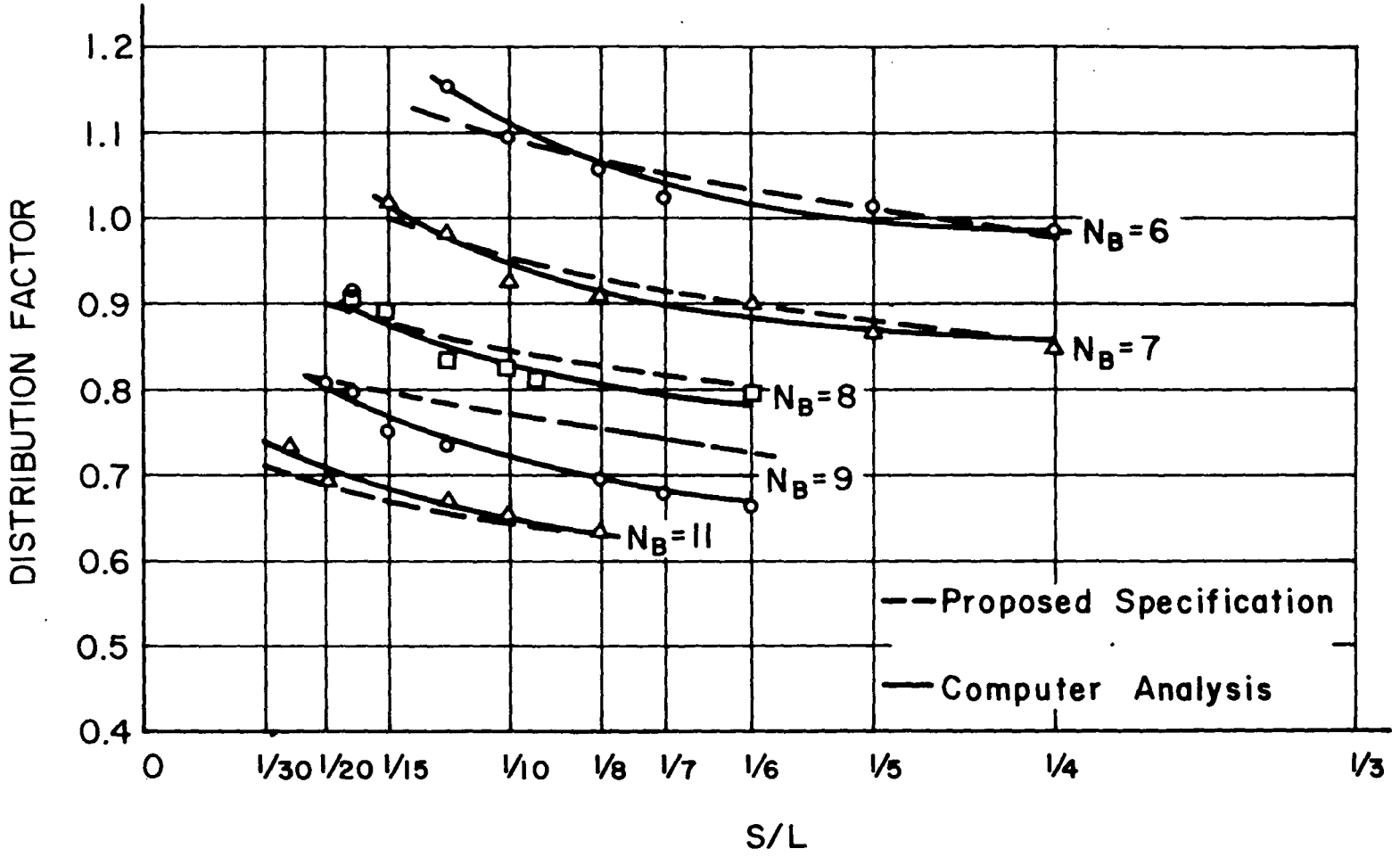

Fig. 37 Distribution Factors for Exterior Beams - W = 48 ft. N_L = 4

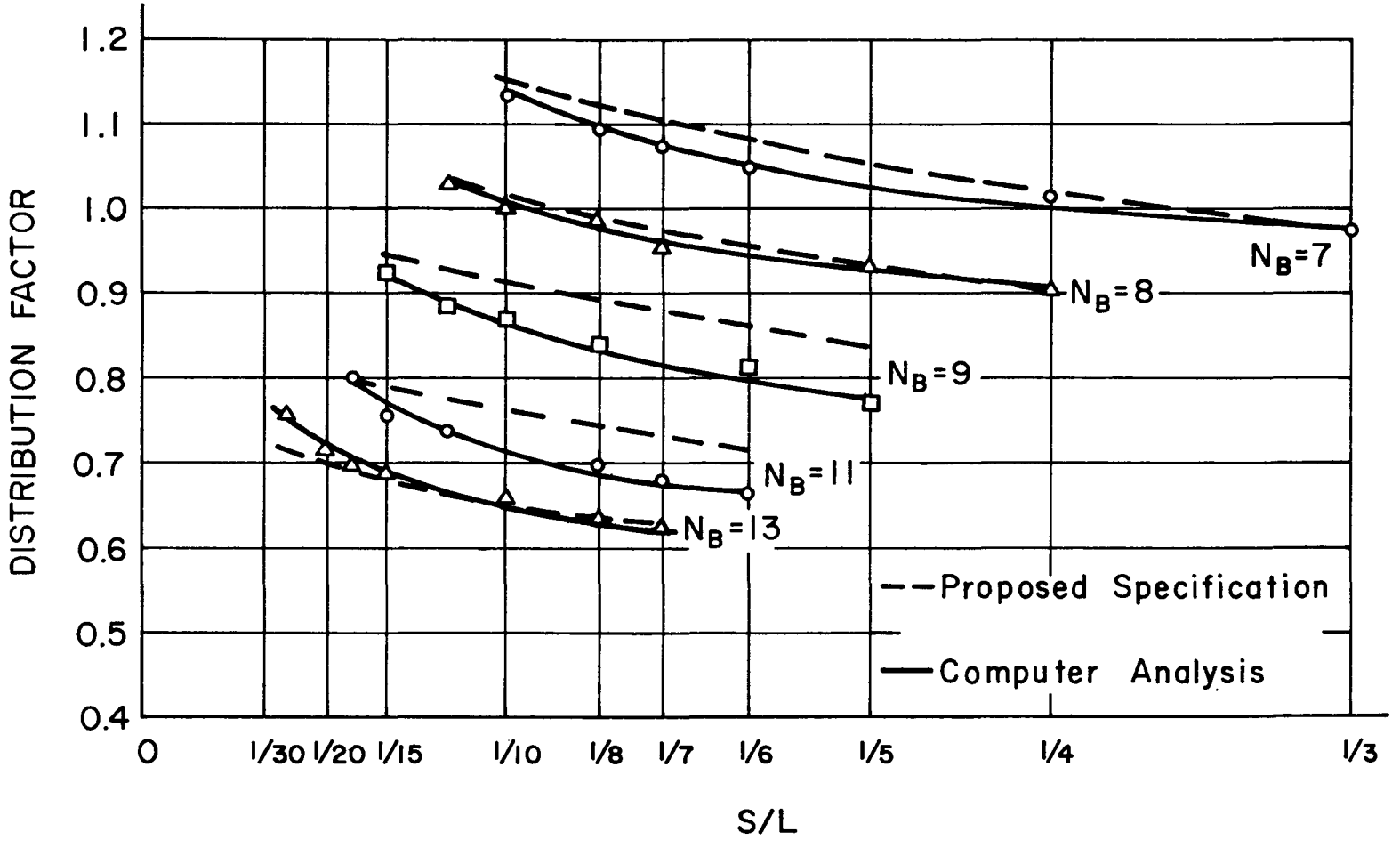

Fig. 38 Distribution Factors for Exterior Beams - W = 60 ft. N_L = 5

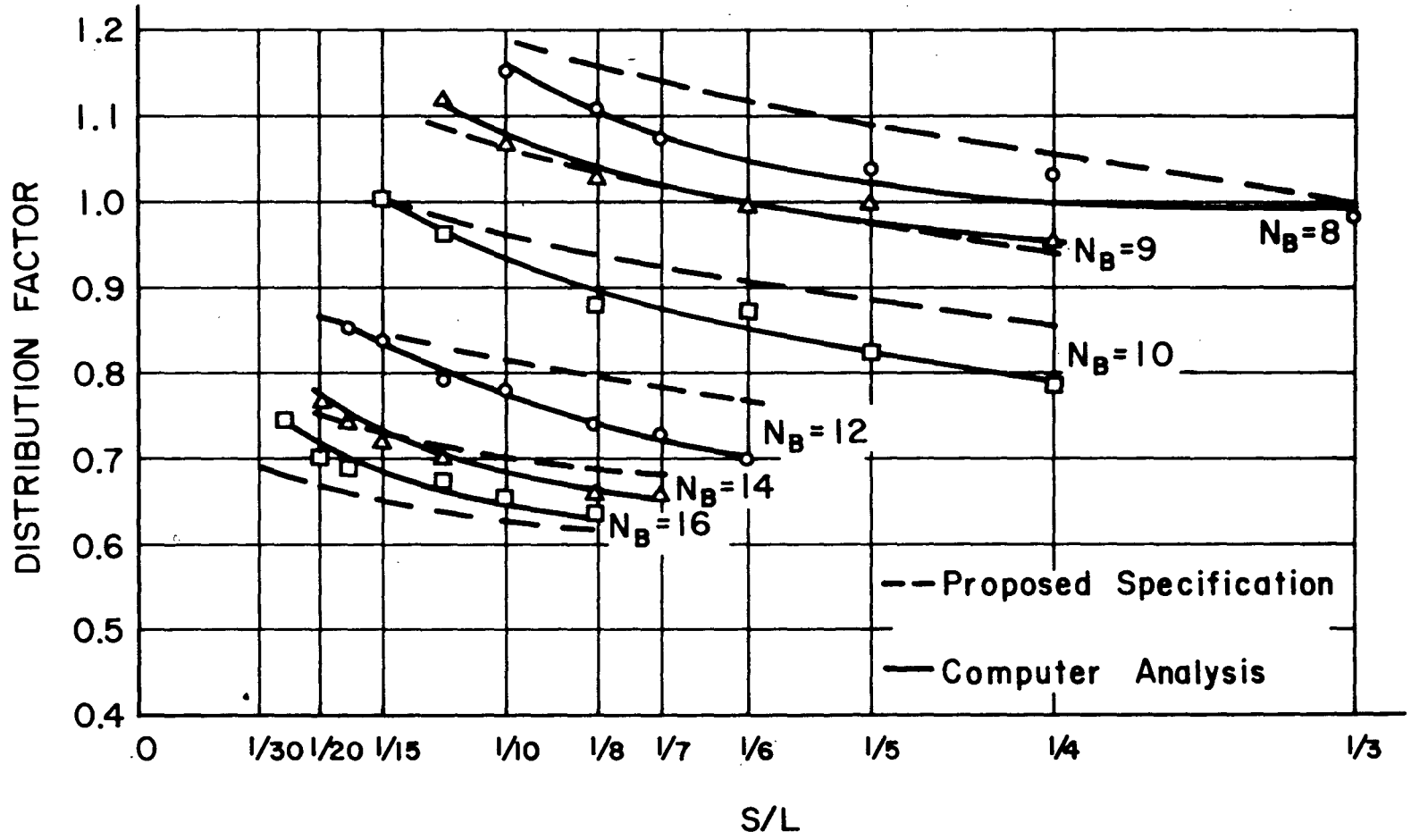

Fig. 39 Distribution Factors for Exterior Beams - W = 72 ft. N_L = 6

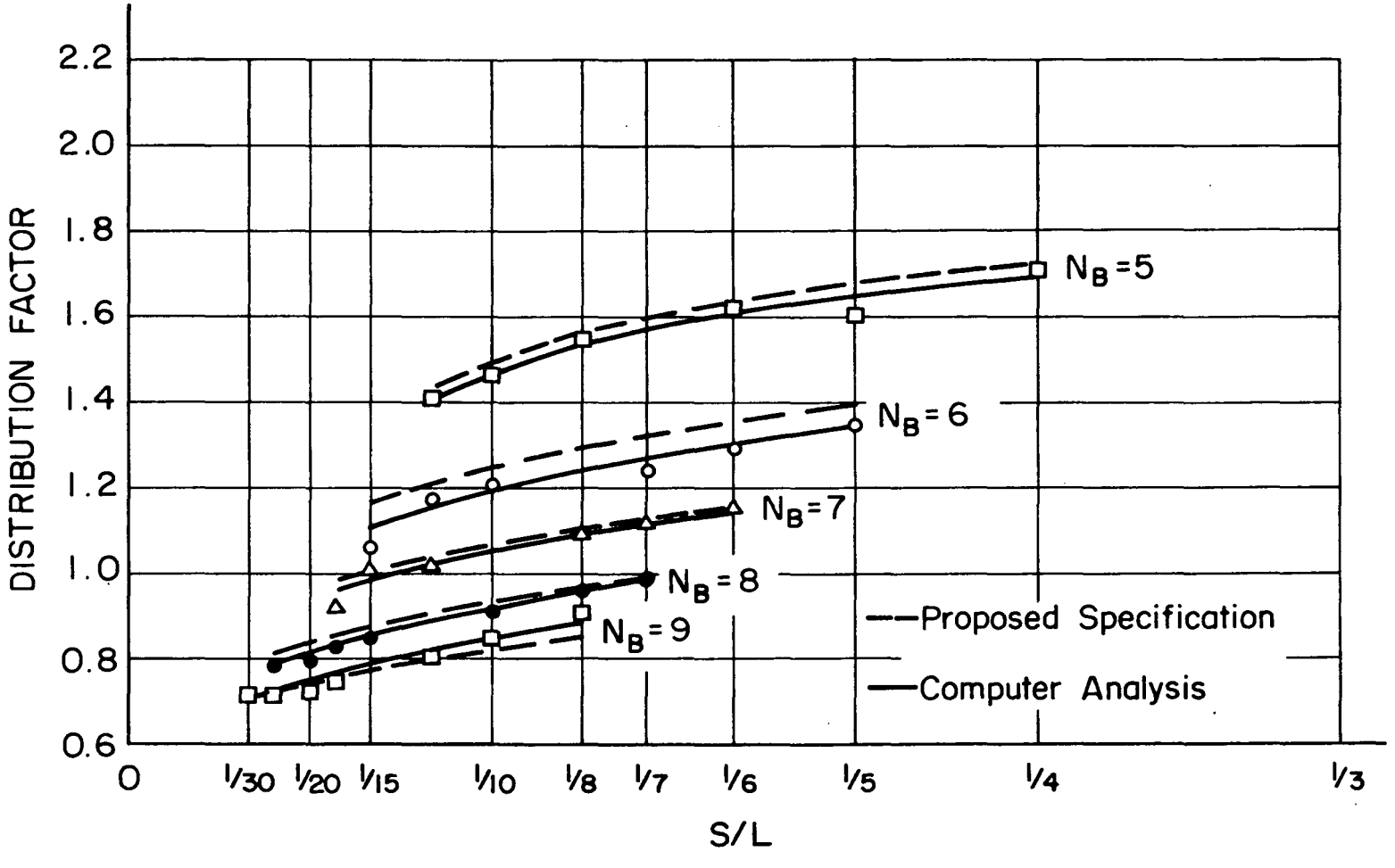

Fig. 40 Distribution Factors for Interior Beams - W = 36 ft. N_L = 2

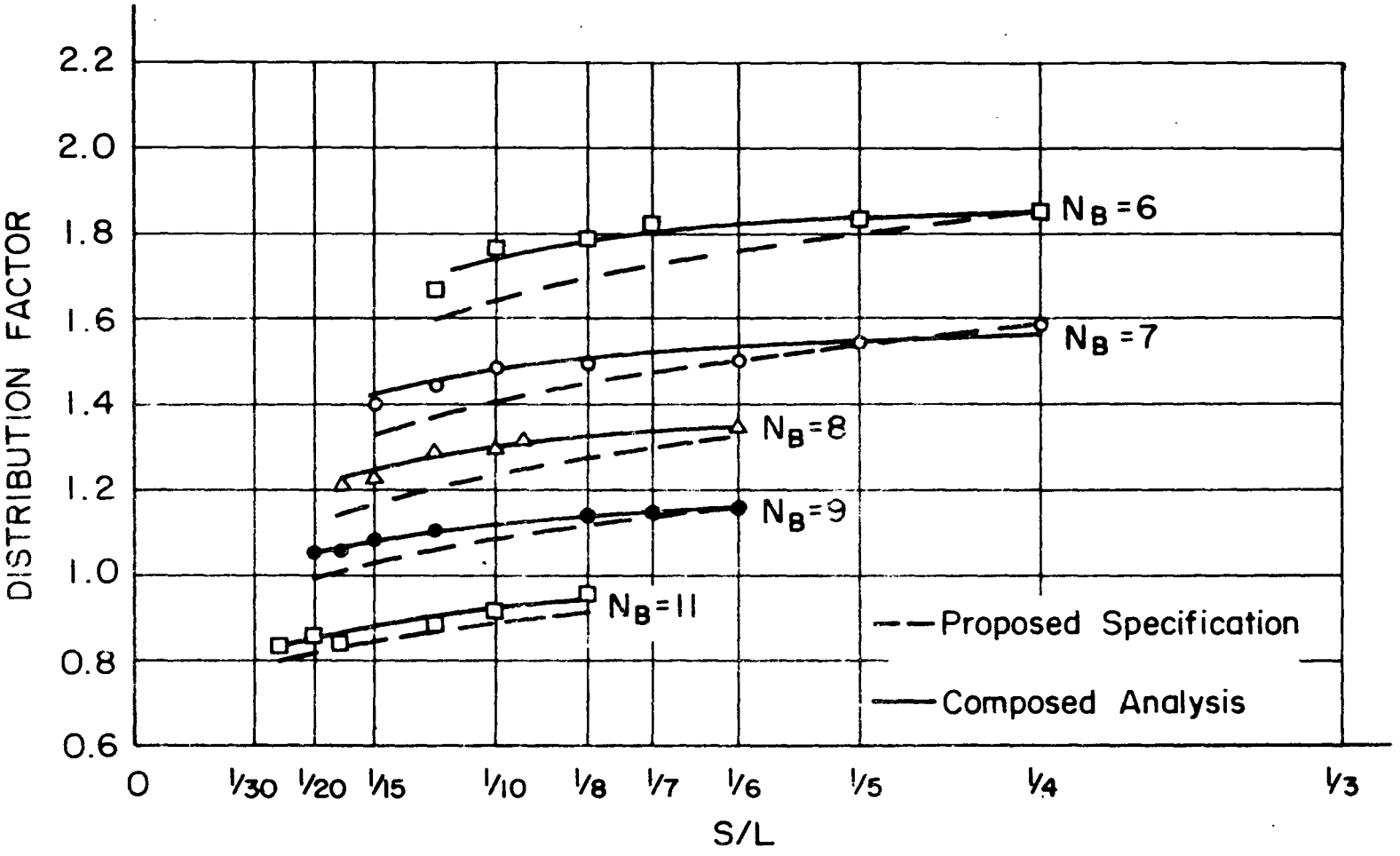

Fig. 41 Distribution Factors for Interior Beams - W = 48 ft. $N_L = 3$

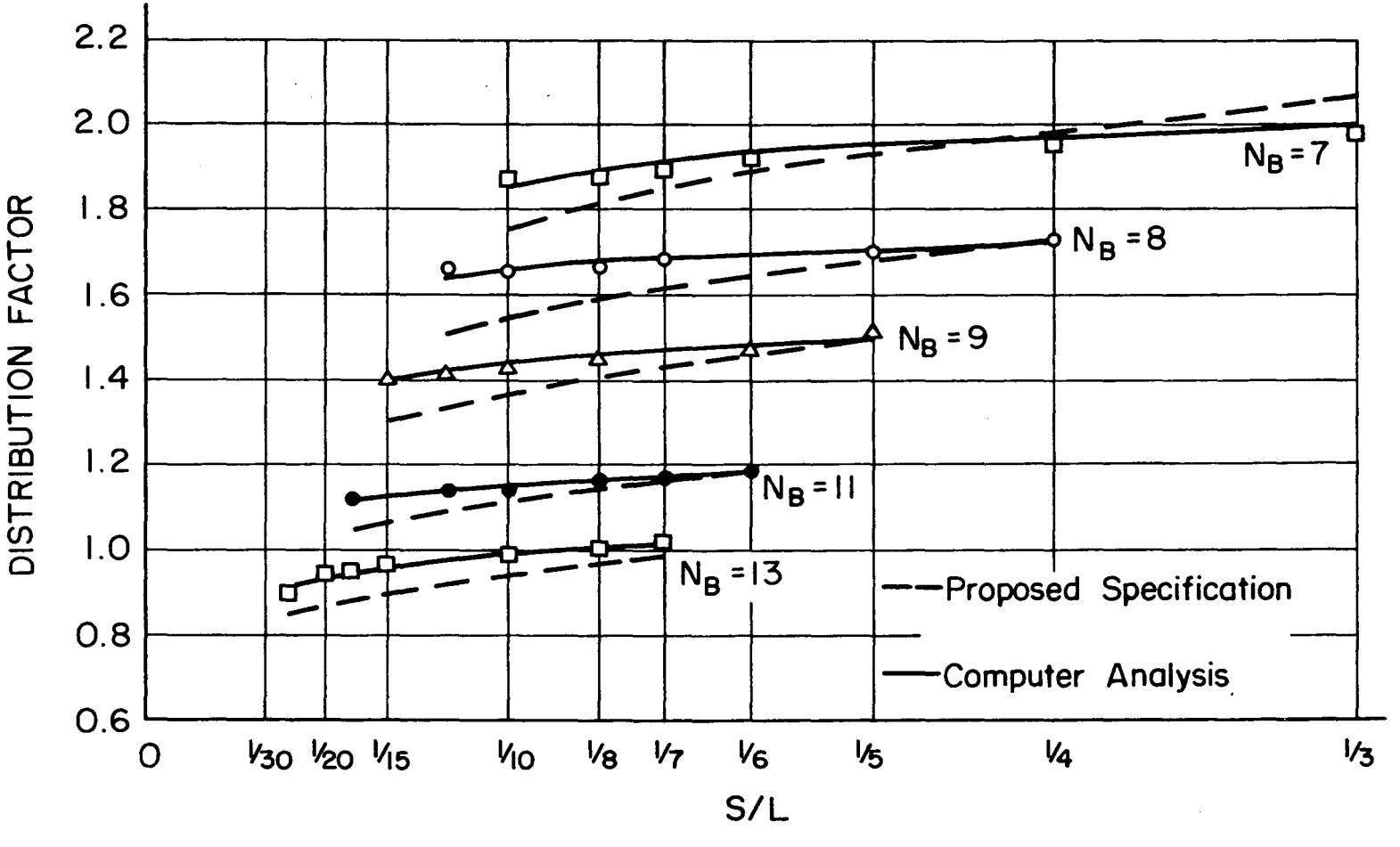

Fig. 42 Distribution Factors for Interior Beams - W = 60 ft. $N_L = 4$

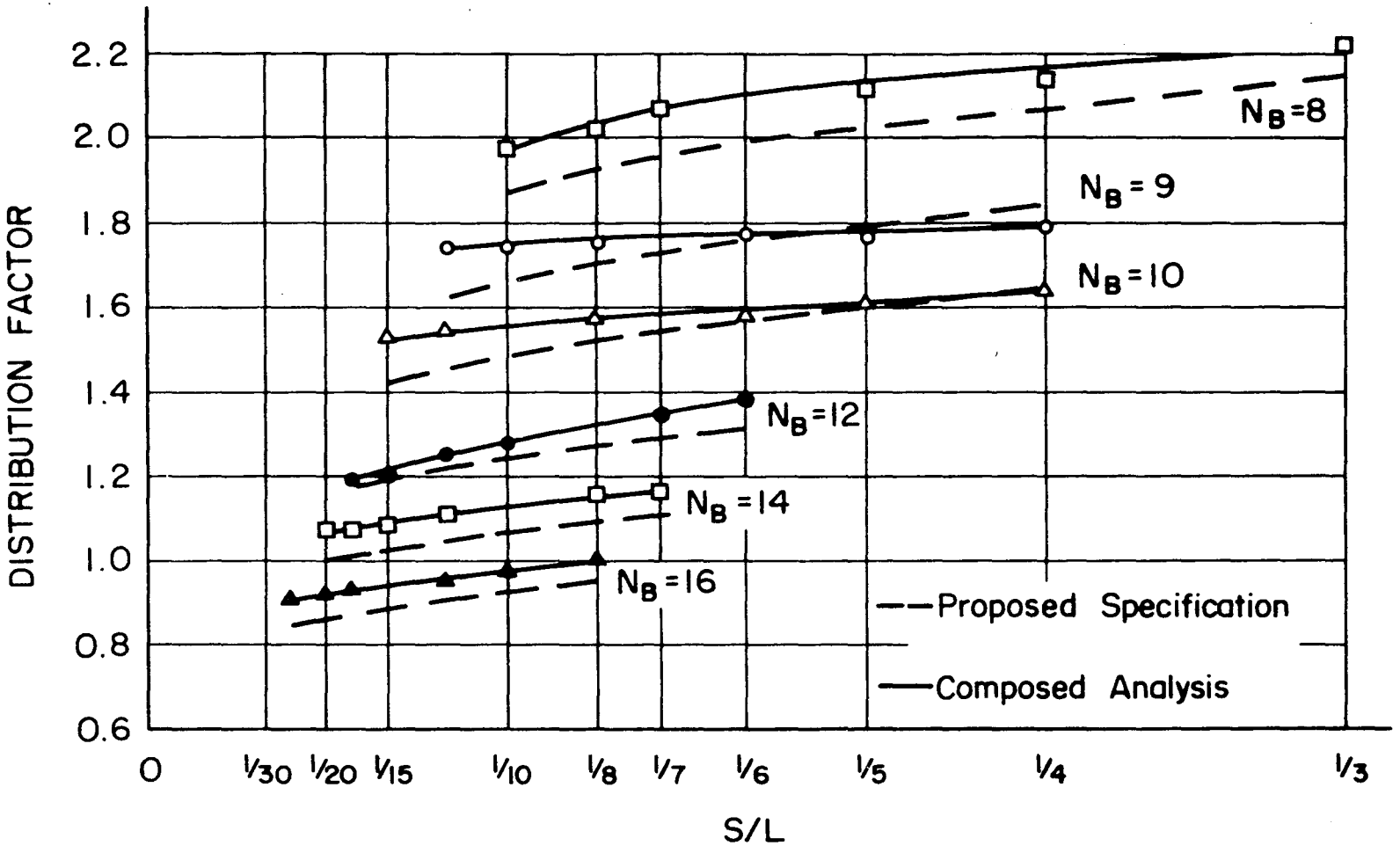

Fig. 43 Distribution Factors for Interior Beams - W = 72 ft. $N_L = 5$

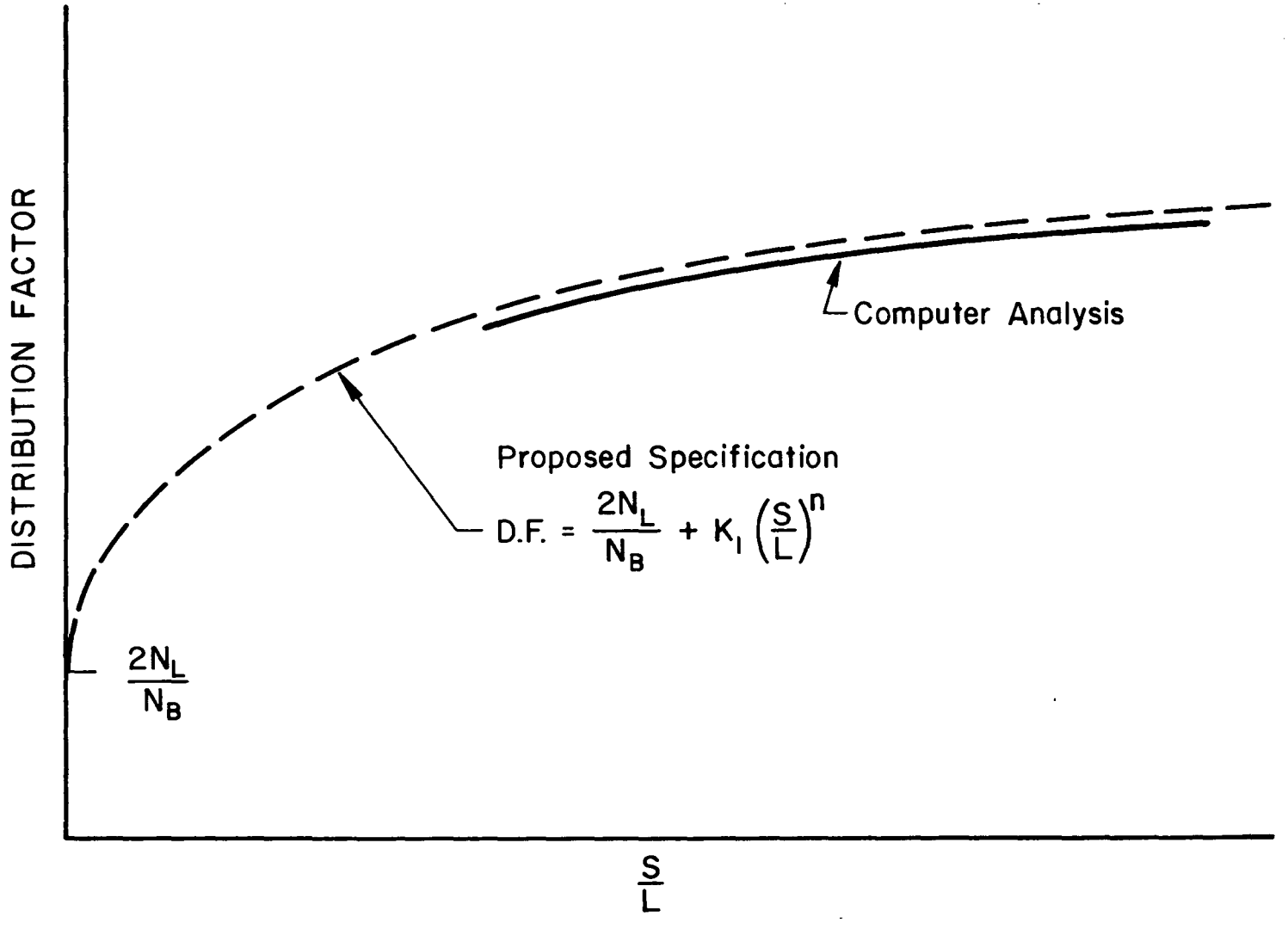

Fig. 44 Development of Proposed Specification for Interior Beams

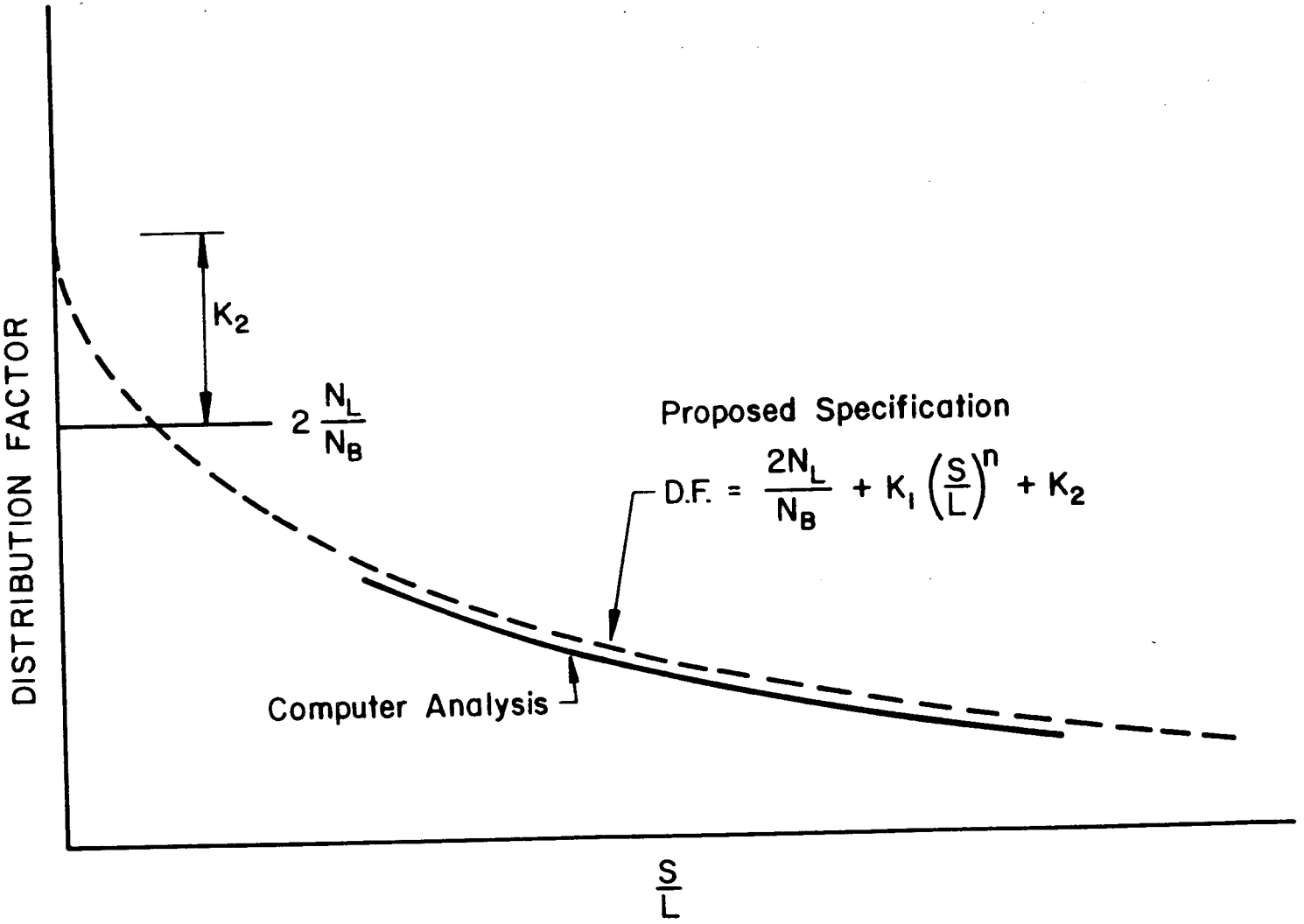

Fig. 45 Development of Proposed Specification for Exterior Beams

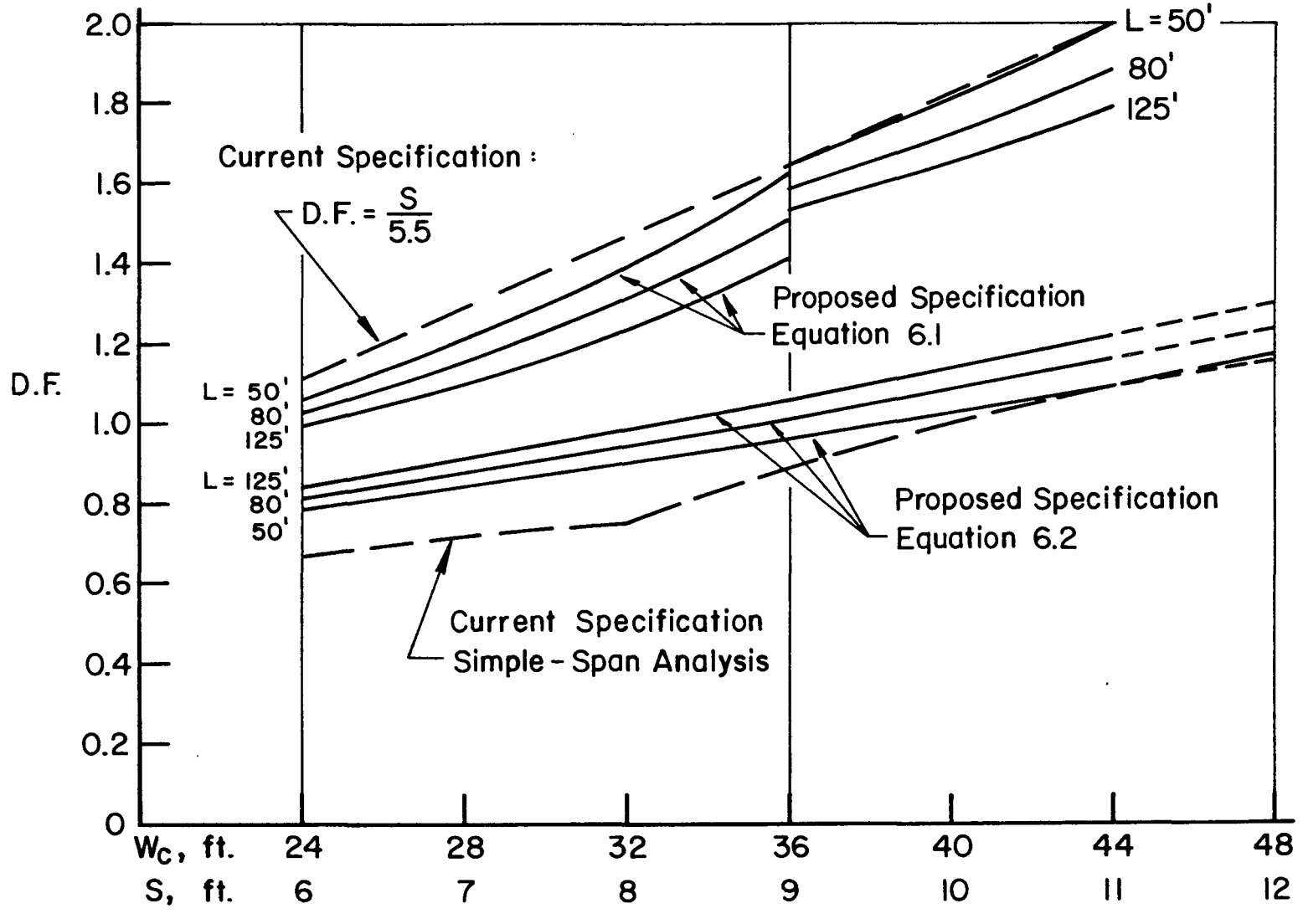

Fig. 46 Comparison of Proposed and Current Specifications - $N_8 = 5$

11. REFERENCES

1. American Association of State Highway and Transportation Officials
   STANDARD SPECIFICATIONS FOR HIGHWAY BRIDGES, Eleventh Edition, Washington, D. C., 1973.

2. American Association of State Highway and Transportation Officials
   INTERIM SPECIFICATIONS - BRIDGES, Washington, D. C., 1974.

3. Adini, A. and Clough, R. W.
   ANALYSIS OF PLATE BENDING BY THE FINITE ELEMENT METHOD, Report submitted to the National Science Foundation, Grant No. G7337, University of California, Berkeley, California, 1960.

4. Chen, C. H. and VanHorn, D. A.
   STATIC AND DYNAMIC FLEXURAL BEHAVIOR OF A PRESTRESSED CONCRETE I-BEAM BRIDGE - BARTONSVILLE BRIDGE, Lehigh University, Fritz Engineering Laboratory Report No. 349.2, January 1971.

5. Chen, C. H. and VanHorn, D. A.
   SLAB BEHAVIOR OF A PRESTRESSED CONCRETE I-BEAM BRIDGE - LEHIGH BRIDGE, Lehigh University, Fritz Engineering Laboratory Report No. 349.5, July 1971.

6. DeCastro, E. S. and Kostem, C. N.
   USER'S MANUAL FOR PROGRAM PLATE, Lehigh University, Fritz Engineering Laboratory Report No. 400.13, January 1975.

7. Eby, C. C., Kulicki, J. M., Kostem, C. N. and Zellin, M. A.
   THE EVALUATION OF ST. VENANT TORSIONAL CONSTANTS FOR PRESTRESSED CONCRETE I-BEAMS, Lehigh University, Fritz Engineering Laboratory Report No. 400.12, June 1973.

8. Pennsylvania Department of Transportation
   STANDARDS FOR BRIDGE DESIGN (PRESTRESSED CONCRETE STRUCTURES), DB-201, March 1973.

9. Timoshenko, S. P. and Woinowsky, K.
THEORY OF PLATES AND SHELLS, New York, McGraw-Hill Book Company, Inc. 1959.

10. VanHorn, D. A. and Chen, C. H.
STRUCTURAL BEHAVIOR OF A PRESTRESSED CONCRETE I-BEAM BRIDGE - LEHIGHTON BRIDGE, Lehigh University, Fritz Engineering Laboratory Report No. 349.4, October 1971.

11. Wegmuller, A. W. and VanHorn, D. A.
SLAB BEHAVIOR OF A PRESTRESSED CONCRETE I-BEAM BRIDGE - BARTONSVILLE BRIDGE, Lehigh University, Fritz Engineering Laboratory Report No. 349.3, May 1971.

12. Wegmuller, A. W. and Kostem, C. N.
FINITE ELEMENT ANALYSIS OF PLATES AND ECCENTRICALLY STIFFENED PLATES, Lehigh University, Fritz Engineering Laboratory Report No. 378A.3, February 1973.

13. Wegmuller, A. W. and Kostem, C. N.
EFFECT OF IMPERFECTIONS ON THE STATIC RESPONSE OF BEAM-SLAB TYPE HIGHWAY BRIDGES, Proceedings of the Specialty Conference on the Finite Element Method in Civil Engineering, Canadian Society of Civil Engineering, McGill University, Montreal, Quebec, Canada, pp. 974-970, June 1972.

14. Zellin, M. A., Kostem, C. N., and VanHorn, D. A.
STRUCTURAL BEHAVIOR OF BEAM-SLAB HIGHWAY BRIDGES, A SUMMARY OF COMPLETED RESEARCH AND BIBLIOGRAPHY, Lehigh University, Fritz Engineering Laboratory Report No. 387.1, May 1973.

15. Zellin, M. A., Kostem, C. N., VanHorn, D. A. and Kulicki, J. M.
LATERAL DISTRIBUTION OF LIVE LOAD IN PRESTRESSED CONCRETE I-BEAM BRIDGES, Lehigh University, Fritz Engineering Laboratory Report No. 387.2A, June 1975.

16. Zienkiewicz, O.
FINITE ELEMENT METHOD IN ENGINEERING SCIENCE, New York, McGraw-Hill Book Company, 1971.